Lawrence Berkeley National Laboratory
Recent Work

Title
Classical and Semiclassical Aspects of Chemical Dynamics

Permalink
https://escholarship.org/uc/item/2bg1h0rh

Author
Gray, Stephen Kevin

Publication Date
1982-08-01

Lawrence Berkeley Laboratory

UNIVERSITY OF CALIFORNIA

Materials & Molecular Research Division

CLASSICAL AND SEMICLASSICAL ASPECTS OF
CHEMICAL DYNAMICS

Stephen Kevin Gray
(Ph. D. thesis)

August 1982

DISCLAIMER

Classical and Semiclassical Aspects
of Chemical Dynamics

Stephen Kevin Gray
(Ph.D. thesis)

Lawrence Berkeley Laboratory
University of California
Berkeley, California 94720

August 1982

Classical and Semiclassical Aspects of Chemical Dynamics

by

Stephen Kevin Gray

Abstract

It is argued that a classical or semiclassical picture is useful for understanding a variety of problems in chemical dynamics. To demonstrate this, three very different problems are studied.

Tunneling in the unimolecular reactions $H_2C_2 \rightarrow HC_2H$, $HNC \rightarrow HCN$, and $H_2CO \rightarrow H_2 + CO$ is studied with a classical Hamiltonian that allows the reaction coordinate and transverse vibrational modes to be considered directly. A combination of classical perturbation theory and the semiclassical WKB method allows tunneling probabilities to be obtained, and a statistical theory (RRKM) is used to construct rate constants for these reactions in the tunneling regime. In this fashion, it is found that tunneling may be important, particularly for low excitation energies.

Nonadiabatic charge transfer in the reaction $Na + I \rightarrow Na^+ + I^-$ is treated with classical trajectories based on a classical Hamiltonian that is the analogue of a quantum matrix representation. The charge transfer cross section obtained is found to agree reasonably well with the exact quantum results. An approximate semiclassical formula, valid at high energies, is also obtained.

The interaction of radiation and matter is treated from a classical viewpoint. The excitation of an HF molecule in a strong laser is described with classical trajectories. Quantum mechanical results are also obtained and compared to the classical results. Although the detailed structure of the pulse time averaged energy absorption

cannot be reproduced classically, classical mechanics does predict the correct magnitude of energy absorption, as well as certain other qualitative features. The classical behavior of a nonrotating diatomic molecule in a strong laser field is considered further, by generating a period advance map that allows the solution over many periods of oscillation of the laser to be obtained with relative ease. Classical states are found to form beautiful spirals in phase space as time progresses. A simple pendulum model is found to describe the major qualitative features.

William H. Miller

Table of Contents

Intended for Sir Isaac Newton in Westminster Abbey:

Nature and Nature's laws lay hid in night;
God said, *Let Newton be!* and all was light.

...by Alexander Pope (1688-1744)

Acknowledgements

It is a pleasure to acknowledge Professor William H. Miller for his great patience, guidance, and support throughout these past four years.

I have also benefited from numerous and stimulating discussions with the following past and present members of our eclectic research group : Dr. Charles Cerjan, Dr. Boyd Waite, Dr. Lynn Hubbard, Shenghua Shi, Dominic Ali, Steven Schwartz, Tucker Carrington, and especially Peter Dardi, who deftly collaborated with me on some aspects of the laser-molecule problem.

The illuminating remarks of Professor Robert Wyatt, Dr. Yitzhak Weissman, and Professor M. A. Lieberman are also deeply appreciated.

The electronic structure wizardry of Dr. Yukio Yamaguchi, Dr. Yoshihiro Osamura, and Professor H.F. Schaefer supplied the necessary fuel for the tunneling calculations described here. Dr. Michel Dupuis is also to be thanked for providing me with a foolproof version of his electronic structure code.

Douglas Fox is to be thanked for maintaining our minicomputer and for providing much needed technical advice.

I would also like to acknowledge some of my other good friends, who have kept me happy over the years : Saul Zackson, Shankar Subramanian, Bob Sherburne, Derek White, Doug Lichty, Doug Templeton, Jon Kowallis, John Verosky, and Bosco Weenie.

Of course a special thanks is also due my fiancée, Anne Olson, whose patience, love, and understanding have been instrumental to the successful completion of this work.

Finally, Professor James S. Wright, who initially sparked my interest in theoretical chemistry, is to be thanked for his continued encouragement, advice and friendship.

I. Introduction

Although molecules are inherently quantum mechanical in nature, there is great appeal, from both an aesthetic and practical viewpoint, to use classical and semiclassical methods in the description of basic molecular phenomena. The validity of such approaches is limited, of course, to problems for which the de Broglie wavelength may be considered small in comparison with, say, the dimensions of the interaction region.

The aesthetic appeal of classical mechanics, especially to chemists, is that molecular events, such as bimolecular collisions and reactions, may be depicted with classical trajectories - that is the coordinates and momenta of the relevent atoms may be followed explicitly as a function of time. This gives a mechanistic view of the reaction that has served frequently in the analysis and prediction of, for example, molecular beam experiments[1]. The practicality of classical mechanics is that, given the potential of interaction, the solution of the classical equations of motion, i.e. Hamilton's equations, is not too difficult with the aid of modern computers, even for reactions involving as many as six or seven atoms[2]. In contrast, reactive quantum scattering calculations are complicated by the many channels, or basis functions, that must be included, as well as by serious convergence problems. It is amusing to consider a famous test case of chemical dynamics, the $H + H_2$

hydrogen atom exchange reaction in 3d. The first numerically accurate classical trajectory prediction of the various cross sections for this reaction, as a function of collision energy, was made in 1965 by Karplus, Porter, and Sharma[3]. Only in 1975, and with the expense of almost excessive human and computer time, was an accurate quantum solution obtained[4], and this solution was for a very small range of collision energies. At present (1982) the solution for $H + H_2$ is still the only example of an accurate quantum solution for a realistic (i.e. no constraints such as collinearity) reactive chemical system. In contrast, many classical trajectory studies have appeared, for reactions ranging from[5] $F + H_2 \rightarrow HF + H$, to[6] $H + C_2H_4 \rightarrow C_2H_5$. Of course reactive quantum scattering theory is far from dead, and several groups are working on problems associated with it. Benchmark calculations for other three atom systems, such as $F + H_2$, are expected in the near future. For a discussion of the current status of reactive quantum scattering theory, see Wyatt's recent review[7]. However it would be fair to say that a full quantum solution of, say, $H + C_2H_4$, will not appear in the near future and may never appear, owing to the immense practical difficulties.

Of course quantum effects, ultimately arising from the uncertainty principle and superposition, are observable in many experiments and approximate quantum theories may be used to describe them. A partic - ularly appealing approximate quantum theory is semiclassical mechanics[8].

Semiclassical mechanics constructs essentially a limiting or asymptotic solution to the Schrodinger equation for the case $\hbar \to 0$, which is the classical limit of small de Broglie wavelength. The well-known[9] WKB tunneling and quantization formulae are examples of semiclassical analysis. The result of taking the classical limit is that classical trajectories, and even a more generalized trajectory that may be complex-valued, are retrieved. However, these trajectories are used in constructing complex amplitudes that must be added before an overall probability, the square of the S matrix, may be obtained[8]. Most chemically interesting quantum effects, including interference oscillations in cross sections and tunneling, can arise out of a semiclassical treatment. To obtain an "exact" asymptotic solution of the Schrodinger equation for anything but a simple system has turned out to be almost comparable in difficulty to actually solving the Schrodinger equation directly. But the concepts involved in semiclassical mechanics have greatly aided in the interpretation of many results in chemical dynamics and, moreover, approximate semiclassical methods, such as the WKB method, are exceedingly easy to apply and often can be quite accurate.

The present thesis applies these classical and semiclassical approaches to a variety of chemical dynamics problems. In sec. II, tunneling in the unimolecular reactions $HNC \to HCN$, $H_2C_2 \to HC_2H$, and $H_2CO \to H_2 + CO$, is treated with a classical Hamiltonian

that allows the "reaction coordinate" and transverse vibrational modes
to be considered directly[10]. A combination of classical perturbation
theory and the WKB method allows tunneling probabilities to be
obtained, and a statistical theory (RRKM) is used to construct rate
constants for these reactions due to tunneling[11]. In this fashion
it is found that tunneling may play a significant role in the
microcanonical rate constant, particularly at low excitation energies.

In sec. III, nonadiabatic reactions, such as the charge transfer
reaction, $Na + I \rightarrow Na^+ + I^-$, are considered. These sorts of reactions
involve different quantum mechanical electronic states and thus are
generally thought of as being pure quantum events. However, a novel
classical Hamiltonian treatment, due to Miller, Meyer, and McCurdy[12],
allows one to take the quantum mechanical matrix elements and construct
a classical Hamiltonian. It is shown that purely classical trajectories
can then reasonably approximate the charge transfer cross section for
Na + I. An approximate semiclassical formula, based on this classical
Hamiltonian, and valid at high energies, is also derived.

In sec. IV, the interaction of radiation and matter is treated
classically. The excitation of an HF molecule by a strong laser is
described with classical trajectories. Quantum mechanical results are
also obtained and compared to the classical results. As might be
expected, averaged quantities are well described by the classical
analysis. However, the detailed structure, including rotations, of
the classical and quantum energy absorption spectra do have significant

differences. The classical behavior of a nonrotating diatomic

molecule in a strong laser is also considered, borrowing some

methods from nonlinear dynamics. A method of obtaining the

solution over many periods of oscillation of the laser, by generating

a period advance map[13], is given. The classical solution is seen

to consist of spirals in phase space, representing very graphically

the nature of the resonance between molecule and laser. Through

certain approximate transformations, it is possible to represent the

problem as a simple pendulum[14], with the momentum of the pendulum

being related to the energy of the molecule, and the angle of the

pendulum being the difference between molecular and laser phases.

Finally, sec. V gives some brief concluding remarks.

II. Tunneling in Unimolecular Reactions

A. Preliminaries

Unimolecular reactions, such as molecular decompositions and rearrangements, have been extensively studied, and textbooks such as that of Robinson and Holbrook[15], and review articles such as that by Hase[16], give detailed accounts of many aspects. One aspect rarely discussed, however, is the role of quantum mechanical tunneling. One reason is that the effect of tunneling on the thermal rate constant is expected to be quite small. However, tunneling may play an important role in the microcanonical (energy-dependent) rate constant[11,17], particularly at low excitation energies of the molecule. Today's laser techniques allow, in fact, an experimental determination of state specific rate constants, and some interesting examples include the work of Reddy and Berry[18] on the methyl and allyl isocyanide isomerizations. Indeed, if a laser could excite a molecule to an energy below its classical threshold for reaction, the entire rate of reaction measured would be due to tunneling. This feat, however, has not yet been accomplished in the laboratory.

In sec. IIB, we outline the simple tunneling correction to unimolecular rates given by Miller[11] (see also Forst[17]), and apply it to the isomerization of vinylidene to acetylene. An explanation of the experimental difficulty in observing vinylidene is made on the basis of these results. Next, in sec. IIC, the reaction path

Hamiltonian of Miller, Handy and Adams[10], for polyatomic systems, is discussed. A WKB tunneling probability formula is developed with this Hamiltonian, and then applied to tunneling in the hydrogen isocyanide isomerization, HNC → HCN. In sec. IID the unimolecular decomposition of formaldehyde, $H_2CO \rightarrow H_2 + CO$, is discussed in terms of the present semiclassical reaction path model.

B. Simple Tunneling Correction to Unimolecular Rates, with Application to Vinylidene Isomerization

RRKM theory (so named after its originators O.K. Rice, J. Ramsperger, L.S. Kassel and R.A. Marcus) is the basic theory of unimolecular reactions[15,16]. It may be considered a transition state theory because it assumes the existence of a transition state or critical configuration which may be considered the point of no return. If a molecule attains this configuration during the course of reaction, then it is assumed to react, and not return to reactants. This concept will be modified below to allow a certain leakage due to tunneling. RRKM theory is a statistical theory because it assumes that all possible quantum states of the transition state (and also reactants) are equally probable. As a corollary to the above two assumptions, energy re-distribution within the molecule is considered to be faster than unimolecular reaction. Within these approximations, the microcanonical rate constant is[11]

$$k(E) = N^{\ddagger}(E)/[2\pi\hbar\rho(E)] \quad , \qquad \text{II-1}$$

where $N^{\ddagger}(E)$ is the sum of states at the transition state, and

$\rho(E) = dN_o/dE$ is the density of states for the reactant. More

explicitly, the sum of states for the transition state and reactant

are given by

$$N^{\ddagger}(E) = \sum_{\underset{\sim}{n}} h(E - \varepsilon^{\ddagger}_{\underset{\sim}{n}}) \qquad \text{II-2a}$$

$$N_o(E) = \sum_{\underset{\sim}{n}} h(E - \varepsilon_{\underset{\sim}{n}}) \qquad , \qquad \text{II-2b}$$

where $h(x)$ is the usual step function,

$$h(x) = \begin{cases} 0, & x < 0 \\ 1, & x > 0 \end{cases} \qquad ,$$

and $\varepsilon^{\ddagger}_{\underset{\sim}{n}}$ and $\varepsilon_{\underset{\sim}{n}}$ are vibrational energy levels of the transition state

and reactant. The sums in eq. II-2 are over all possible quantum

number combinations $\underset{\sim}{n} = (n_1, n_2, \ldots)$. It is common to use a separable

harmonic oscillator (or normal mode) approximation to obtain the

energy levels, with $\{\omega^{\ddagger}_i\}$ and $\{\omega_i\}$ being the respective harmonic

frequencies. Thus, measuring the energy relative to the reactant

minimum of energy,

$$\varepsilon_{\underset{\sim}{n}} = \sum_{i=1}^{F} \hbar\omega_i \, (n_i + 1/2)$$

$$\varepsilon^{\ddagger}_{\underset{\sim}{n}} = V^{\ddagger}_o + \sum_{i=1}^{F-1} \hbar\omega^{\ddagger}_i \, (n_i + 1/2) \qquad ,$$

where F is the number of degrees of freedom and $V^{\ddagger}_o$ is the barrier

height relative to the reactant (without any zero-point energy corrections). Notice that the transition state is summed over only F - 1 degrees of freedom, since the reaction coordinate s is assumed not to be harmonic, but rather to have a potential energy profile $V_o(s)$, with a barrier at s = 0 $(V_o(0) = V_o^{\ddagger})$.

The key idea is to replace the sum of states at the transition state, eq. II-2a, by a sum of tunneling probabilities if the total energy E is below the classical threshold, $E_{th} = V_o^{\ddagger} + \Sigma_{i=1}^{F-1} \hbar\omega_i^{\ddagger}/2$:

$$N^{\ddagger}(E) \rightarrow T(E) = \Sigma_{\underset{\sim}{n}} P(E - \epsilon_{\underset{\sim}{n}}^{\ddagger}) \quad , \qquad \text{II-3}$$

where $P(E_s)$ is the 1d tunneling probability for energy E_s in the reaction coordinate. If $V_o(s)$ is only known near s = 0, the transition state, one could use, for example, an Eckart potential barrier assumption and the corresponding tunneling probability[11,18]. Alternatively, if $V_o(s)$ is reasonably well defined, one could use the WKB method[9] to obtain P. With eq. II-3, the microcanonical rate constant in the tunneling energy regime is given by[11]

$$k(E) = T(E)/[2\pi\hbar\rho(E)] \qquad . \qquad \text{II-4}$$

As a final point, angular momentum has been neglected in the above considerations. Miller[11] has shown that its inclusion is not difficult, and experience has shown its effect is not great for

typical low total angular momentum situations.

To use the theory in its simplest form, one needs to know the geometries and total electronic energies of the reactant, transition state, and preferably also the product. One also needs to know the normal mode frequencies of the reactant and transition state. To obtain these, it is necessary to evaluate second derivatives of the Born – Oppenheimer electronic energy with respect to the nuclear coordinates. The normal mode analysis then consists of diagonalizing the appropriately mass – weighted second derivative or force constant matrix (see sec. IIC). For the reactant, one obtains $F = 3N - 6$ positive eigenvalues corresponding to the ω_i^2 , and six zero (or near zero) eigenvalues, that correspond to overall rotations and translations. For the transition state, one finds $F - 1$ positive eigenvalues that correspond to the $\omega_i^{\ddagger 2}$. The other nonzero eigenvalue is negative, which implies an imaginary frequency $i\omega_b$. The presence of one imaginary frequency indicates the potential along one degree of freedom, the reaction coordinate, has the local form of an inverted parabola or barrier. (Actually, in the case of the reactant, exper – imental information may be available on the frequencies, so that it may not be absolutely necessary to obtain the ω_i a priori.)

To obtain the required geometries, one notes that each is an extrenum on the potential surface, so that root searching techniques, coupled with information on the gradient of the potential, are required. The recently developed analytic gradient techniques[19] facilitate the

required work. Also, if second derivative information is readily

available, which will certainly be the case in the very near future[20],

a new approach to finding transition states, due to Cerjan and Miller[21],

may be used.

An interesting application of the theory is to the vinylidene

isomerization to acetylene,

$$\begin{matrix} H \\ \diagdown \\ H \diagup \end{matrix} C=C: \quad \rightarrow \quad H-C\equiv C-H \quad .$$
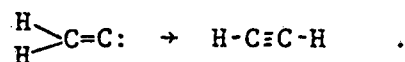
Osamura and Schaefer[22] performed the required electronic structure

calculations described above, at a rather high "level" (with the

configuration interaction(CI) of single and double electronic

excitations relative to the Hartree-Fock reference – see Ref. 22

for the details). Fig. 1 shows the three stationary point geometries

and Table I gives the vibrational frequencies. As a check on the

theoretical calculations, one may note that the theoretical geometry

for acetylene agrees to within 1% with the experimental geometry

and the theoretical vibrational frequencies for acetylene are within

10% of the experimental frequencies. The classical barrier $V_o^{\ddagger}$ is

found to be 6 kcal/mol relative to vinylidene, and acetylene is

lower in energy than vinylidene by 40 kcal/mol. Electronic structure

barrier heights are usually too high and, upon further refinements

of the basis set, the barrier usually decreases. Osamura and Schaefer

therefore applied a correction to their barrier, that empirically

corrects for some omissions in their calculation. Their "best"

classical barrier is estimated to be $V_o^{\ddagger} = 4$ kcal/mol (thus the zero –

point corrected barrier is found to be $V_{ZP} = V_o^{\ddagger} + (\Sigma_{i=1}^{F-1} \hbar\omega_i^{\ddagger} - \Sigma_{i=1}^{F} \hbar\omega_i)/2$

$= 4 - 1.8 = 2.2$ kcal/mol).

The tunneling probability was estimated from the Eckart barrier

formula given in Ref. 11. The density of states for the reactant

was estimated from the Whitton–Rabinovitch semiempirical formula[15],

although it should be noted that the simpler semiclassical expression[15],

$$\rho(E) = E^{F-1}/[(F-1)! \prod_{i=1}^{i=F} \hbar\omega_i] \quad ,$$

could have been equally used, since numerical comparisons of the rate

calculated with the above formula and the Whitton–Rabinovitch formula

did not differ by more than a few percent.

Fig. 2 displays the rate constant results. The dashed curve is

the rate calculated with the 6 kcal/mol barrier and the solid curve

is the rate with the "best" barrier of 4 kcal/mol. It is clear

from Fig. 2 that the rearrangement rate is very high, and for

excitation energies of less than 1 kcal above the zero–point energy

of vinylidene, the rate to form acetylene is $\gtrsim 10^{10} s^{-1}$. This is in

harmony with the experimental work of Skell and co-workers[23a], which

indicates a rearrangement rate of greater than $10^{10} s^{-1}$, and also

with the experiments of Reiser and co-workers[23b], which failed

to detect any evidence of vinylidene. Basicly, one does not observe

vinylidene because its lifetime, $\sim 1/k \sim 10^{-10} - 10^{-12}$ sec, is so short

that it rearranges to acetylene before it has time to collide and react with other molecules (which would indicate its presence). The time between collisions in such experiments is $\sim 10^{-7}$ s, i.e. much longer that the lifetime of vinylidene .

Before going on with some other applications and extensions, it should be noted that there is some uncertainty in these results due to uncertainty in the barrier height. As can easily be seen from Fig. 2, the rate is extremely sensitive to the value chosen for the barrier. In fact, Krishnan et al[24] have challenged the present barrier, claiming that the zero-point corrected barrier is less than 1 kcal/mol, and possibly even zero. This would imply that tunneling per se is not the reason for vinylidene being difficult to observe. Rather, because then even very small excitation energies are above the barrier, it is simply energetics, and not tunneling, that leads to the quick rearrangement to acetylene. Unfortunately, it is not clear at present which calculation is correct, since Krishnan et al [24] base their conclusions on high level perturbation theory results and Osamura and Schaefer[22] use a high level variational treatment - i.e. both methods have different strong and weak points.

C.   Reaction Path Hamiltonian and the HNC → HCN Reaction

C1.   The Reaction Path Hamiltonian

In the previous section, the F degrees of freedom of the transition state were decomposed into a reaction coordinate, along with F - 1 bound vibrational degrees of freedom. What distinguished the reaction coordinate was that the frequency associated with it (obtained from a normal mode analysis at the transition state) was imaginary, implying an inverted parabola or barrier potential along its direction. This analysis was entirely local and only valid very close to the transition state geometry. Naturally, as the molecular coordinates change from this geometry, the frequencies associated with the F - 1 vibrational modes will change. Furthermore, they will, in general, be coupled to one another in some sort of dynamical fashion. In the limit of the reactant geometry, the frequencies of these modes will have changed to take on F - 1 of the reactant mode frequencies, and the potential profile along the reaction coordinate will now appear bound, with frequency corresponding to the other reactant mode. Similar arguments apply to the product limit. The effect of the changing frequencies and couplings between the modes can be incorporated into the calculation of the tunneling probabilities associated with a unimolecular reaction. In this section, a more rigorous formulation of the reaction coordinate and the modes normal to it, valid at intermediate geometries, will be given and a classical Hamiltonian, the reaction path Hamiltonian of Miller, Handy, and Adams[10],

will be discussed.

Consider an N atom system with a transition state on its potential surface separating the relevent reactant and product regions. If $R_{i\gamma}$ denotes the Cartesian coordinates of the nuclei, with $i = 1,2,...,N$, and $\gamma = x,y,z$, it is usually most convenient to work in the mass - weighted coordinates,

$$x_{i\gamma} = \sqrt{m_i}\ R_{i\gamma}\quad,$$

since then the masses m_i do not enter into the equations explicitly. One now defines a curve through the 3N dimensional coordinate space that passes through the reactant, transition state, and product geometries. Although there are many such curves, the most relevant is the reaction path, which is defined as the zero kinetic energy trajectory from the transition state down to the product and reactant regions. In Appendix A it is shown that if s is the distance travelled along the reaction path, the associated mass - weighted Cartesian coordinates must satisfy

$$\partial x_{i\gamma}/\partial s = -c\partial V/\partial x_{i\gamma}\quad,\qquad\qquad\text{II-5}$$

where $c^{-2} = \sum_{i\gamma}(\partial V/\partial x_{i\gamma})^2$, and V is the usual Born - Oppenheimer potential energy. Thus, starting from the transition state, which will always be taken as $s = 0$, one may solve the first order

differential equations, eqs. II-5, to obtain $x_{i\gamma}(s)$, if $\partial V/\partial x_{i\gamma}$ can be readily evaluated.

We constrain the system to have zero total angular momentum so that there are $F = 3N - 6$ relevent degrees of freedom (the six overall rotations and translations being ignored). One of the coordinates is chosen to be the reaction coordinate s. The other $F - 1$ coordinates then correspond to vibrational motion orthogonal to this reaction coordinate and are denoted by Q_k. Miller, Handy and Adams[10] performed a canonical transformation from the usual Cartesian coordinates and momenta $(x_{i\gamma}, p_{i\gamma})$ to these new coordinates and their associated momenta (s, Q_k, p_s, P_k), which resulted in the Hamiltonian ,

$$H(p_s, s, \underset{\sim}{P}, \underset{\sim}{Q}) = \sum_{k=1}^{F-1} \left(\tfrac{1}{2}P_k^2 + \tfrac{1}{2}\omega(s)^2 Q_k^2 \right) + V_0(s)$$

$$+ \tfrac{1}{2} \frac{\left[p_s - \sum_{k,k'=1}^{F-1} Q_k P_{k'} \, B_{k,k'}(s) \right]^2}{\left[1 + \sum_{k=1}^{F-1} Q_k \, B_{k,F}(s) \right]^2} \quad , \qquad \text{II-6}$$

where it has been assumed that for fixed s, the potential along each vibrational degree of freedom Q_k is harmonic. $V_0(s)$ is the (non-harmonic) potential along the reaction coordinate, $\omega_k(s)$ are the harmonic frequencies associated with the Q_k and the $B_{kk'}(s)$ are elements

which couple the various vibrational modes with one another (B_{kF} denotes the direct coupling of mode k to the reaction coordinate).

The frequencies $\omega_k(s)$ and coupling elements $B_{kk'}$ in eq. II-6 are obtained as follows. The 3N by 3N force constant matrix $\underset{\approx}{K}$ is defined to be the matrix of (mass-weighted) second derivatives,

$$K_{i\gamma,i'\gamma'} \equiv \frac{\partial^2 V}{\partial x_{i\gamma} \partial x_{i'\gamma'}} \quad , \quad \text{II-7}$$

evaluated at the coordinates on the reaction path. The matrix $\underset{\approx}{P}$ is a matrix that projects onto the directions corresponding to the overall translations and rotations, as well as the reaction coordinate direction (which is proportionate to the gradient vector). The explicit form for $\underset{\sim}{P}$ is given in Ref. 10. The projected force constant matrix is then defined to be

$$(\underset{\sim}{1} - \underset{\sim}{P}) \cdot \underset{\approx}{K} \cdot (\underset{\sim}{1} - \underset{\sim}{P}) \quad , \quad \text{II-8}$$

and has seven zero eigenvalues corresponding to the overall translations and rotations, as well as the reaction coordinate direction. The other $3N - 7 = F - 1$ nonzero eigenvalues are the ω_k^2, with associated eigenvectors denoted by $L_{i\gamma,k}(s)$. Let the normalized negative gradient vector be the $k = F$ eigenvector :

$$L_{i\gamma,F}(s) = - c \partial V / \partial x_{i\gamma} \quad .$$

The coupling elements are then given by

$$B_{k,k'}(s) = \sum_{i,\gamma} \frac{\partial L_{i\gamma,k}(s)}{\partial s} L_{i\gamma,k'}(s) \quad . \qquad \text{II-9}$$

The terms $B_{kF}(s)$ couple the various normal modes to the reaction coordinate and are also related to the curvature $\kappa(s)$ of the reaction path :

$$\kappa(s) = \left[\sum_{k=1}^{F-1} B_{k,F}(s)^2 \right]^{\frac{1}{2}} = \left[\sum_{i,\gamma} x_{i\gamma}''(s)^2 \right]^{\frac{1}{2}} ,$$

The harmonic oscillator coordinates (Q_k, P_k) are not always the most convenient ones. The action - angle variables (n_k, q_k) corresponding to these coordinates are defined by[10]

$$Q_k = \sqrt{(2n_k + 1)/\omega_k} \, \sin q_k$$

$$P_k = \sqrt{(2n_k + 1)\, \omega_k} \, \cos q_k \quad ,$$

and will be useful in the perturbative arguments that follow. The Hamiltonian in terms of these variables is given by

$$H(p_s, s, \underset{\sim}{n}, \underset{\sim}{q}) = \sum_{k=1}^{F-1} (n_k + \tfrac{1}{2})\omega_k(s) + V_0(s)$$

$$+ \tfrac{1}{2} \frac{\left[p_s - \sum_{k,k'=1}^{F-1} \sqrt{(2n_k + 1)(2n_{k'} + 1)\omega_{k'}(s)/\omega_k(s)} \, \sin q_k \cos q_{k'} B_{k,k'}(s) \right]^2}{\left[1 + \sum_{k=1}^{F-1} \sqrt{(2n_k + 1)/\omega_k(s)} \, \sin q_k \, B_{k,F}(s) \right]^2} \qquad \text{II-10}$$

In eq. II-10 the diagonal elements $B_{kk}(s)$ are defined as

$$B_{k,k}(s) \equiv - \frac{\omega_k'(s)}{2\omega_k(s)} \quad ,$$

where here the prime denotes differentiation with respect to s. (Note that in the Q_k, P_k Hamiltonian, eq. II-6, $B_{kk} = 0$.)

C2. An Improved Rate Constant Formula

In sec. C1, a more rigorous definition of the reaction-coordinate and associated reaction path Hamiltonian was given in which the frequencies of the normal modes change as s, the reaction coordinate, changes, and also certain couplings between the modes occur. It is possible to incorporate these effects into a calculation of the rate constant. This will be accomplished with the classical perturb- ation theory described in Born's famous book[25]. The basic idea is to take the original Hamiltonian, in terms of the zero-order action-angle variables (eq. II-10), $H(p_s, s, \underset{\sim}{n}, \underset{\sim}{q})$, and through certain canonical transformations arrive at yet another Hamiltonian, $H(p_s, s, \underset{\sim}{N}) = E$, which does not depend explicitly on the new angle variables conjugate to $\underset{\sim}{N}$. Effectively, for fixed p_s and s, one has averaged over the F - 1 vibrational modes. One then, in the spirit of the old quantum theory, associates the new actions $\underset{\sim}{N}$ with the quantum numbers of the modes at the transition state and calculates a tunneling probability for each combination of $\underset{\sim}{N}$ via the WKB approximation,

$$T(E) = \sum_{\underset{\sim}{N}} [\, 1 + e^{2\theta(E, \underset{\sim}{N})}]^{-1} \quad , \qquad \text{II-11}$$

where θ is the 1d barrier penetration integral,

$$\theta(E,\underset{\sim}{N}) = \int_{s_<}^{s_>} ds \; \text{Im} \; p_s(s,E,\underset{\sim}{N}) \quad . \qquad\qquad \text{II-12}$$

This is completely analagous with the simple treatment of sec. IIB, except that implicit in eqs. II-11 and II-12 are the (average) effects of changing frequencies and mode couplings. The micro − canonical rate constant is then given as before (cf. eq. II-4).

The transformation $H(p_s,s,\underset{\sim}{n},\underset{\sim}{q}) \rightarrow H(p_s,s,\underset{\sim}{N})$ is very difficult to do exactly. We will carry it out to second order in perturbation theory, which, although not exact, suffices for the present application to hydrogen isocyanide rearrangement, since the effects to be included actually are small. (There are, of course, better, but more numerical ways of accomplishing such transformations[26] and these could possibly be used for more pathological examples.)

Considering the coupling elements B to be the perturbation, one can write the Hamiltonian as

$$H(p_s,s,\underset{\sim}{n},\underset{\sim}{q}) = H_0(p_s,s,\underset{\sim}{n}) + H_1(p_s,s,\underset{\sim}{n},\underset{\sim}{q}) + H_2(p_s,s,\underset{\sim}{n},\underset{\sim}{q}) \qquad \text{II-13a}$$

where H_0 is given by

$$H_0(p_s,s,\underset{\sim}{n},\underset{\sim}{q}) = \sum_{k=1}^{F-1} (n_k + \tfrac{1}{2})\omega_k(s) + V_0(s) + \tfrac{1}{2}p_s^2 \quad , \qquad \text{II-13b}$$

and H_1 and H_2 are given by

$$H_1(p_s,s,\underset{\sim}{n},\underset{\sim}{q}) = -p_s C_1 - p_s^2 C_2 \qquad \text{II-13c}$$

$$H_2(p_s,s,\underset{\sim}{n},\underset{\sim}{q}) = \tfrac{1}{2} C_1^2 + \tfrac{3}{2} p_s^2 C_2^2 + 2p_s C_1 C_2 \qquad \text{II-13d}$$

with

$$C_1 \equiv \sum_{k,k'} B_{k,k'}(s)\sqrt{(2n_k + 1)(2n_{k'} + 1)\omega_{k'}(s)/\omega_k(s)} \; \sin q_k \cos q_{k'}$$

$$\text{II-13e}$$

$$C_2 \equiv \sum_k B_{k,F}(s)\sqrt{(2n_k + 1)/\omega_k(s)} \; \sin q_k \quad .$$

Following Born[25], classical perturbation theory then gives the
Hamiltonian in terms of the good action-angle variables as a perturb -
ation series :

$$E(p_s,s,\underset{\sim}{N}) = E_0(p_s,s,\underset{\sim}{N}) + E_1(p_s,s,\underset{\sim}{N}) + E_2(p_s,s,\underset{\sim}{N}) + \cdots \qquad \text{II-14a}$$

where

$$E_0(p_s,s,\underset{\sim}{N}) = H_0(p_s,s,\underset{\sim}{N}) \qquad \text{II-14b}$$

$$E_1(p_s,s,\underset{\sim}{N}) = \overline{H}_1(p_s,s,\underset{\sim}{N}) \qquad \text{II-14c}$$

$$E_2(p_s,s,\underset{\sim}{N}) = \overline{H}_2(p_s s,\underset{\sim}{N})$$

$$\text{II-14d}$$

$$-\tfrac{1}{2} \sum_{\underset{\sim}{k}} \frac{\left| \underset{\sim}{k} \cdot \frac{\partial}{\partial \underset{\sim}{N}} \; H_{\underset{\sim}{k}}^{(1)}(p_s,s,\underset{\sim}{N}) \right|^2}{\underset{\sim}{k} \cdot \underset{\sim}{\omega}(s)} \quad ,$$

with

$$\overline{H}_i(p_s,s,\underset{\sim}{N}) = (2\pi)^{-(F-1)}\int_0^{2\pi}d\underset{\sim}{q}\; H_i(p_s,s,\underset{\sim}{N},\underset{\sim}{q}) \qquad \text{II-15a}$$

$$H_{\underset{\sim}{k}}^{(1)}(p_s,s,\underset{\sim}{N}) = (2\pi)^{-(F-1)}\int_0^{2\pi}d\underset{\sim}{q}\; e^{-i\underset{\sim}{k}\cdot\underset{\sim}{q}} H_1(p_s,s,\underset{\sim}{N},\underset{\sim}{q}) \qquad \text{II-15b}$$

Using eqs. II-14 and II-15, a straightforward calculation gives

$$E_0(p_s,s,\underset{\sim}{N}) = \tfrac{1}{2}p_s^2 + V_0(s) + \sum_k (N_k + \tfrac{1}{2})\omega_k(s) \qquad \text{II-16a}$$

$$E_1(p_s,s,\underset{\sim}{N}) = 0 \qquad \text{II-16b}$$

$$E_2(p_s,s,\underset{\sim}{N}) = A(s,\underset{\sim}{N}) + p_s^2\, B(s,\underset{\sim}{N}) - p_s^4\, C(s,\underset{\sim}{N}), \qquad \text{II-16c}$$

where

$$A(s,\underset{\sim}{N}) = \tfrac{1}{2}\sum_{k<k'} B_{k,k'}(s)^2 (N_k + \tfrac{1}{2})(N_{k'} + \tfrac{1}{2})\frac{\omega_k(s)^2 + \omega_{k'}(s)^2}{\omega_k(s)\omega_{k'}(s)}$$

$$+ \sum_k \left(\frac{\omega_k'(s)}{4\omega_k(s)}\right)^2 (N_k + \tfrac{1}{2})^2 \qquad \text{II-16d}$$

$$B(s,\underset{\sim}{N}) = \tfrac{3}{2}\sum_k B_{k,F}(s)^2\frac{N_k + \tfrac{1}{2}}{\omega_k(s)} - \tfrac{1}{8}\sum_k \frac{\omega_k'(s)}{\omega_k(s)^3}^2 (N_k + \tfrac{1}{2})$$

$$- \tfrac{1}{2}\sum_{k<k'} B_{k,k'}(s)^2 \frac{\left[\omega_k(s)(N_{k'} + \tfrac{1}{2}) - \omega_{k'}(s)(N_k + \tfrac{1}{2})\right]}{\omega_k(s)^2 - \omega_{k'}(s)^2}\frac{\left[\omega_k(s)^2 + \omega_{k'}(s)^2\right]}{\omega_k(s)\omega_{k'}(s)},$$

$$\text{II-16e}$$

$$C(s,\underset{\sim}{N}) = \tfrac{1}{2}\sum_k \frac{B_{k,F}(s)^2}{\omega_k(s)^2} . \qquad \text{II-16f}$$

With the Hamiltonian expressed in terms of (p_s, s) and the good action-angle variables, it is then easy to use energy conservation, i.e.,

$$E_0(p_s, s, \underset{\sim}{N}) + E_1(p_s, s, \underset{\sim}{N}) + E_2(p_s, s, \underset{\sim}{N}) = E \quad ,$$

to define $Im\ p_s(s, E, N)$. One finds

$$Im\ p_s(s, E, \underset{\sim}{N}) = \sqrt{2(V - E + A)}$$

$$X \left[B + \tfrac{1}{2} + \sqrt{(B + \tfrac{1}{2})^2 + 4C\ (V - E + A)} \right]^{-\tfrac{1}{2}} \qquad \text{II-17a}$$

where A,B,C are as defined in eq. II-16 and

$$V = V_0(s) + \sum_k (N_k + \tfrac{1}{2})\omega_k(s) \qquad . \qquad \text{II-17b}$$

From eqs. II-17 one can caluclate the barrier penetration integral via eq. II-12, the corresponding tunneling probability from eq. II-11, and finally the microcanonical rate from eq. II-4.

To summarize, the present model is vibrationally adiabatic in that the transformation to good action angle variables $(\underset{\sim}{n}, \underset{\sim}{q}) \rightarrow (\underset{\sim}{N}, \underset{\sim}{Q})$ is performed holding p_s and s fixed as parameters. This is an approximation. Also, the transformation was carried out to only second order perturbation theory and is thus only valid for small coupling perturbations.

C3. Tunneling in HNC $\rightarrow$ HCN

The first step is to obtain the relevant portion of the reaction path and the corresponding frequencies and couplings. Yamaguchi and Schaefer[27] performed the required electronic structure calculations within the self-consistent field (SCF) Hartree-Fock approximation (see Ref. 27 for details). They also performed a limited number of higher level (configuration interaction) calculations. They found, for example, that the geometry of the transition state predicted by the SCF theory was within 3 % of the more exact CI result. The CI barrier height (relative to HNC), however, was 36 kcal/mol compared to the SCF value of 40 kcal/mol. Since tunneling is quite sensitive to the barrier height, the results we report will be as a function of the total energy relative to the barrier height, $E - V_o^{\ddagger}$, which should be somewhat insensitive to the choice of $V_o^{\ddagger}$.

To determine the reaction path $x_{i\gamma}(s)$, one starts at the transition state and takes a step in the direction of the eigenvector associated with the imaginary frequency, $L_{i\gamma,F}(0)$:

$$x_{i\gamma}(\Delta s) \simeq x_{i\gamma}(0) \pm L_{i\gamma,F}(0)\Delta s,$$

where Δs is an appropriate step size and the $+$ or $-$ takes one to one or the other side of the transition state. Subsequent steps are then determined from

$$x_{i\gamma}(s_j) = x_{i\gamma}(s_{j-1}) + L_{i\gamma,F}(s_{j-1})\Delta s \quad ,$$

where $L_{i\gamma,F}(s)$ is the negative normalized gradient vector (cf. the

r.h.s. of eq. II-5). This approach is basicly Euler's method[28] of

solving the differential equations given by eqs. II-5, and represents

the simplest way to find a reaction path. Unless the step size in s

is chosen very small, however, the reaction path generated by the

above approach will oscillate about the true path. Although there

are ways to patch up this difficulty[29], or avoid it[21], we chose simply

to smooth out the nonphysical oscillations "by hand", which should be

satisfactory, since only a small portion of the reaction path near

the transition state yields significant tunneling probabilities.

The relevant portion of the reaction path is shown in Fig. 3, where

s is reported in units of $amu^{1/2} \text{Å}$ ($1\ amu^{1/2} \text{Å} = 80.679\ m_e^{1/2} a_o$). A

step size of $\Delta s = 0.1\ amu^{1/2} \text{Å}$ was used in the calculations. The SCF

force constant matrix was evaluated for $s = 0$, ± 0.3, and $\pm 0.5\ amu^{1/2} \text{Å}$.

The coupling elements $B_{kk'}$ and frequencies ω_k were obtained from

the eigenvalues and eigenvectors of the projected force constant matrix

(see eq. II-8). The $B_{kk'}$ were obtained from eq. II-9 using finite

differences to estimate the derivatives. Since $F = 3$, there are only

two frequencies, essentially the H - (CN) stretch, and the C - N

stretch. The reaction coordinate ($k = F = 3$), is mostly the bending

vibration. As was mentioned earlier, some CI calculations were

also performed. Owing to the expense of such calculations, Yamaguchi

and Schaefer were only able to calculate the CI force constant matrix

at the transition state. To obtain the best estimates of the frequencies

away from the transition state, $\omega_k(s)$, the SCF frequencies were

scaled by $\omega_k^{CI}(0)/\omega_k^{SCF}(0)$. The potential $V_o(s)$ was fit to an Eckart function[18] with the CI energetics and the CI imaginary frequency at $s = 0$. Fig. 4 displays the relevant scaled frequencies and the potential $V_o(s)$. Fig. 5 displays the relevent couplings $B_{kk'}$. B_{12} couples the two modes orthogonal to the transition state to one another, B_{13} couples the H – CN stretch to the reaction coordinate, and the other coupling B_{23}, which couples the CN stretch to the reaction coordinate, was found to be small and essentially zero within the present numerical error ($\pm 10^{-3} m_e^{-1/2} a_o$). It should be noted that these couplings are relatively small, especially in comparison with the curvature couplings in the H + H_2 problem[10].

The microcanonical rate constant, $k(E)$, for the HNC → HCN reaction is shown in Fig. 6, as a function of the energy relative to the classical barrier height ($V_o^{\ddagger} = V_{sp}$ in the figure). The classical threshold is denoted by an arrow. Below this energy the rate is seen to vary exponentially with the energy, a characteristic feature of tunneling. To see the importance of tunneling, one could note that an ideal experiment, performed in a molecular beam, would be capable of measuring rates faster than $10^5 s^{-1}$ (the time of flight across a molecular beam chamber is $\sim 10^{-5} s$). Fig. 6 indicates that rates this fast occur for energies as low as 8 kcal/mol below the classical threshold.

Finally, to assess the importance of including the coupling elements $B_{kk'}$ in the tunneling probability, the calculations were

carried out with all the B's set to zero. This decreases the rate

constant, but not by much; it is 5% smaller at $E-V_o^{\ddagger} = 3$ kcal/mol,

10% smaller at $E-V_o^{\ddagger} = 0$, and 15% smaller at $E-V_o^{\ddagger} = -2$ kcal/mol.

Over the physically significant energy region, the tunneling is

not influenced much by the coupling elements. This is primarily

because the reaction path is relatively flat throughout the relevent

region (see Fig. 3). In the case of $H + H_2$, the reaction path[10]

was very curved in the region of the transition state, implying

large and significant couplings B_{kF}.

D. Tunneling in the Unimolecular Decompostion of Formaldehyde

D1. Preliminaries

The photodissociation of formaldehyde has attracted considerable

theoretical and experimental interest in recent years[30]. Let us

consider the collisionless limit of the process, with the following

idealized sequence of events. First a laser electronically excites

formaldehyde from its ground singlet (S_o) state to a single ro -

vibrational state of the first excited singlet state (S_1) ,

$$H_2CO(S_o) + \hbar\omega \rightarrow H_2CO^*(S_1) \quad , \qquad \text{II-19a}$$
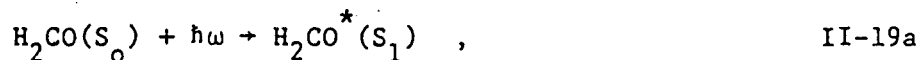
which then decays by either re-emitting a photon (fluorescence),

$$H_2CO^*(S_1) \rightarrow H_2CO(S_o) + \hbar\omega' \quad , \qquad \text{II-19b}$$
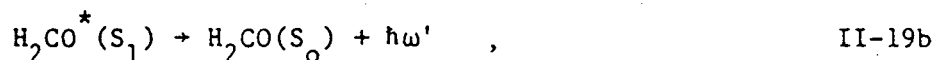
or by undergoing a radiationless transition to a highly vibrationally

excited S_o state,

$$H_2CO^*(S_1) \rightarrow H_2CO^\ddagger(S_o) \quad , \qquad\qquad \text{II-19c}$$

which then may decompose unimolecularly,

$$H_2CO^\ddagger(S_o) \rightarrow H_2 + CO \qquad . \qquad\qquad \text{II-19d}$$

The symmetry is such that molecular products H_2 and CO only correlate with the ground S_o state. It has been assumed that the laser excitation energy is not too much above the $S_o \rightarrow S_1$ origin so that radical products (HCO + H) are energetically inaccessible.

The experimental results[30,31] are consistent with very fast nonradiative decay rates for S_1. Furthermore, it appears that this nonradiative decay is small when D_2CO is used instead of H_2CO. A particularly attractive idea is, therefore, that tunneling[32,11] (in reaction II-19d) plays a significant role - i.e. that there is a very fast nonradiative decay from S_1 to S_o that is coupled with tunneling to form molecular products.

Recently, Goddard, Yamaguchi, and Schaefer[33] have performed extensive and highly accurate _ab initio_ configuration interaction calculations on the S_o surface, and in the subsequent section their results will be used (along with some supplementary calculations by

Yamaguchi and Schaefer) to obtain accurate rate constants[34] for reaction II-19d.

D2. Reaction Path and Tunneling Calculations

Tables II and III give the harmonic frequencies of stable (S_o) formaldehyde and the harmonic frequencies and barrier height of the transition state of reaction II-19d, obtained from ab initio calculations[33,34] at various levels of sophistication. The level of theory is increasing from left to right, with SCF denoting calculations made with a single (Hartree-Fock) configuration and CI denoting calculations with many (literally tens of thousands) configurations. The reader may consult Refs. 32-34 for more technical details. The "experimental frequencies " of Table II are the harmonic frequencies inferred from experiment[35]. The "scaled frequencies" in Table III are the best estimates of the transition state frequencies, obtained by empirically modifying the DZP-CI frequencies by

$$(\omega_i^{scaled})_{TS} = (\omega_i^{DZP-CI})_{TS} \times (\omega_i^{exptl}/\omega_i^{DZP-CI})_{H_2CO} \quad .$$

One point to be made about Tables II and III is that ab initio electronic structure theory estimates frequencies reasonably well, even at rather "low" levels of theory, such as the DZ-SCF level. Thus if one considers the RRKM rates predicted with the various levels of theory, and adjusts appropriately for the different barrier heights by, e.g., comparing $k(E - V_o^{\ddagger})$ rather than $k(E)$,

there will not be much variation in the predicted rates. Using

the RRKM + tunneling model described in sec. IIB, we obtained

Table IV, which indeed confirms these expectations. Thus for

the energy region for which the rate constant is 10^5 or larger,

there is less than a factor of three variation in the rate

constants predicted by the various levels of theory.

Fig. 7 shows the potential energy profile along the reaction

path in the vicinity of the transition state, as given by the

DZP-CI calculations. It has been previously determined that

for these sort of tunneling calculations, one need only consider

the region on either side of the transition state to where the

potential has fallen off to about 8 kcal/mol below its value

at the transition state. The points in Fig. 7 are the ab initio

values, and the solid line is an Eckart potential function[18] fit

to the ab initio energetics and curvature at the transition state.

Thus it appears that the Eckart potential form is well suited

for this problem.

Ab initio force constant matrices were calculated at the DZP - CI

level at values of the reaction coordinate $s = \pm 0.21$ and 0 $\text{amu}^{1/2}\overset{o}{A}$;

these are points at which $V_o(s)$ has fallen to about 8 kcal/mol below

its value at the transition state. The frequencies and couplings

were obtained as before (sec. IIC) from the projected force constant

matrix. The frequencies are listed in Table V. Owing to certain

technical difficulties, the out-of-plane bend, ω_6, was only estimated

roughly (see Ref. 33 for more explanation). However, since it is one of the lower frequencies, its variation with s is not expected to have a significant effect on the microcanonical rate. (But if the energy were not completely randomized, then it is possible that certain mode specific effects, related explicitly to this out-of-plane bend, could play a role[36].)

The coupling elements $B_{kk'}$ were rougly estimated using a finite differences approximation to eq. II-9 and the three sets of eigenvectors obtained for $s = \pm 0.21$ and 0. It will turn out that the actual effect of the coupling is small, so that a more accurate determination is unnecessary. Within the numerical error, the most significant nonzero couplings may be considered constant over the -0.21, 0.21 interval in s and are found to be $B_{13} \cong 0.01$, $B_{34} \cong 0.015$, $B_{1F} \cong 0.005$, and $B_{3F} \cong -0.009 \ m_e^{1/2} a_o$.

The tunneling rates are presented in Table VI. Column A is just the simple RRKM + tunneling rate of sec. IIB, with the DZP-CI values for all relevent parameters. Column B is the same as A but with the Eckart potential replaced by the actual $V_o(s)$ points and a WKB approximation to the tunneling probability. Column C is the same as B, except that the frequencies are allowed to vary along s (i.e. the potential has the form of eq. II-17b), with each $\omega_k(s)$ being defined by a quadratic fit to the points in Table V. Column D includes the effect of coupling between the modes, using the perturbative formulae of sec. IIC. Column E

is the same as Column D, but with the couplings all multiplied by a factor of two, to see the effect of larger coupling.

One sees from Table VI how relatively insensitive the rate is to the level of rigour used to describe the tunneling dynamics. For example, the simplest model, Column A, differs from the most rigorous model, Column D, by less than 20% for energies for which the rate is significant ($\gtrsim 10^5$ s^{-1})

Let us now summarize our best predictions of the microcanonical rate for reaction II-19d at the experimental excitation origin for $S_o \rightarrow S_1$, $\hbar\omega = 80.6$ kcal/mol. The zero-point energy of formaldehyde is 16.8 kcal/mol (using the experimental frequencies of Table II), so that the total energy is then 97.4 kcal/mol. Using the best classical barrier of 92 kcal/mol we see that $E - V_o^{\ddagger} = 5.4$ kcal/mol. Interpolating from Column D, Table VI, and applying a factor of two due to symmetry[11], gives

$$k = 5.9 \times 10^6 \text{ s}^{-1} \quad .$$

It is amusing to note that this result is in remarkable agreement with an earlier estimate of Miller, that used the simplest RRKM + tunneling theory and some significantly different parameters.

This magnitude of k near the origin of excitation has been shown[30] to be consistent with the experimental results, since it is significantly larger than typical radiative decay rates ($\sim 2 \times 10^5$s^{-1}). Also, if one replaces hydrogen by deuterium, the mass effect reduces

k by about a factor of[11] 40, making it comparable to or less than the radiative decay rates, which is again consistent with the experimental observations[30,31].

However, this picture may not be perfect because there is still some uncertainty about the barrier height. Recent work by Frisch, Krishnan, and Pople[37] has suggested that the zero-point corrected barrier is V_{ZP} = 80 kcal/mol, which is to be contrasted with the best estimate of Goddard, Yamaguchi, and Schaefer[33], V_{ZP} = 87 kcal/mol. The result of Frisch et al is based on a perturbation theory approach that actually includes certain configurational effects not included by Goddard et al in their extensive many configuration variational calculation. On the other hand, the variational calculation includes more completely some configurational effects. Whatever the final outcome, one can still use Table VI to estimate the rate. Suppose, for example, that upon further refinements, the true zero-point corrected barrier is found to be 83 kcal/mol. Then the classical barrier is 83 + 16.8 - 11.8 = 88 kcal/mol, where the zero-point energies have been taken out (11.8 kcal is the best estimate of the transition state zero-point energy obtained from Table III). Thus $E - V_o^{\ddagger}$ = 97.4 - 88 = 9.4 kcal. From Table VI, one interpolates $k = 2 \times 10^8 \text{ s}^{-1}$, where again the factor of two due to symmetry[11] has also been included. Here, we have used the previous observation that although the barrier height may vary, the rate as a function of $E - V_o^{\ddagger}$ remains relatively constant.

D3.   A Closer Look at the Formaldehyde Decomposition Reaction Path

Up until now, we have been only looking at a rather small
portion of the reaction path that was important for tunneling.
However, if one wishes to do a more detailed theoretical study,
as, for example, in Ref. 36 where mode specific effects are considered,
a wider and more detailed view of the path is necessary. To
obtain such a view, including the frequency and coupling variations,
would be exceedingly expensive with a high level of electronic
structure theory. However, as has already been noted, the
frequencies are reasonably well described with a relatively low
level of theory, such as DZ-SCF.

In the following, we have used the computer code written by
King, Dupuis, and Rys[38] to obtain the reaction path, frequencies,
and couplings at the simple DZ-SCF (i.e. one configuration Hartree-
Fock) level.

The Reaction Path

The equilibrium and transition state geometries are both planar,
and within the DZ-SCF level are[32]
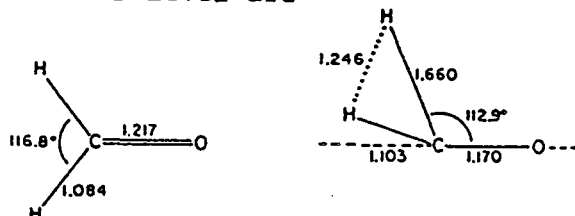
(with bond distances in Å). As usual, the negative normalized
gradient vector in mass-weighted coordinates (eq. II-5) was

followed, with the initial step being in the direction of the

eigenvector of the imaginary frequency at the transition state

(see the procedure in sec. IIC). A step size $\Delta s = 0.05$ amu$^{1/2}$Å

was found to be sufficient, and, owing to the steepness of the

potential, no nonphysical oscillations were apparent upon subsequent

steps. (As a check, certain portions of the path were reproduced

with a smaller step size of 0.025 amu$^{1/2}$Å.) A total of 28 steps

were taken from the transition state towards equilibrium

formaldehyde, and only 10 towards molecular products $H_2 + CO$.

The reaction path is planar, since the gradient vector is always in

the plane of the molecule. The corresponding potential profile is

shown in Fig. 8. It will be noticed that the barrier is about

114 kcal (but, if desired, could be readily scaled to whatever

barrier height is desired). It was found that the reaction

cooridinate (with imaginary frequency 2320i at the transition state)

corresponds to the $\omega_6(b_2) = 1349$ cm^{-1} mode in equilibrium

formaldehyde. This is also evident from Fig. 8, since in the

vicinity of H_2CO (s = -1.4 amu$^{1/2}$Å), the potential indeed has the

form $V_o(s) \approx (1/2)\omega_6(b_2)^2\Delta s^2$, i.e. the curvature near equilibrium

formaldehyde is less in absolute magnitude than the curvature of the

potential at the transition state.

The Frequencies

As usual, the frequencies were obtained from the eigenvalues

of the projected force constant matrix. This was done for a

total of 30 geometries along the reaction path, allowing for a very clear view of how the frequencies change with s.

There is a slight problem of nomenclature for the frequencies. The standard numbering of the reactant frequencies, employed in the previous section in Table II is not in one to one correspondence with the standard numbering of the transition state frequencies in Table III. Thus, for example, the reaction coordinate frequency, as discussed above, corresponds to $\omega_6(b_2)$ of the equilibrium formaldehyde frequencies. This is not to be confused with the $\omega_6(a'')$ transition state frequency, which is really the out-of-plane bend. To represent the $\omega_k(s)$ we have chosen to use the labels of the transition state.

In Fig. 9 is shown the variation of the frequencies with s. There are some quite interesting features here. The two CH stretches (ω_1 and ω_2 in the transition state labelling scheme) approach each other closely near equilibrium formaldehyde and appear to have a sort of avoided crossing near s = -1.1. In the product limit, it appears that these two frequencies turn into the only two nonzero product frequencies, corresponding to H_2 and CO. Notice also that the out-of-plane bend, ω_6, has a rather deep "well" near s = -0.4. The out-of-plane bend, by symmetry, does not couple with any of the other modes and thus may cross other frequencies, as it crosses ω_4 near s = -0.2. The ω_5 frequency is absent, since it is the reaction coordinate. The above features

have been independently verified by Yamashita, Yambe, and Fukui[39].

The Coupling Elements

As before, the coupling elements were obtained with a finite difference approximation to eq. II-19. This approximation should be reasonably good here, since the spacing between points is now typically small (0.05 $amu^{1/2}$Å). Fig. 10 ahows some of the couplings. An interesting observation, which holds for the other couplings, is that B_{21} is large whenever the associated frequencies become close to each other. Thus B_{21} is quite large where the two CH stretches approach very closely, near $s = -1.1$. Generally speaking, Fig. 10 shows that the couplings can be quite large. However, it is amusing to note that in the vicinity of the transition state, the couplings are generally not too large. This is very fortunate, and indicates that the tunneling analysis discussed in the last section is reasonably justified.

As a final point, we may compare the couplings, obtained from many SCF calculations, to the couplings obtained in the previous section on the basis of only a few CI points. We had previously found that the only significant couplings were approximately $B_{13} \approx 0.01$, $B_{34} \approx 0.015$, $B_{1F} \approx 0.005$, and $B_{3F} \approx -0.009$. From the SCF calculations, we find $B_{13} \approx 0.004$, $B_{34} \approx 0.02$, $B_{1F} \approx 0.00$, and $B_{3F} \approx -0.009$, in satisfactory agreement, in view of the significant differences between the two calculations.

E. Summary

In secs. IIA-IIC, tunneling in several unimolecular reactions was treated with varying levels of theoretical sophistication.

In sec. IIA, the microcanonical rate constant for the isomerization of vinylidene to acetylene was predicted with a simple RRKM + tunneling model due to Miller[11,22], and was found to be consistent with the available experimental evidence. The model used ignored the dynamical effects of coupling between the various normal modes with each other, and with the reaction coordinate. It is difficult to say whether or not the neglect of these effects is serious without doing a much more detailed study. Nonetheless the calculations reported suffice as a reasonable first guess.

In sec. IIB, a more sophisticated dynamical model, based on the reaction path Hamiltonian[10] was developed to account for the mode coupling effects. A combination of classical perturbation theory and the WKB method was used to obtain the tunneling probability and thus micro-canonical rate constant. An application to hydrogen isocyanide isomer-ization showed that the effects of coupling, at least for this reaction, are not very significant. Thus over the significant energy range, the coupling effects did not alter the rate by more than 15%. The obvious reason for this lack of importance is the smallness of the coupling elements $B_{kk'}$ in the reaction path Hamiltonian formalism. Although in general it is difficult to predict <u>a priori</u> if the coupling elements will be small, inspection of the reaction path shows that the reaction

proceeds very smoothly, without any abrupt changes in the nature of the vibrational modes, implying that the reaction is relatively adiabatic. Furthermore, the reaction path itself has very little curvature in the region of the transition state, implying that the B_{kF} which couple the vibrational modes to the reaction path are quite small. Not all reactions are this nice. In the case of $H + H_2$, the curvature effects are known to alter ther tunneling probability by an order of magnitude or more[10].

In sec. IIC the decomposition of formaldehyde was treated with the methods of secs. IIA and IIB. The rate constant obtained was found to be compatible with experiment. Again it was found that the effects of mode coupling play a relatively insignificant role, changing the overall rate by not more than 20%. As with hydrogen isocyanide, the couplings in the region of the transition state were relatively small.

In sec. IID, however, a wider view of the formaldehyde reaction path was obtained. It was seen that although the couplings are not very large near the transition state, they can indeed become large along other parts of the reaction path. This suggests that a more detailed dynamical treatment (i.e. nonperturbative and nonstatistical) may indeed show that mode coupling is more important.

As pointed out earlier, the effect of tunneling in unimolecular reactions has not been treated very much in the literature (see Forst[17] for some brief remarks) and the applications presented here represent the first serious effort at illucidating its importance.

III. Charge Transfer from a Classical Perspective

A. Preliminaries

One of the classic problems of chemical dynamics is collisional ionization[40], for example the reactions

$$Na + I \rightarrow Na^+ + I^- \qquad \text{III-1a}$$

$$Cs + Br_2 \rightarrow Cs^+ + Br_2^- \qquad \text{III-1b}$$

$$H^+ + H_2 \rightarrow H_2^+ + H \qquad . \qquad \text{III-1c}$$
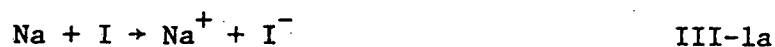
The problem is nonadiabatic in that at least two potential curves (or surfaces) must be considered, along with the associated couplings. Quantum mechanics provides the natural language for the description of such processes. However, given a quantum mechanical Hamiltonian, it is possible to work backwards, and obtain a classical Hamiltonian. Then, purely classical dynamics may be used to describe the problem. Such an approach has been adopted by McCurdy, Meyer, and Miller[12] and has been successfully applied to the study of fine structure transitions in certain atom-atom and atom-molecule collisions. Of course for reactions as simple as III-1a, it is possible to do an accurate quantum mechanical treatment[41]. However, for the related charge-transfer reactions such as III-1b and III-1c, an accurate quantum analysis is much more difficult, whereas the corresponding classical analogue approach to be described is still quite feasible.

Another classical approach to such problems, to be distinguished

from the present, is the surface-hopping trajectory method of Tully and

Preston[42]. In this approach, classical trajectories are followed on a

single surface up to a crossing point, where then a hop to another

surface may take place according to a certain probability. This

method mixes both classical and quantum dynamics and, as pointed out

by Miller[43], can lead to a poor description of dynamical resonances.

Nonetheless the Tully-Preston method has been quite successful in

some applications, such as to reaction III-1c.

In the following, we will treat explicitly a two-state model of

reaction III-1a, although the method can be generalized easily to

related reactions.

B. The Classical Analogue

In the quantum mechanical formulation of the problem, the

Hamiltonian operator is sandwiched between elements of a complete and

orthonormal set of basis functions to obtain an equivalent matrix

representation. Commonly, two sorts of basis set are employed[44]. In

one set, the potential terms are made diagonal, and in the other the

kinetic terms are made diagonal. These are called, respectively,

adiabatic and diabatic representations. It is possible to obtain a

classical analogue for either case, but we consider here only the

diabatic representation.

Considering a two-state model of the simplest charge transfer

reaction, III-1a, the quantum diabatic Hamiltonian representation of

the stationary state Schrodinger equation is

$$(\underset{\approx}{T} + \underset{\approx}{V}(R) - \underset{\approx}{1}E)\psi_\ell(R) = 0 \quad ,$$

where $\psi_\ell(R)$ is the ℓ'th partial wave, R is the internuclear distance,
E the total energy, and ($\hbar = 1$)

$$\underset{\approx}{T} = \underset{\approx}{1}[-(2\mu)^{-1}d^2/dR^2 + \ell(\ell + 1)/2\mu R^2)$$

$$\underset{\approx}{V} = \begin{pmatrix} V_{00} & V_{01} \\ V_{10} & V_{11} \end{pmatrix} \quad ,$$

with $\mu = m_{Na}m_I/(m_{Na} + m_I)$. For the present application, $V_{00}(R)$ may
be considered a covalent Na-I interaction and $V_{11}(R)$ the ionic
Na^+-I^- interaction. In the diabatic representation V_{00} and V_{11} may
cross, but the potential matrix is nondiagonal. Had the adiabatic
representation been employed, a noncrossing rule would hold, $\underset{\approx}{V}$ would
be diagonal, and the coupling terms would be in the kinetic energy[44].

By expanding $\underset{\approx}{V}$ in terms of Pauli spin matirces and then representing
the spin operators in terms of classical action-angle variables, Meyer
and Miller[12c] showed that the corresponding classical analogue of the
matrix Hamiltonian above is

$$H_{cl}(P,R,n,q) = P^2/2\mu + \ell^2/2\mu R^2 + (1-n)V_{00} + nV_{11}$$
$$+ 2V_{01}\sqrt{(n+1/2)(3/2-n)}\cos q \quad . \qquad \text{III-2}$$

The idea now is that the electronic degree of freedom is represented

by the action-angle variables (n,q). A value of n near zero will correspond to mostly covalent states, whereas a value of n near one will correspond to mostly ionic states. (There are other ways of obtaining the classical Hamiltonian[12], but for the two-state model the spin analogy is the simplest.)

C. Classical Trajectories for $Na + I \rightarrow Na^+ + I^-$

The diabatic matrix elements of Faist and Levine[41] were employed in a relatively standard quasiclassical trajectory study[45] with the classical Hamiltonian of eq. III-2. For various fixed centre-of-mass energies E, the initial positions and momenta were taken as $R_o = 160$Å, $P_o = -\sqrt{2\mu E}$, $n_o = 0$, and $q = 2\pi\zeta$, where ζ is a random number between 0 and 1. It was also necessary to average over the orbital angular momentum ℓ, which is related to the classical impact parameter b through $\ell^2 = 2\mu E b^2$. We adopt the usual quasiclassical procedure[45] of choosing b from $b = \sqrt{\zeta'} \, b_{max}$, where ζ' is another random number between 0 and 1. The value of b_{max} must be such that no charge transfers will take place for larger values of b. A value of 9 Å was found satisfactory (initial and final electronic actions were the same to three significant figures). It will be noticed that the initial internuclear separation (the "practical" asymptotic limit) is rather large (160Å). This is because b is typically large for such charge transfer reactions (crudely, one could imagine many charge transfers taking place near the diabatic curves' crossing point of about 7 Å – see, e.g., the "harpoon mechanism"[1]), and thus the centrifugal term $\ell^2/2\mu R^2 = Eb^2/R^2$ can be significant even for seemingly large values of

the internuclear separation R. A standard (variable step-size,

5'th order predictor-corrector) routine was then used to integrate

Hamilton's equations,

$$\dot{P} = - \partial H_{cl}/\partial R$$
$$\dot{n} = - \partial H_{cl}/\partial q$$
$$\dot{R} = \partial H_{cl}/\partial P$$
$$\dot{q} = \partial H_{cl}/\partial n \quad ,$$

with H_{cl} given by eq. III-2, until R was sufficiently large ($\geqslant 15$Å),

and P was positive. A crude 'binning' procedure was used to determine

the cross section for charge transfer. If the final action n_f is

between 1/2 and 3/2, then the trajectory is termed reactive. (There

are better ways of analysing the products, such as the moment method[46].)

The charge transfer cross section is then given by the well-known

Monte-Carlo formula[45],

$$\sigma(E) = \pi b_{max}^2 N_r/N \quad ,$$

where N_r is the number of charge transfers and N the number of

trajectories run at the energy E. The Monte-Carlo error, that is

one standard deviation, is given by[45]

$$\delta\sigma = \sqrt{(N-N_r)/N \cdot N_r} \ \sigma \quad .$$

About 400 trajectories were run at each energy, with the corresponding Monte-Carlo error in the cross sections being about 10%.

The results of the calculations are shown in Fig. 11. For comparison, the essentially exact quantum mechanical results of Faist and Levine[41] are shown as the solid curve. It is clear that the present classical model is qualitatively correct, and somewhat quantitative. It is conceivable, therefore, that the classical analogue approach might be useful for studying more complex charge transfer reactions, such as III-1b and III-1c , where it is difficult to obtain the quantum result.

D. A Semiclassical Model

The encouraging results of the previous section suggest that a semiclassical model, based on the classical analogue Hamiltonian, might be appropriate. We follow here the semiclassical perturbation theory approach of Miller and Smith[47]. The classical analogue Hamiltonian is written as

$$H = H_o + H_1 \quad , \qquad \qquad \text{III-3a}$$

where

$$H_o = P^2/2\mu + \ell^2/2\mu R^2 + (1 - n)V_{00} + nV_{11} \quad , \qquad \text{III-3b}$$

and

$$H_1 = 2\sqrt{(n+1/2)(3/2-n)} \; V_{01}\cos q \quad . \qquad \text{III-3c}$$

The semiclassical S matrix for a transition $n_1 \to n_2$ is then given approximately by[47],[48]

$$S_{n_2 \leftarrow n_1} = (2\pi)^{-1} \int_0^{2\pi} d\bar{q}\; e^{-i\Delta n \bar{q}}\; e^{-iA}, \qquad \text{III-4a}$$

with

$$A = \int_{-\infty}^{\infty} dt\; H_1(t) \quad \text{III-4b}$$

In eq. III-4, $\bar{q}$ is the initial value of the angle variable associated with the electronic action. To find the time dependence of H_1, one assumes that it arises out of the zero-order trajectory determined by eq. III-3b :

$$
\begin{aligned}
\dot{q} &= V_{11} - V_{00} \\
\dot{R} &= \sqrt{2\mu(E - \ell^2/2\mu R^2 - (1-n)V_{00} - nV_{11})}/\mu \\
\dot{n} &= 0 \\
\dot{P} &= \ell^2/\mu R^3 - (1-n)\partial V_{00}/\partial R - n\partial V_{11}/\partial R \quad .
\end{aligned}
\qquad \text{III-5}
$$

The value of n in eq. III-5, which is constant to zero order, is taken as $(n_1 + n_2)/2 = 1/2$. As discussed by Miller and Smith[47], this is one way of symmetrizing the S matrix (but not the only way). The time evolution of q is given by

$$q(t) = \bar{q} + \int_{t_0}^{t} (V_{11} - V_{00})\, dt = \bar{q} + \int_{t_0}^{t} \omega\, dt \quad ,$$

with $\omega = V_{11} - V_{00}$. Inserting this explicit (but approximate) time dependence for $q(t)$ into eq. III-4b, and changing integration variables from t to R ($dt = \mu P^{-1}dR$) results in

$$A = 2\mu[\int_{\infty}^{R_t} V_{01}(\cos\bar{q} \cos \int_{R_t}^{R} P^{-1}\mu\omega dR' - \sin\bar{q} \sin \int_{R_t}^{R} P^{-1}\mu\omega dR')P^{-1} dR$$

$$+ \int_{R_t}^{\infty} V_{01}(\cos\bar{q} \cos \int_{R_t}^{R} P^{-1}\mu\omega dR' - \sin\bar{q} \sin \int_{R_t}^{R} P^{-1}\mu\omega dR')P^{-1}dR] \quad , \quad \text{III-6}$$

where $P = \pm \sqrt{2\mu(E - \ell^2/2\mu R^2 - (V_{00}+V_{11})/2)}$, and R_t is the turning point (R value s.t. P = 0).

In the first integral of eq. III-6, one sets $P < 0$, corresponding to an incoming trajectory, and in the second integral $P > 0$, which corresponds to an outgoing trajectory. This then leads to

$$A = Z \cos\bar{q} \quad , \quad \text{III-7}$$

where

$$Z = 4\mu \int_{R_t}^{\infty} V_{01} \cos \int_{R_t}^{R} P^{-1}\mu\omega \, dR' \, P^{-1}dR \quad . \quad \text{III-8}$$

Eq. III-4a for the S matrix then becomes

$$S_{n_2 \leftarrow n_1} = (2\pi)^{-1} \int_0^{2\pi} d\bar{q} \, e^{-i\Delta n\bar{q}} \, e^{-iZ\cos\bar{q}}$$

$$= J_{\Delta n}(Z) \quad , \quad \text{III-9}$$

where $J_{\Delta n}$ is a regular Bessel function of order Δn. In the case of charge transfer, one has simply

$$P_{1 \leftarrow 0} = |S_{1 \leftarrow 0}|^2 = J_1^2(Z) \quad . \qquad \text{III-10}$$

The argument Z may be evaluated along the zero-order classical trajectory with eq. III-8. Numerical difficulties may arise (since $P = 0$ at $R = R_t$) and it may be best to do the integral directly in the time representation. In this case,

$$Z = 4\int_0^\infty dt \, V_{01}(t) \cos \int_0^t \omega(t') dt' \quad , \qquad \text{III-11}$$

where the zero of time is understood to be the classical turning point R_t. The time dependence of V_{01} and ω arises from eqs. II-5. An even simpler time dependence would be to assume a straight line trajectory so that

$$R(t) = \sqrt{b^2 + (P/\mu)^2 t^2} \quad .$$

To illustrate this model, let us consider the Landau – Zener[49] model,

$$
\begin{aligned}
V_{00} &= -F_0 (R - R_x) \\
V_{11} &= -F_1 (R - R_x) \qquad \text{III-12} \\
V_{01} &= \text{constant} \quad .
\end{aligned}
$$

In addition, it will be assumed that the collision is at zero impact parameter and that the nuclear velocity is constant. The zero-order motion is then

$$
\begin{aligned}
P(t) &= P \\
n(t) &= n = 1/2 \\
R(t) &= Pt/\mu + R_x \\
q(t) &= P(F_o - F_1)t^2/2\mu + \bar{q} \quad ,
\end{aligned}
\qquad \text{III-13}
$$

where $t = 0$ has been chosen to correspond to the crossing point R_x. We now have

$$
H_1(t) = 2V_{01}[\cos\bar{q} \cos P(F_o-F_1)t^2/2\mu - \sin\bar{q} \sin P(F_o-F_1)t^2/2\mu] \quad ,
$$

and thus

$$
A = \int_{-\infty}^{\infty} dt \, H_1(t) = 2V_{01}\sqrt{\pi\mu/P(F_o-F_1)} \; (\cos\bar{q} - \sin\bar{q}) \quad .
$$

The semiclassical S matrix is then given by

$$
S_{n_2 \leftarrow n_1} = (2\pi)^{-1} \int_0^{2\pi} d\bar{q} \; e^{-i\Delta n\bar{q}} \, e^{-iZ(\cos\bar{q} - \sin\bar{q})/\sqrt{2}} \quad ,
$$

with

$$
Z = 2\sqrt{2} \; V_{01}\sqrt{\pi\mu/P(F_o - F_1)} \quad .
$$

50

The probability of a transition then reduces to

$$P_{1 \leftarrow 0} = |S_{1 \leftarrow 0}|^2 = J_1^2(Z) \quad , \qquad\qquad \text{III-14}$$

where the identity

$$J_n(\sqrt{a^2+b^2}) \; e^{in\alpha} \equiv (2\pi)^{-1} \int_0^{2\pi} dx \; e^{i[a \sin x + b \cos x]} \; e^{-inx} \quad ,$$

with $\alpha = \tan^{-1}(b/a)$, has been used.

The correct quantum mechanical result for the Landau-Zener model is[49] $P_{1 \leftarrow 0} = 1 - e^{-Z^2/4}$. It is thus evident that in the limit $Z \to 0$ both the approximate semiclassical result, eq. III-14, and the exact quantum result agree, since then $J_1(Z) \to Z/2$, and both formulae give $P_{1 \leftarrow 0} \to Z^2/4$. Table VII gives a more detailed comparison of the semiclassical and quantum results. For small arguments Z, i.e. large velocities and/or small slope differences (F_0-F_1), the semiclassical result is reasonable. It is interesting to note that it gives better results than both the standard classical trajectory method and primative semiclassical mechanics in this regime (see Ref. 12b for the classical and primative semiclassical results). As might be expected, however, the approach fails for larger arguments Z. In this regime, the semiclassical perturbation theory is inapplicable (even probability conservation, $P_{0 \leftarrow 0} + P_{1 \leftarrow 0} = 1$, breaks down as Z becomes large). In fact, by inspection of eq. III-14, one sees that the maximum value that $P_{1 \leftarrow 0}$ can take on is about 0.35,

since that is about the largest value that J_1^2 can take on. None-theless, for the range $Z \lesssim 1$, the perturbative model does seem adequate. Thus, if one does not have a simple linear approximation to the diabatic matrix elements, so that the Landau-Žener model is not directly applicable, one could perhaps use eqs. III-10 and III-11 to obtain the nonadiabatic transition probabilities in the limit of small arguments Z.

We now apply this semiclassical model to the Na + I problem. One should keep in mind that this should be a rather severe test since the charge transfer probabilities are quite high here and the semi-classical model is really only valid when the probabilities are small. The charge transfer cross section is given by

$$\sigma(E) = 2\pi \int_0^{\infty} b \ db \ P(b) \quad ,$$

with $P(b) = J_1^2(Z)$, with Z given by eq. II-11. The $R(t)$ dependence, in principle, should be obtained by solution of eqs. III-5. However, for the present application we are only concerned with the high energy regime, where the semiclassical model is most valid. In this regime, the simple straight line trajectory approximation should be good, $R(t) = \sqrt{b^2 + (P/\mu)^2 t^2}$.

A simple trapazoidal rule integration was performed over b to obtain σ, and each $Z(b)$ was also obtained by a trapazoidal rule integration of eq. III-11. The result is shown as a dashed line in Fig. 11. As expected, the model is adequate for the very high

energies, but quite poor for the lower energies. For other sorts of two state processes, that occur with lower probabilities, one might expect this model to be more applicable.

E. Concluding Remarks

The success of the classical trajectory analysis of sec. IIIC suggests that the classical analogue might be useful for studying more complex sorts of charge transfers, such as $M + X_2 \rightarrow M^+ + X_2^-$, where M is an alkali atom and X_2 a halogen molecule[40]. These sorts of reactions have been treated with Tully-Preston surface hopping approaches with some success, and it would be interesting to see if the classical analogue would be as useful. It may also be interesting to examine $H^+ + H_2 \rightarrow H_2^+ + H$, which also involves exchange of an atom[42].

The semiclassical perturbation theory of sec. IIID is less generally applicable, since it is only valid in the case of small coupling and transition probabilities (i.e. high energy). However, in this limit it may be useful since, unlike the Landau-Zener model[49], for example, it can be used with any desired forms for the matrix elements V_{00}, V_{11}, and V_{01}.

IV. Classical Aspects of the Laser Excitation of Molecules

A. Overview

With the development of high-powered lasers, physical chemists

have been exploring the nature of multiphoton and overtone absorption

in molecules[50]. There is a growing need for simple theoretical models

to interpret and predict the results of such experiments. However,

the correct theoretical treatment, a detailed solution of the

Schrodinger equation, including the molecule-radiation interaction,

is still out of reach for most systems of chemical interest. Many

theoreticians have thus turned to a classical description of the

process[51], which is at least more tractable. There are then two

obvious questions that must be answered. First, how realistic is

the classical description ? In sec. B we answer this question for a

vibrating and rotating diatomic in a strong laser, since in this case

it is also possible to obtain an accurate quantum solution. The

second question that arises is, given that a classical description is

correct to some extent, what is the nature of such a solution ? We

answer this question in sec. C for a model nonrotating diatomic in

a strong laser by looking carefully at how classical states evolve with

time, using a novel period advance map method[13] to generate the solution.

A very simple model, based on a pendulum[14], is then invoked to explain

many of the classical features, which include spirals in phase space.

B. Classical and Quantum Mechanical Studies of HF in an Intense Laser Field.

B1. Preliminaries

The simplest molecule-laser problem is a diatomic molecule interacting with a strong laser. Accurate, numerical classical and quantum solutions may be obtained for this problem. Because of the small number of quantum states involved, this represents a particularly severe test of classical mechanics. Previously, Walker and Preston[52] have performed both quantum and classical calculations for a model, nonrotating HF molecule. Their results, with laser intensities $\gtrsim 10 \text{TW/cm}^2$ ($1\text{TW} = 10^{12}$ Watts), indicated good agreement between classical and quantum predictions of energy absorption averaged over laser pulse times, except near multiphoton resonances. Various other aspects of the problem of a diatomic interacting with a laser have been examined using either classical[53] or quantum[54] models.

In this section, we examine the detailed behavior of a vibrating and rotating diatomic molecule in an intense laser field, and the validity of classical mechanics to describe this problem. The classical and quantum equations of motion are solved numerically for both rotating and, for comparison, nonrotating models of HF, initially in its ground state. Laser intensities of 1.0 and 2.5 TW/cm^2

are used, with frequencies in the range of the fundamental transition. Energy absorption and transition probabilities are calculated as a function of pulse time, as well as the pulse averaged absorption. Most of the work is for maximum pulse lengths between 0.9 and 2.0 ps (between 100 and 250 optical cycles), although it was necessary to integrate the quantum solution near multiphoton resonances for much longer times. It is found that classical mechanics does not correctly describe the time behavior of the system. Furthermore, classical rotational state distributions are completely incorrect. Classical mechanics, however, does give the correct magnitude of pulse averaged energy absorption. In addition, classical mechanics correctly indicates the presence of increased multiphoton absorption for frequencies lower than the one-photon resonance, although, in agreement with Walker and Preston's results[52], specific resonance peaks are not resolved and only a small amount of multiphoton absorption occurs. The effect of laser phase, which is often neglected, is also studied and found to be only a small effect on the quantum results and little or no effect on the classical results.

B2. Methods

Classical Mechanics

The Hamiltonian for a vibrating and rotating diatomic molecule, with reduced mass μ, in spherical coordinates r, θ and ϕ is

$$H_o = \frac{P_r^2}{2\mu} + \frac{1}{2\mu r^2} (p_\theta^2 + p_\phi^2/\sin^2\theta) + V(r) \quad , \quad \text{IV-1}$$

where p_r, p_θ, and p_ϕ are momenta canonically conjugate to r, θ and φ, and V(r) is the Born–Oppenheimer potential function. In the absence of external fields, there are three conserved quantities which are the vibrational action,

$$N_v = -\frac{\hbar}{2} + \frac{1}{2\pi} \oint p_r dr ,$$

the rotational angular momentum,

$$\sqrt{J(J+\hbar)} = (p_\theta^2 + \frac{p_\phi^2}{\sin^2 \theta})^{\frac{1}{2}} ,$$

and the z projection of the angular momentum $M = p_\phi$. If an oscillating electric field of frequency ω, z polarization, and phase δ is introduced, the Hamiltonian becomes

$$H = H_o - d(r) \cos \theta \, E_o \sin (\omega t + \delta) \quad , \qquad \text{IV-2}$$

where d(r) is the molecular dipole function and E_o is the field strength, which is related to the intensity by[55] $E_o = (8\pi I/c)^{1/2}$. Eq. IV-2 is valid in the limit of high photon density, which is certainly true in the present study. For lower intensities, the classical formalism developed by Miller[56] could be used.

With the interaction present, the vibrational action N_v and rotational angular momentum J are no longer conserved. However, with the present choice of polarization, M is still conserved since H has no φ dependence. The complete classical solution involves

specification of the appropriate initial conditions and solution of Hamilton's equations :

$$\dot{p}_r = -\frac{\partial H}{\partial r} = \frac{1}{\mu r^3} (p_\theta{}^2 + p_\phi{}^2/{}_{\sin^2\theta}) - \frac{\partial V}{\partial r} + \frac{\partial d}{\partial r} \cos \theta \ E_o \ \sin \ (\omega t + \delta)$$

$$\dot{p}_\theta = -\frac{\partial H}{\partial \theta} = p_\phi{}^2/{}_{\mu r^2 \sin^3\theta} - d \ (r) \ \sin \ \theta \ E_o \ \sin \ (\omega t + \delta)$$

$$\dot{r} = \partial H/_{\partial p_r} = p_r/_\mu$$

$$\dot{\theta} = \partial H/_{\partial p_\theta} = p_\theta/_{\mu r^2}$$

IV-3

Approximate analytic orbits have been obtained[57] for a rotating Morse oscillator with no external field, and these are used to determine the diatomic initial conditions (see Appendix B for details). This approximation is excellent for the vibration-rotation states of importance here. The laser phase δ is also averaged over in most cases (i.e. each trajectory has δ chosen randomly between 0 and 2π), although it will be shown to be unimportant.

The energy absorbed as a function of pulse length is defined by

$$<E(t)>_{CL} = \frac{1}{N} \Sigma_{i=1}^N H_o(p_r{}^i(0), p_\theta{}^i(0), r^i(0), \theta^i(0), \delta^i; t) - E_1 \qquad IV-4$$

where N is the number of trajectories and E_1 is the initial molecular energy, which is the present study is the ground state (v=0, j=0) energy.

The final vibrational action N_v after a pulse length t is also calculated with the rotating Morse oscillator approximation[57]. J is calculated directly from $J(J+\hbar) = p_\theta^2 + p_\phi^2/\sin^2\theta$. (Note : $p_\phi = 0$ here since J = 0 initially.) With $\hbar = 1$, N_v and J are boxed according to the nearest integers v,j such that $v-1/2 \leq N_v \leq v+1/2$ and $j-1/2 \leq J \leq j+1/2$, which is the usual quasiclassical quantization procedure. The transition probability into a particular v,j state, as a function of pulse length is

$$P_{v,j}^{CL}(t) = N_{v,j}(t)/N \qquad \qquad \text{IV-5}$$

where $N_{v,j}(t)$ is the number of trajectories at time t with final actions in the v,j box.

Of course, a single trajectory integrated out to some large pulse length T contributes to all intermediate pulse time results. Similar to Walker and Preston[52], the pulse averaged energy as a function of laser frequency ω is defined as

$$\bar{E}_{Cl}\,(\omega) = \frac{1}{T} \int_0^T \left\langle E(t) \right\rangle_{CL} dt \qquad . \qquad \text{IV-6}$$

For comparison, nonrotating calculations were also performed. These calculations were done essentially in the same manner as described by Walker and Preston[52].

More technical details will be discussed later.

Quantum Mechanics

Although Leasure, Milfeld, and Wyatt[54] have developed an efficient means of determining the long time solution, the time scale of interest here is short enough (usually less than 20 ps) that direct integration of the coupled quantum equations is possible.

The total wavefunction is expanded as

$$\Psi_m (r,\theta,\phi,t) = \Sigma_{v,j}\, C_{vjm}(t)\chi_{vjm}(r,\theta,\phi) \qquad \text{IV-7}$$

with

$$\chi_{vjm}(r,\theta,\phi) = R_v(r)\, Y_{jm}(\theta,\phi)/r \quad .$$

The Y_{jm} are spherical harmonics and R_v are Morse eigenfunctions[58]. Strictly speaking, R_v should also depend on j, but in the present problem, with only small values of j being important, such rotational corrections should be small. As in classical mechanics, the z component of the angular momentum, $m\hbar$, is conserved. Since the present study involves j = 0 initially, m is zero throughout. In all subsequent equations m is understood to be zero.

Inserting eq. IV-7 into the time-dependent Schrodinger equation results in the coupled equations

$$i\hbar\,\dot{C}_{vj}(t) = E^o_{vj}\, C_{vj} + \Sigma_{v'j'}\, D_{v'j'vj}\, C_{v'j'}\, E_o \sin(\omega t + \delta) \, , \qquad \text{IV-8}$$

where the E_{vj}^o are eigenvalues of $\hat{H}_o$ and the $D_{v'j'vj}$ are matrix elements

$$D_{v'j'vj} = -\int_0^\infty R_{v'} \, d(r) \, R_v dr \times \begin{cases} \left[\dfrac{(j + 1)^2}{(2j + 1)(2j + 3)} \right]^{\frac{1}{2}}, & j' = j + 1 \\[4mm] \left[\dfrac{j^2}{(2j - 1)(2j + 1)} \right]^{\frac{1}{2}}, & j' = j - 1 \end{cases}$$

. IV-9

It will be shown later, as with the classical results, that the laser phase δ does not appreciably effect the results. For efficiency, the majority of the quantum calculations are made with a fixed δ of $\pi/2$. The coefficients C_{vj} of eq. IV-8 must be complex. Thus, writing $C_{vj} = X_{vj} = i \, Y_{vj}$, one obtains the coupled real equations

$$- \hbar \, \dot{Y}_{vj} = E_{vj}^o X_{vj} + \Sigma_{v'j'} D_{v'j'vj} X_{v'j'} E_o \sin (\omega t + \delta)$$

IV-10

$$\hbar \, \dot{X}_{vj} = E_{vj}^o Y_{vj} + \Sigma_{v'j'} D_{v'j'vj} Y_{v'j'} E_o \sin (\omega t + \delta) .$$

For comparsion with the classical results, we will also be interested in the transition probabilities

$$P_{vj}^{QM}(t) = \left| C_{vj}(t) \right|^2 ,$$

IV-11

the energy absorption

$$\langle E(t) \rangle_{QM} = \Sigma_{vj} \, P_{vj}^{QM}(t) \, E_{vj}^o - E_1 ,$$

IV-12

and the pulse length averaged energy absorption,

$$\overline{E}_{QM}(\omega) = \frac{1}{T} \int_0^T \langle E(t) \rangle_{QM} \, dt \quad . \qquad\qquad \text{IV-13}$$

We also study the nonrotating case in a similar fashion. One may obtain the nonrotating equations by omitting all factors that include j and m in eqs. IV-7 through IV-12.

Computational Details

A Morse potential, $V = D(e^{-\alpha(r-r_e)} - 1)^2$, was used, with the parameters corresponding to HF taken from Ref. 52 : $D = 0.22509$, $\alpha = 1.1741$, and $r_e = 1.7329$ a.u. Since relatively low v states are involved, a linear approximation to the dipole function is satisfactory, $d(r) = d_0 + d_1(r-r_e)$, with[54c] $d_0 = 0.716$ and $d_1 = 0.310$ a.u. (1Debye = 0.39343 a.u.). Some work, in fact, was done with a quadratic form for $d(r)$[53c], and that did not significantly affect out results.

Laser intensities of 1.0 and 2.5 TW/cm^2 were used, which correspond to field strengths E_0 of 0.005338 and 0.008440 a.u., respectively. (1Volt/cm = 1.9447 x 10^{-10} a.u.) The matrix elements $D_{v'j'vj}$ of eq. IV-9 were evaluated numerically, although analytical forms do exist[58]. Some typical elements are $D_{1100} = 0.022$, $D_{2211} = 0.028$ and $D_{2011} = 0.032$ a.u.

For the classical rotating HF calculations, 1000 trajectories with random initial conditions (see Appendix B) were run for most frequencies. Monte-Carlo errors in the quantities of interest were

between 10 and 15 %. For the nonrotating calculations, 50 trajectories were run for each frequency. In this case it is more efficient to increment the vibrational angle variable in a step-wise fashion between 0 and 2π than to pick it randomly. The classical equations of motion were integrated with a standard predictor-corrector routine[59] to either 0.9 or 1.5 ps. The trajectories were back-integrable to four significant figures in all variables. Integration of the classical equations beyond about 1.5 ps is extremely difficult due to the accumulation of error. The integration of oscillatory nonlinear differential equations over long time periods is still a current problem of numerical analysis[60].

By between 0.9 and 1.5 ps, the pulse averaged energy absorption, eq. IV-6, appears to be converging, but has not yet fully converged. However, reasonable estimates of the converged $\bar{E}_{CL}$ can be obtained, since $\langle E(t) \rangle_{CL}$ has either leveled off to some extent or is oscillating with a small amplitude.

The quantum equations of motion, eqs. IV-10, were integrated with the same predictor-corrector routine as the classical equations. An adequate basis set for HF with the intensities and time scale of interest consisted of the first five v and first five j states, i.e. a 25 term expansion. The nonrotating quantum solutions were obtained in a similar fashion, with five v states being sufficient. Most of the quantum solutions were integrated to 2 ps, although when the laser frequency was near a multiphoton resonance, it was necessary to

integrate to times in the 10 to 20 ps range in order to obtain converged pulse time averages. Interestingly, because the quantum equations are linear, it is possible to integrate the 50 coupled quantum equations to times exceeding 20 ps, which is much longer than it is practical to integrate only four nonlinear classical equations.

To aid in the interpretation of the results, Table VIII gives some relevant E_{vj}^{o} levels for HF, calculated with the rotating Morse oscillator formula[57].

B3.   Results and Discussion

The quantum and classical pulse time averaged energy absorption spectra are plotted in Fig. 12a for nonrotating and Fig. 12b for rotating HF, with laser intensity 1.0 TW/cm^2. The plot for nonrotating HF is similar to plots of Walker and Preston[52] for higher intensities . At 1.0 TW/cm^2, though, the quantum structure is more resolved.   The major features are a narrow two-photon resonance at $\bar{\nu} = \omega/2\pi c$ = 3879 cm^{-1} (i.e. the v=0 to v=2 absorption) , and a broad one-photon resonance at $\bar{\nu}$ = 3966 cm^{-1} (the v=0 to v=1 absorption). The classical spectrum shows just one very broad peak with a maximum near 3940 cm^{-1}. While the classical spectrum does not have any quantum structure, examination of the classical state distribution does show the presence of a small amount of two-photon absorption, as the frequency is lowered.   Details of this will be given later .

For rotating HF, the spectra (Fig. 12b) are qualitatively

similar to the nonrotating case. There are three peaks in the

quantum spectrum : one broad peak near $\bar{v} = 4006$ cm^{-1}, which

corresponds to the $(v,j)=(0,0)$ to $(1,1)$ one-photon resonance,

and two narrow peaks near 3937 cm^{-1} and 3879 cm^{-1}, which correspond

to the two-photon resonances $(0,0) \rightarrow (2,2)$ and $(0,0) \rightarrow (2,0)$,

respectively. The classical spectrum has one very broad peak

which actually peaks near the $(0,0) \rightarrow (1,0)$ resonance at 3966 cm^{-1}.

Overall, the classical solution gives a general idea of the absorption.

As in the nonrotating case, the classical result predicts more

two-photon absorption for frequencies red-shifted from the one-

photon resonance, as will be discussed below.

In Fig. 13, the rotating HF average energy absorption for an

intensity of 2.5 TW/cm^2 is shown. Qualitatively, the quantum peaks

become broader and overlap more than the 1.0 TW/cm^2 case. There

appears to be a small power shifting of the resonance peaks toward

higher frequencies (see Ref. 54c for a discussion of this effect),

but this has not been clearly resolved here. Classically, the

absorption also broadens relative to 1.0 TW/cm^2, and the peak

maximum appears to shift to lower frequencies, indicating more multi-

photon absorption.

We now turn to look at the rotationally averaged transition

probabilities (later, we will examine specific v,j probabilities).

Table IX shows the quantum and classical time averaged probabilities

at various frequencies for rotating and nonrotating HF, with laser

intensity I = 1.0 TW/cm^2. Each peak of the quantum solution can be seen to be either a one or a two photon absorption, with both processes observed appreciably only where peaks overlap. At higher intensities the peaks will broaden and overlap more. The classical results do indicate the presence of some two-photon absorption as frequency is decreased. But classically, there is a very gradual change which results in the very broad single peak in the spectrum of Fig. 12, rather than the abrupt changes as in the quantum results.

To show some of the effects of increasing intensity, average probabilities for rotating HF at 2.5 TW/cm^2 are given in Table X. For this larger intensity, both classically and quantum mechanically the excited states become more populated.

We now examine the energy absorption and transition probabilities as a function of time. In Fig. 14, a comparison of classical and quantum energy absorption as a function of time is given for nonrotating HF with $\bar{\nu}$ = 3966 cm^{-1} being the laser frequency, which corresponds to the v = 0 → 1 resonance. The quantum results show oscillations with a period of about 0.75 ps with no sign of damping out to 1.5 ps. At this frequency and intensity (1.0 TW/cm^2) the solution is well approximated by a two level system (i.e. the Rabi model[61a]). In contrast, the classical result oscillates with a frequency of about 0.4 ps and a smaller amplitude. Also, it appears as though the oscillations

may be damping.

Fig. 15 shows the classical and quantum time-dependent energy absorption for rotating HF with $\bar{\nu} = 4006$ cm^{-1}, the one-photon $(0,0) \rightarrow (1,1)$ resonance. The results are similar to those in Fig. 14 for nonrotating HF. In this case, though, the classical result appears to level off even faster. The behavior of the quantum solution is again well approximated by the two level Rabi model[61a]. The quantum solution has been followed for up to 20 ps with no clear sign of damping.

The quantum result for the two-photon resonance at 3937 cm^{-1}, the $(0,0) \rightarrow (2,2)$ resonance, is considerably different (Fig. 16). The complicated nature of the oscillations may be contrasted with the simple Rabi oscillations of Fig. 15. From Fig. 16 it can be seen that the two-photon absorption is a long time process. The corresponding classical result (Fig. 17) also seems to show some aspects of the slower growth in absorption, although the solution is reasonably level by 0.9 ps.

In Figs. 18,19 and 20, plots are shown for some transition probabilities as a function of time, again for I = 1.0 TW/cm^2. Here, the classical solution is actually broken up into rotational levels, so that the discrepancy with quantum mechanics can be seen. The results for $\bar{\nu} = 4006$ cm^{-1} are given in Fig. 18. The quantum solutions for P_{01} and P_{10} are not shown since they are very small ($\leq 10^{-2}$). Qualitatively, the probabilities show the same behavior as the energy absorption, i.e. the classical

solutions tend to level off more and the quantum solutions

appear periodic. Note that in reality there are high frequency,

small amplitude oscillations that are superimposed on the

quantum probabilities, which have not been clearly resolved,

and thus give rise to some roughness, particularly near peak maxima.

The classical probabilities for rotating HF at $\bar{\nu} = 3937$ cm^{-1}

are shown in Fig. 19. It can be seen that the v = 2 state gets

significantly populated, but the v = 1 state is also significantly

populated. The quantum probabilities at this frequency are shown

in Fig. 20. The resonant probability $P_{22}(t)$ displays a long

period which essentially matches that of the energy absorption in

Fig. 16. Another reasonably significant probability is P_{11}, which

is not shown. $P_{11}(t)$ displays higher frequency oscillations that

can reach a maximum of about 0.13. The other two-photon resonance,

at 3879 cm^{-1}, is not shown here. Qualitatively, the classical

results for this frequency show much less excitation than for 3937

cm^{-1}. There is a small amount of v = 1 excitation and no v = 2

excitation. Essentially no rotational excitation is seen in the

classical results for this frequency. The quantum results for 3879

cm^{-1} show somewhat less excitation into the (1,1) state than for

3937 cm^{-1}, and again the resonant probability, P_{20}, displays a

long period.

Finally, we turn now to the effect of laser phase. Based

on the classical and quantum equations of motion, eqs. IV-3 and

IV-8, without additional approximations, one would expect the

solutions to be dependent on the choice of laser phase δ.

Without allowing for the details of how the field is turned on,

a complete study should involve averaging over the laser phase to

obtain the most meaningful results[62].

The laser phase dependence, however, disappears from the

quantum equations in the rotating wave approximation[61], as has

been recently shown[63]. However, for sufficiently large field

strengths or de-tuning of ω from resonance, the rotating wave

approximation will breakdown[61c]. Thus, for example, Moloney and

Meath[62] have shown the laser phase dependence of probabilities

as a function of time for a two state model. They found

increasing phase effects for larger field strengths and at

multiphoton resonances.

The situation is not quite as clear in the classical analysis.

However, if only the relative difference between the laser phase

and vibrational phase is important, then it would be sufficient to

average over only the vibrational phase, without averaging over

the laser phase, i.e. the laser phase would not matter. The

conditions for this to be true probably include that ω be close

to resonance.

To assess the effect of laser phase δ on the present problem,

consider first nonrotating HF. For an intensity of 1.0 TW/cm^2 and

frequencies of 3966 cm^{-1} and 3879 cm^{-1}, the classical solutions

were obtained for fixed δ of 0 and $\pi/2$. 500 trajectories were run

for each solution to ensure no statistical error. Over the entire 1.5 ps range, the energy absorption as a function of time for the two phases agreed to between 2 and 4 significant figures. The quasiclassical probabilities were also in excellent agreement. Similarly, the nonrotating quantum results for the same conditions showed very little phase dependence.

We also examined rotating HF at 1.0 TW/cm^2 for the possibility of phase effects. Within the Monte-Carlo error, no clear phase effect can be distinguished in the classical results. However, slight discrepancies in the time-dependent quantum solutions may be seen, since no statistical error is present. Table XI lists some relevant probabilities and $\langle E(t) \rangle_{QM}$ for $\delta = 0$ and $\pi/2$, at $\bar{v} = 4006$ cm^{-1}. Other phases were also examined, but the largest differences were between these two phases. Despite the laser frequency being almost exactly on resonance, slight differences may be noted, particularly in the probabilities. These differences become larger near peak maxima and can be as much as 4 %. However, such differences are comparable in amplitude to the high frequency oscillations that are superimposed on the Rabi oscillations, and do not appreciably effect the overall behavior. Table XII presents similar results for $\bar{v} = 3937$ cm^{-1}. Although this is a two-photon resonance, the discrepancies due to laser phase are comparable to the $\bar{v} = 4006$ cm^{-1} results. Thus, for intensities ~ 1.0 TW/cm^2, and the present frequency range, the effect of laser phase is small and can be neglected for most

practical purposes.

B4. Summary

The detailed dynamics of both rotating and nonrotating models for HF in an intense laser field has been investigated with both classical and quantum mechanics.

It is found that classical mechanics does not predict the correct rotational state distributions. Also, the time behavior of the classical solution can be qualitatively different from the quantum one. Classical mechanics does give the correct magnitude of pulse averaged quantities, such as the average energy absorption, but does not give the detailed resonance peaks for multiphoton absorptions. Classical mechanics does correctly indicate the presence of increased multiphoton absorption as the frequency is red-shifted from the one-photon resonance, but it predicts far too little such absorption.

The laser phase has clearly been shown to be unimportant for the intensities and frequencies studied here, but could conceivably be important for other parameter ranges.

It is difficult to extend these conclusions to polyatomic systems in intense lasers, which are of greater interest. These results do indicate that some care should be taken when classical mechanics is applied to molecular systems. There is the possibility, however, that the increased number of states in a polyatomic could make   classical mechanics a better approximation to quantum mechanics than for the present case of a diatomic. The same may be true for a diatomic initially in anexcited state, or in a more intense field, where more states may become populated.

C. The Period Advance Map and the Simple Pendulum Model

C1. Preliminaries

In sec. B it was remarked that classical mechanics is sometimes used in the theoretical description of laser-molecule processes[51]. Although some important cautionary notes were given, particularly with regard to the fine details of the absorption, classical mechanics does describe many features of the absorption in a qualitatively correct manner. Moreover, as the number of degrees of freedom is increased, or as the intensity is raised, it is expected that classical mechanics would provide a better description.

Given that a classical description of molecular energy absorption is to some extent correct, there is still a need to understand more clearly the nature of this description. Most classical trajectory studies, such as those described in sec. B, are essentially numerical experiments, involving the solution of many coupled nonlinear differential equations. There is a need to understand how and why a solution comes out as it does and, moreover, to build more general models of the process that do not require any detailed numerical calculations.

In this section, the simplest model of a laser induced process, the excitation of a nonrotating diatomic molecule in an intense laser, is examined classically in some detail. First, a new approach to the solution, based on generating a map from

initial conditions to the solution after one period of oscillation

of the laser, is presented. Repeated applications of this period

advance map[13] then allow the solution over many periods of

oscillation to be obtained with relative ease. The behavior

of the solution, as a function of time, or the number of

oscillations of the laser field, is found to be quite interesting,

with spirals or "whorls" developing in phase space. Such

behavior has been discussed by Berry and co-workers[64] for simpler

maps, and can be related to some elementary properties of the

period advance map. We then go on to show that a very simple

model, due primarily to Chirikov[14], and based on the orbits of

a pendulum, is capable of describing this behavior reasonably

well. The pendulum model is found to be a useful tool for

understanding other features of the absorption, such as certain

trends in the average energy absorption as a function of initial

vibrational state of the molecule.

In sec. C2, the period advance map and its generation are

discussed. Sec. C3 applies the method to the problem of a

nonrotating HF molecule in an intense (1 TW/cm^2) laser field.

Sec. C4 uses the pendulum model to interpret the results of

sec. C3, and sec. C5 discusses energy absorption trends in

a qualitative fashion with the pendulum model. Finally, in

sec. C6, some brief concluding remarks are given.

C2. The Period Advance Map

Consider a one-dimensional nonlinear oscillator, driven by a periodic force $f(x,t) = f(x,t + \tau)$. The Hamiltonian is written

$$H(p,x,t) = p^2/2\mu + V(x) + f(x,t) \quad , \qquad \text{IV-14}$$

where p and x are the canonically conjugate momentum and position, μ is the mass, and V(x) is the unperturbed potential function. Hamilton's equations are periodic in time and read

$$\dot{p}(t) = - \partial H/\partial x = \dot{p}(t + \tau)$$
$$\dot{x}(t) = \partial H/\partial p = \dot{x}(t + \tau). \qquad \text{IV-15}$$

In many applications, such as those in Ref. 51, the periodicity of eqs. IV-15 is not used as a practical simplification. Rather, a direct numerical integration, for each trajectory in a given ensemble, is performed over many periods τ of the driving force. If eqs. IV-15 were linear, however, Floquet analysis[54,65] does allow one to make effective use of the periodicity. Moreover, in the quantum analogue of the problem, because the differential equations for the coefficients of the wavefunction are always linear, even when the corresponding classical equations are nonlinear, the periodicity again simplifies the calculations[52,54]. It was the apparent lack of a practical scheme, making use of the periodicity of the nonlinear classical equations, that was the

original motivation for this work.

The approach taken here is based on the period advance map[13], which

maps initial conditions (p_o, x_o) to the corresponding solution at $t = \tau$,

(p_τ, x_τ) :

$$(p_\tau, x_\tau) = T(p_o, x_o) \quad . \qquad\qquad \text{IV-16}$$

An elementary property of the periodicity of eqs. IV-15 is that once the

solution over the first period is known, then it is known for all

subsequent period advances by repeatedly applying the map :

$$(p_{r\tau}, x_{r\tau}) = T^r(p_o, x_o), \quad r = 1, 2, 3, \ldots \qquad \text{IV-17}$$

In addition to the useful and practical property IV-17, it is a

straightforward consequence of Liouville's theorem that T is an

area preserving map[13].

A functional representation of eq. IV-16 is

$$T_p(p_o, x_o) = p_\tau$$

$$T_x(p_o, x_o) = x_\tau \qquad , \qquad\qquad \text{IV-18}$$

where T_p and T_x are two-dimensional functions spanning the relevant

phase space. To obtain approximations to T_p and T_x, one may simply

define a grid of initial conditions (p_o^i, x_o^j) and for each grid point (i,j)

numerically integrate over one period of the motion to obtain T_p^{ij} and T_x^{ij}. Any appropriate two-dimensional fitting function may be used to define the approximations to T_p and T_x. Of course to obtain accurate approximations, a dense grid of initial points, such as a 100 x 100 grid, must be used. However, the numerical integration of even a very dense grid over only one period of the driving force is usually a very quick and easy task. Furthermore, once T has been satisfactorily determined, the solution over many periods of oscillation is known from eq. IV-17.

In the calculations reported below, use was made of two-dimensional cubic spline functions to define T_p and T_x. The advantage of using splines is that they pass uniquely through all the data points, and can be shown to have desirable minimum curvature properties[66a]. A cubic spline is a piecewise continuous interpolating polyanomial with continuous first and second derivatives. A possible disadvantage of using splines is then that higher order derivatives may not be continuous. However, no problems were encountered in the present application. The explicit algorithm used here is that of Ref. 66b, with the one-dimensional splines required by this algorithm chosen to be the natural cubic splines of Ref. 66a.

C3. Application to a Diatomic in an Intense Laser

Action-Angle Variables

Frequent use will be made of the Morse oscillator action-angle variables, so it is convenient to define them here. The Hamiltonian for a Morse oscillator, in the absence of any driving force, is

$$H_o(p,x) = p^2/2\mu + D(e^{-\alpha x}-1)^2 \quad , \qquad \text{IV-19}$$

where D is the dissociation energy, and α is a positive constant related to the curvature of the potential. For convenience, x has been taken to be the displacement from equilibrium. It is possible to change variables from (p,x) to action-angle variables (n,q) such that $H_o = H_o(n)$, i.e. the new Hamiltonian is a function of the action n only. Rankin and Miller[67] have done this for the Morse oscillator, with the result

$$H_o(n) = (n + \hbar/2)\omega_o - (n + \hbar/2)^2\omega_o^2/4D \quad , \qquad \text{IV-20}$$

where $\omega_o = \sqrt{2D\alpha^2/\mu}$. The unperturbed motion is then given by $\dot{n} = 0$, and $\dot{q} = \omega(n)$, where the oscillator frequency is

$$\omega(n) = \partial H_o/\partial n = \omega_o - (n + \hbar/2)\omega_o^2/2D \quad . \qquad \text{IV-21}$$

The old variables (p,x) are related to the new variables (n,q) by

$$x(n,q) = \alpha^{-1} \ln[\ (D + \sqrt{DH_o(n)} \ \cos q)/(D - H_o(n))]$$

$$p(n,q) = \mu\omega(n)\partial x/\partial q$$

$$= -\mu\alpha^{-1}[\ \omega_o - (n + \hbar/2)\omega_o^2/2D \ ] \frac{\sqrt{DH_o} \ \sin q}{(D + \sqrt{DH_o} \ \cos q)}$$

IV-22

The phase convention in eqs. IV-22 has been chosen so that $q = 0$ is an outer turning point and $q = \pi$ is an inner turning point.

It should be noted that n corresponds closely with the vibrational quantum number v. Thus if one replaces n with $v\hbar$, $v = 0,1,\ldots$, eq. IV-20 gives the correct energy eigenvalue formula for the Morse oscillator. We use atomic units ($\hbar = 1$) throughout, so that classically n can take on any value $\geqslant -1/2$ and $0 \leq q \leq 2\pi$.

Generating the Period Advance Map

To mimic a nonrotating HF molecule in a strong laser, a Morse potential was used with a driving force linear in x (i.e. the linear dipole approximation),

$$H(p,x,t) = p^2/2\mu + D(\ e^{-\alpha x} - 1 \ )^2 - \epsilon x \ \cos\Omega t,$$

IV-23

with $\epsilon = \sqrt{8\pi I/c} \, d_1$, where I is the laser intensity, c the speed of light, and d_1 the slope of the dipole. For HF, as before, we have[52] $D = 0.22509$, $\alpha = 1.1741$ and $\mu = 1744.8$ a.u. With[54] $d_1 = 0.3099$ a.u., $\epsilon = 0.00165$ a.u. for a 1 TW/cm^2 laser intensity. The laser frequency was taken to be the fundamental transiton frequency, i.e. $\Omega = H_o(1) - H_o(0) = 0.01807$ a.u. The period is then $\tau = 2\pi/\Omega = 347.7$ a.u. (or 0.00841 ps).

The period advance map was then obtained by the method described in sec. C2. A suitable grid for the present purposes was a 100 x 100 grid with x_o and p_o evenly spaced between $-0.3573 \le x_o \le 0.6274$ and $-14.61 \le p_o \le 14.61$. These limiting values allow for excitations up to $n = 3$. As a check on the accuracy of the map so obtained, comparsion was made with trajectories that were directly integrated over r periods of the driving force. In Table XIII is shown the root mean square deviations of the predicted $p_{r\tau}, x_{r\tau}$ values from the map and the directly integrated trajectories for an ensemble of 50 trajectories with $n = 0$ initially and q evenly spaced between 0 and 2π. The map is seen to be accurate over the first few hundred periods. However, the numerical interpolation error builds up, particularly in $p_{r\tau}$, as r increases, and the map cannot be expected to be very accurate beyond $r \sim 400$. This error could be improved, of course, if a finer grid, particularly in p_o, were used, but the present form is sufficient for our purposes.

It should be noted that although it was necessary to integrate numerically 10,000 trajectories over one period of the driving force, the resulting map contains information that would be much more difficult to obtain by direct integrations over many periods of oscillation. For example, the behavior of the entire phase plane will be examined below with the map.

Repeated Iterations of the Map

If one takes some initial set of (p,x) points and repeatedly maps them, plotting each mapped point, one obtains the surface of section plot shown in Fig. 21a. Points on each curve labeled A through E will, upon successive mappings (or periods of oscillation), yield points on the same curve. Thus, for example, if one starts with some point on curve C, it will, upon repeated mappings, travel counterclockwise around C in uneven but discrete jumps. The period 1 fixed points, i.e. those points satisfying (p,x) = T(p,x), lie, by the symmetry of the underlying Hamiltonian, on the x axis. These points are classified as being stable elliptic (o in Fig. 21) or unstable hyperbolic(•) fixed points depending on whether mapped points, in a small region about each fixed point, fall on closed ellipses or open hyperbolas. The elliptic or hyperbolic nature of each fixed point was also verified by a linearization of the map about each fixed point[68]. With T defined in terms of the cubic splines, the required derivatives could be obtained analytically.

As a check on the accuracy of the map, the fixed points were also found by direct integrations of trajectories and agreed, to six significant figures, with the map predictions. Incidentally, there is one more fixed point, that lies at $x = \infty$, so that the total number of fixed points is even, as would be expected[68]. There are also higher order fixed points, $(p,x) = T^s(p,x)$, $s > 1$, which will be mentioned later on.

Also, the approximate positions of the period 1 fixed points can be predicted remarkably well with some simple arguments given in Appendix C.

It may appear, from Fig. 21a, that the motion is quite complicated. However, if one plots the curves in action-angle space, with n and q as defined previously, one obtains Fig. 21b. The curves in (n,q) space bear a close resemblance to orbits of a simple pendulum[14,69]. In fact, this analogy will be made more clear in sec. C4. By symmetry, the three relevant fixed points now lie at either q = 0 or q = π. The two most important of these points are (n,q) = (0.61726, π), which is stable, and (0.36030, 0), which is unstable. Notice that these points have action values near n = 1/2, which is the action where the molecular frequency is in resonance with the laser frequency ($\omega(1/2) = \Omega$). The other fixed point, which lies at (-0.48206, 0), and is stable, corresponds to the molecule having practically no energy. Some orbits, very near this point, must close around it. However, this occurs only in a very small region and most orbits , even for n values as small as -0.4, appear as "rotations" (e.g. curve E in Fig. 21b). We will not concern ourselves with the region very close to this point.

As a final point on the surface of section plots, no "chaotic" regions were noticable with the present perturbation strength ϵ. Of course these regions do exist,[14] particularly near the separatrix curves B and D, which are the sets of points which eminate from and approach the unstable fixed point, but are small in area and difficult to see on the scale of the plots.

It is of interest to see how a line in action-angle space, which corresponds to an initial classical vibrational state, behaves under the mapping. In Fig. 22 is shown the result of mapping points that lie initially on a line in (n,q) space with $n_0 = 1/2$ and q_0 between 0 and 2π. It is seen that the line distorts into quite a remarkable structure. Spirals or whorls develop near the stable fixed point (o). Although not shown here, even more applications of the map results in the whorls winding more and more about the stable fixed point. The behavior near the unstable fixed point (•) is also interesting. Initially no point lies on the unstable fixed point, but very quickly under the mapping points begin to approach it closely. Fig. 23 shows the results of mapping points that lie initially on lines with $n_0 = 0$ and 1. The behavior of these initial states is similar to $n_0 = 1/2$, with, for example, whorls again evolving about the stable fixed point.

Berry and co-workers[64] have considered the fate of curves under mappings. They expect to see whorls near stable fixed points, which indeed are observed here. In the next section, this behavior will be seen to also arise out of the pendulum analogy[14]. Berry and co-workers[64] also predict "tendrils", or chaotic and snake-like convolutions, to develop near the unstable fixed point. Tendrils are not observed here. The reason that the tendrils are hard to see is that they are associated with the chaotic motion near the separatrix. As we have already noted, this region is quite small here, so that tendrils are not evident on the scale of Figs. 22 and 23. However,

if one expanded the scale, and looked very carefully, tendrils may be evident.

Another interesting manifestation of the whorls is evident in a coarse-grained glance at the entire phase plane evolving under the map. Consider dividing the initial phase space into, say, a 120 x 120 grid of points with $-1/2 \leq n_o \leq 5/2$, and $0 \leq q \leq 2\pi$. Each point of this grid is then mapped and the resulting new action at time $r\tau$, $n_{r\tau}(n_o, q_o)$, is plotted in a coarse-grained fashion. If $n_{r\tau}$ is between $-1/2$ and $1/2$, corresponding to a crude $n = 0$ state, white coloring is used. If $n_{r\tau}$ is between $1/2$ and $3/2$, corresponding to an $n = 1$ state, grey coloring is used. If $n_{r\tau}$ is between $3/2$ and $5/2$, an $n = 2$ state, diagonal lines are used. Finally, if $n_{r\tau}$ is between $5/2$ and $7/2$, an $n = 3$ state, dots are used. At time zero (i.e. $r = 0$), one has simply rectangular blocks with white on bottom, grey on top of the white, and diagonal lines on top of the grey. After 20 periods of oscillation of the laser, one obtains Fig. 24a, which shows a developing whorl in the $n = 1/2$ resonance region. Notice that the axes in Fig. 24 are always the initial action and angle variables, and the coloring represents the coarse-grained action at time $r\tau$ that evolved from those initial conditions. After 40 and 60 oscillations one obtains Figs. 24b and 24c, with the whorl winding more tightly in the resonance region. Although not shown here, this has been followed for up to 400 periods of the driving force, with the whorls winding tighter and tighter, representing very graphically how molecules absorb and emit

energy in the vicinity of a resonance.

C4. The Pendulum Model

The remarkable similarity of the surface of section plot Fig. 21b and the pendulum phase plane orbits[14,69] can be made more concrete. In fact, Chirikov[14] has developed a theory of classical resonance based on this analogy. Here, similar ideas are applied to the forced Morse oscillator problem of sec. C3.

Derivation of the Pendulum Hamiltonian

In action-angle variables, the full Hamiltonian is

$$H(n,q,t) = H_o(n) - \epsilon x(n,q) \cos\Omega t \quad . \qquad \text{IV-24}$$

In our problem, $x(n,q)$, defined by eq. IV-22, is an even function of q so that the perturbation may be expanded in a cosine Fourier series with the result

$$x(n,q) \cos\Omega t = \sum_{k=o}^{\infty} V_k(n) \ [\ \cos(kq - \Omega t) + \cos(kq + \Omega t) \ ] \ , \qquad \text{IV-25}$$

where

$$V_k(n) = (2\pi)^{-1} \int_{-\pi}^{\pi} dq \ x(n,q) \ \cos kq \quad . \qquad \text{IV-26a}$$

The integral of eq. IV-26a may be evaluated analytically[70] for $x(n,q)$ given by eq. IV-22, to yield explicit expressions for the Fourier coefficients,

$$V_k(n) = - d^{-k}/\alpha k \quad , \quad k \neq 0$$

$$V_o(n) = \alpha^{-1} \ln \left(- \sqrt{H_o/D} \, d/2 \right) \quad , \qquad \text{IV-26b}$$

where $d = - \sqrt{D/H_o} \left(1 + \sqrt{1 - H_o/D} \right)$.

Now the important terms in the expansion of eq. IV-25 are those with slowly varying arguments. If one is looking at a region of phase space with the action n near n_1, the primary resonance defined by

$$\omega(n_1) - \Omega = 0 \quad , \qquad \text{IV-27}$$

where $\omega(n)$ is the oscillator frequency given by eq. IV-21, then the term $q - \Omega t$ is slowly varying, since $\dot{q} - \Omega \approx \omega(n_1) - \Omega = 0$. Thus one may keep only the relevant (k=1 is eq. IV-25) term in the Fourier expansion, which results in the approximate Hamiltonian, valid near $n = n_1$, of

$$H(n,q,t) \approx H_o(n) - \varepsilon V_1(n) \cos(q - \Omega t) \quad , \qquad \text{IV-28}$$

where the $\cos(q + \Omega t)$ term has also been assumed very oscillatory and neglected. Next, one transforms to a new angle variable $\hat{q} = q - \Omega t$, which corresponds to the difference between molecular and laser phases. This may be accomplished with a generator[14,69] $F_3(n,\hat{q},t) = -(n-n_1)(\hat{q}+\Omega t)$, which implicitly defines the new variables $\hat{p}$ and $\hat{q}$ through $\hat{n} = -\partial F_3/\partial \hat{q}$ and $q = -\partial F_3/\partial n$. This results in $\hat{p} = n-n_1$, $\hat{q} = q - \Omega t$, and the new Hamiltonian

$$
\begin{aligned}
K &= H(\hat{p},\hat{q},t) + \partial F_3/\partial t \\
&= H_o(\hat{p} + n_1) - \varepsilon V_1(\hat{p} + n_1) \cos\hat{q} - \hat{p}\Omega \quad .
\end{aligned}
\qquad \text{IV-29}
$$

The final step is to expand H_o about $\hat{p} = 0$ (i.e. $n = n_1$) to quadratic order and V_1 to zero order. Since H_o is already quadratic in n (see eq. IV-20), the expansion of H_o is exact here. The result is

$$
K - H_o(n_1) = \hat{p}^2/2M_1 - \varepsilon V_1(n_1) \cos\hat{q} \quad ,
\qquad \text{IV-30}
$$

where $M_1^{-1} = (\partial \omega/\partial n)_{n_1}$. Eq. IV-30 is the Hamiltonian for a pendulum of mass M_1, which for the Morse oscillator, from eq. IV-21, is

$$
M_1 = - 2D/\omega_o^2 < 0 \quad .
$$

To make the connection with the more familiar positive mass pendulum orbits, one may note that the equations of motion consistent with eq. IV-30,

$$\dot{\hat{p}} = -\partial K/\partial \hat{q} = -\varepsilon V_1(n_1) \sin\hat{q}$$

$$\dot{\hat{q}} = \partial K/\partial \hat{p} = \hat{p}/M_1 \qquad ,$$

are the same as

$$\dot{\hat{p}} = \varepsilon V_1(n_1) \sin\hat{\theta}$$

$$\dot{\hat{\theta}} = \hat{p}/m_1 \qquad , \qquad\qquad\qquad \text{IV-31}$$

with $\hat{\theta} = -\hat{q}$ and $m_1 = -M_1 > 0$. But eqs. IV-31 are consistent with the Hamiltonian

$$K' = \hat{p}^2/2m_1 + \varepsilon V_1(n_1) \cos\hat{\theta} \qquad , \qquad\qquad \text{IV-32}$$

where $(\hat{p},\hat{\theta})$ are the conjugate variables. Thus the well known pendulum orbits[14] $\hat{p}(t),\hat{\theta}(t)$ will determine the approximate motion of a forced Morse oscillator when the action is close to n_1 through $n(t) = \hat{p}(t) + n_1$, and $q(t) = \Omega t - \hat{\theta}(t)$.

The separatrix associated with eq. IV-32 will have maximum and minimum values of action for $\hat{\theta} = \pi$ and $K' = \varepsilon V_1$, if $V_1 > 0$. If $V_1 < 0$, then they occur for $\hat{\theta} = 0$. In either case, the maximum and minimum separatrix actions may be obtained, in terms of the original Morse action variable, from

$$n_1^{\pm} = n_1 \pm 2\sqrt{\varepsilon |V_1| m_1} \qquad . \qquad\qquad \text{IV-33}$$

A similar analysis may be made about other resonances. For example, the next resonance corresponds to an "overtone" resonance, $2\omega(n_2) - \Omega = 0$. In this region of action space, $2q - \Omega t$ is slowly varying so that the $k=2$ Fourier term in eq. IV-25 may be singled out. The same analysis as above, but with a classical generator of the form $F_3(n,\hat{q},t) = - (n-n_2)(\hat{q} + \Omega t)/2$, yields

$$K_2' = \hat{p}^2/2m_2 + \varepsilon V_2(n_2) \cos\hat{\theta} \quad ,$$

where now $\hat{p} = (n-n_2)/2$, $\hat{\theta} = \Omega t - 2q$, and $m_2^{-1} = 4|\partial\omega/\partial n|_{n_2}$. The fixed points associated with the n_2 resonance are actually period 2 fixed points of the period advance map. The maximum and minimum separatrix action values, in the original Morse action, are

$$n_2^{\pm} = n_2 \pm 4\sqrt{\varepsilon|V_2|m_2} \quad . \qquad\qquad \text{IV-34}$$

In order for the pendulum model to be valid, the neglected terms in the Fourier expansion must indeed be rapidly oscillating compared to the terms kept. Chirikov[14] has shown that a condition for this to be so is the condition of moderate nonlinearity,

$$\varepsilon \ll \alpha_r = |\partial\omega/\partial n| \, \omega/n \ll 1/\varepsilon \quad . \qquad\qquad \text{IV-35}$$

It is also necessary that the separatrices associated with, say, the primary resonance n_1 and the next resonance n_2, do not overlap much –

i.e. are well separated from each other. Chirikov[14] defines the

coupling constant of the resonances, s, such that if

$$s = \Delta\omega/\Delta \lesssim 1 \quad , \qquad\qquad \text{IV-36}$$

then the relevant resonances are sufficiently separated from one

another. In eq. IV-36, $\Delta\omega$ could be the frequency full width of the

separatrix of the primary resonance, $\Delta\omega = |\partial\omega/\partial n| \; (n_1^+ - n_1^-) = 4\sqrt{\varepsilon|V_1|/m_1}$,

and Δ the difference between the primary resonance frequency $\omega(n_1)$ and

the next resonance frequency $\omega(n_2)$. If $s \gtrsim 1$, then the overlap of

resonances is associated with chaotic behavior in the vicinity of

the separatrices[14].

Pendulum Approximation to Nonrotating HF in a Strong Laser

For the problem of sec. C3, it is readily found that $n_1 = 1/2$,

$m_1 = 1266$, and $\varepsilon V_1(n_1) \approx 2.04 \times 10^{-4}$, using the formulae given above.

The moderate nonlinearity condition, eq. IV-35, is also found to be

satisfied, since then $\varepsilon \sim 0.002$, and near $n_1 = 1/2$, $\alpha_r \sim 0.02$. The

resonance coupling constant s also satisfies eq. IV-36, since the

next resonance is $n_2 \approx 12$, and is thus well separated from n_1 ($s \lesssim 10^{-1}$).

From the above considerations, one expects that the pendulum

model will be reasonably adequate. Indeed, if one uses eq. IV-33 to

estimate the maximum and minimum separatrix action values, one finds

$n_1^+ = 1.5$ and $n_1^- = -0.5$, in reasonable agreement with the actual values,

which from Fig. 21b are closer to 1.6 and -0.35.

The fixed points of the pendulum described by eq. IV-32, when
converted back to the original action-angle variables, occur at
$(n,q) = (1/2, \pi)$ and $(1/2,0)$, and are stable and unstable respectively.
These fixed points agree reasonably well with the two most important
fixed points of the problem discussed in sec. C3 . The pendulum model
does not have the additional fixed point, near $n = -1/2$, that occurs
in the full problem. However, the immdeiate region near this point
is of no concern to us here, and, furthermore, the pendulum orbits
do actually describe the motion near (but not very near) this point
reasonably well, as might be guessed from inspection of Fig. 21b.

The pendulum equations of motion, eqs. IV-31, were solved
numerically, since although analytical solutions do exist, in terms of
elliptic integrals[14,65], they are somewhat cubersome to use. Fig. 25
shows the result of following the behavior of classical states with
$n_o = 1/2$, 0 and 1, just as was done in sec. C3 . By comparison
with Figs. 22-23 for the full problem, it is seen that the major
qualitative features of the dynamics, including the whorls, arise
out of the pendulum equations of motion. It will also be noticed
from Fig. 25 that there is an artifact in the pendulum solution in
that the action is now no longer bounded from below. Thus some points
actually map to below $n = -1/2$, which is nonphysical since n for the
Morse oscillator is only defined for $n \gtrsim -1/2$.

Tendrils are absent entirely, even under very close scrutiny,
because no chaotic trajectories exist in the pendulum phase space.
The fact that they are also difficult to see in the full problem is

related to the smallness of the resonance coupling parameter s.

It is also easy to see why points, initially not on or extremely close to the unstable fixed point will eventually approach it closely. If one starts with an initial line in (n,q) space, which is also a line in the pendulum phase space $(\hat{p}, \hat{\theta})$, then as long as $\hat{p} = n - n_1$ is within the width of the separatrix, the line must intersect the separatrix twice. Points on the separatrix will tend to move towards an unstable fixed point, or, equivalently, away from another unstable fixed point (cf. curves B and D in Fig. 21b), but never actually reach the unstable fixed point in finite time. Thus, since all the values of n_0 studied are within the separatrix width, necessarily points intersect the separatrix and then approach the unstable fixed point.

The origin of the whorls can be seen in terms of the nonlinearity of the pendulum equations of motion. Because each orbit about the stable fixed point has a different frequency, or rotation number[64,68], a line that intersects these orbits will then wind about the fixed point, with different points winding faster than other points, thus forming a whorl.

C5. Energy Absorption Trends

In this section, the pendulum model of sec. C4 is used to predict qualitative trends in the average energy absorption[53c] of diatomic molecules initially in different vibrational states. Suppose, for

example, one has an initial classical state with n_o fixed and q_o evenly

distributed between 0 and 2π. This corresponds to a horrizontal line

across Fig. 21b. Now each point on the line will evolve, following the

pendulum-like surface of section lines in the figure. Rather than

follow this motion explictly, either by the period advance map, or by

direct integration of trajectories, one can use the pendulum model

to predict in advance whether there will be a net gain or loss of

energy. Suppose n_o lies between the minimum separatrix action n_1^-

and the primary resonance action n_1. Then a substantial number of

points on the initial line will follow elliptic closed orbits about

n_1. But these points then spend most of their time above n_o, since

$n_o < n_1$, which results in a net gain of energy (recall n is a measure of

the energy - eq.IV-20). Conversely, if n_o lies between n_1 and n_1^+,

the maximum in the primary separatrix action, then again the points

will orbit about n_1, but spend most of their time below n_o, resulting

in a net energy loss. If n_o is outside the separatrices, then the

points will simply rotate up and down (as in curve A of Fig. 21b), and,

other things being equal, will not gain or lose much energy. However,

if n_o is increased to within the separatrix corresponding to the next

resonance, i.e. the overtone resonance n_2, there will again be a net

energy gain if n_o is between n_2^- and n_2, and a net energy loss if n_o

is between n_2 and n_2^+.

Recently, Christoffel and Bowman[53c] have looked at the net energy

absorption of nonrotating HF molecules as a function of initial

vibrational action using classical trajectories. They used a larger

perturbation strength than that of secs. C3 and C4 , $\varepsilon \approx 0.011$, and a

slightly different laser frequency, $\Omega = 0.01787$ a.u. The primary

resonance is found from eq. IV-27 to be $n_1 = 0.752$. From eq. IV-33,

the minimum and maximum separatrix actions are $n_1^- = -2.0$ and $n_1^+ = 3.5$.

An action of -2 is nonphysical, but is irrelevant for the arguments that

follow. Similarly, the overtone resonance is found from $2\omega(n_2) - \Omega = 0$,

and is $n_2 = 12.06$. From eq. IV-34 the associated action extrema are

$n_2^- = 9.1$ and $n_2^+ = 15.0$. Rounding off crudely, one would expect

initial actions n_o between 0 and 1 to have a net energy gain, 1 and 4

to have a net energy loss, 4 and 9 to neither gain nor lose much

energy, and once again increased absorption for n_o between 9 and 12.

These expectations are in surprisingly good accord with the observations

of Christoffel and Bowman[53c]. In particular, one could note the

increased absorption for $n_o \gtrsim 9$. The fact that a great deal of energy,

much more than for the lower n_o values, appears to be absorbed for

$n_o \gtrsim 9$ is indicative of the higher order resonances $(n_2, n_3, \ldots)$ being

more closely spaced and overlapping to a large extent, allowing the

molecule to essentially travel up a "chaotic ladder" of separatrix

layers.

This sort of analysis is entirely qualitative, but does have

the advantage that an essentially "back of the envelope" calculation

yields qualitatively correct predictions of energy absorption trends.

Recently, Davis and Wyatt[71] have developed a Poincaré surface of section

approach, based on the numerical integration of only a few classical trajectories, that is complementary to the approach here.

C6. Concluding Remarks

A method of generating period advance maps[13] for one-dimensional forced oscillator problems has been given. An application to a forced Morse oscillator demonstrated that a good deal of dynamical information could be obtained from the approach. The applicability is limited, however, to a relatively modest number (≤ 400) of map iterations (oscillations of the field), but this can be improved somewhat by increasing the initial grid size. Also, if one is only interested in particular dynamical features, such as the fate of a specific initial classical state, it is of course easier to use direct classical trajectories.

The behavior of the nonrotating HF molecule in a strong laser was found to be quite interesting, with classical states developing whorls[64] in the vicinity of the stable fixed point of the map. In fact, the entire phase plane was seen to consist of whorls of excitation and de-excitation. The pendulum model[14] of nonlinear resonance seems quite applicable to problems of this sort and does reproduce some of the major qualitative features. Also, certain dynamical trends, such as the average energy absorption as a function of initial vibrational state, can be qualitatively discussed with this model. Since the pendulum model has been used[14,72] to treat systems with more than 1 or 2 degrees of freedom, there may be some hope in using similar ideas to interpret the behavior of, say, vibrating and rotating diatomic

molecules in lasers, or more general polyatomics, or perhaps two or more lasers[53a] interacting with a molecule. Indeed, in related work, Oxtoby and Rice[72] have treated the autonomous problem of energy re-distribution in polyatomic molecules after excitation using the pendulum model and Chirikov's resonance overlap ideas for the onset of chaotic motion.

As a final point, the quantum analogue of the classical whorls has not been discussed here. Berry and co-workers[64] have discussed this point, and do expect to see certain evidence of whorls in the behavior of the time-dependent probability density .

V. Concluding Remarks

Classical and semiclassical methods have been used to treat a variety of phenomena in chemical dynamics.

Perhaps one of the important advantages of such approaches is that one can study reasonably complicated problems of experimental interest without too much difficulty. Thus in sec. II it was possible to make some connection with experiment in the discussion of tunneling in unimolecular reactions. Unfortunately at present there are no experimental or exact quantum mechanical determinations of the uni-molecular rate constants for the reactions studied in sec. II, so that it is somewhat difficult to calibrate precisely the semiclassical tunneling models developed. At least the results were compatible with the experimental results that were available.

In sec. III the quite different problem of charge transfer was treated with classical trajectories and a perturbative semiclassical model. In the simple alkali-halogen system studied, accurate quantum mechanical results were available for comparison. It was seen that the classical trajectory results predicted reasonably accurate cross sections over a wide range of energies, suggesting it may be useful to try such approaches with more complicated charge transfer reactions. The semi-classical model was also seen to be useful in the limit of high energy. It is interesting that such seemingly quantum mechanical events, such as nonadiabatic charge transfer, can sometimes be adequately explained within a classical or semiclassical framework.

In sec. IV, classical methods were used to study a diatomic molecule interacting with a strong laser. Quantum calculations were also made for comparison. It was found that the classical picture was reasonable for predicting certain averaged results, but could not be relied upon for details such as rotational structure in the absorption spectrum. A more detailed classical analysis of a nonrotating diatomic in a laser, based on a novel method of obtaining the classical solution, was made. A simple pendulum model was used to describe the classical solution, that also proved useful for explaining certain trends in molecular energy absorption.

In conclusion, one must admit that there is some, but not all truth in classical and semiclassical pictures of molecular phenomena, and this line of research is still an interesting and open field for future work (Wyatt's rule[73] still holds: $dK/dW \gg 1$, where $K(W)$ is the knowledge gained as a function of the work exerted).

> Jack: Gwendolen, it is a terrible thing for a man to find out suddenly that all his life he has been speaking the truth. Can you forgive me?

> Gwendolen: I can. For I feel that you are sure to change.

> from Oscar Wilde's "The Importance of Being Earnest"

Appendix A.   The Reaction Path

The concept of a reaction path is ubiquitous in chemistry, but is often ill-understood and poorly defined. For example, in the past it was often thought to be the path of minimum energy from the transition state down to reactant and product geometries. However, it was later pointed out that such a path is non-unique and discontinuous[74].

A more fruitful definition, that does not suffer from the above mathematical faux pas, is the path defined by following the gradient of the Born-Oppenheimer potential[75]. In the following, a very heuristic argument is presented, based on the concept of a zero kinetic energy trajectory connecting reactant, transition state and product geometries, that establishes the differential equations to be satisfied for this path.

Consider the usual (see sec. IIC) mass-weighted Cartesian coordinates, $x_{i\gamma}$. Let $x_{i\gamma}$ be a function of time and Taylor expand it about $t = 0$, which is assumed to correspond to a point on the reaction path. We have

$$x_{i\gamma}(t) - x_{i\gamma}(0) = \partial x_{i\gamma}/\partial t\big|_0 t + (1/2)\partial^2 x_{i\gamma}/\partial t^2\big|_0 t^2, \qquad \text{A1}$$

to second order. But we require that the kinetic energy be zero, so that the velocity $\partial x_{i\gamma}/\partial t = 0$. Also, by Newton's second law,

$$\partial^2 x_{i\gamma}/\partial t^2 = -\partial V/\partial x_{i\gamma} \quad,$$

where V is the Born-Oppenheimer potential surface. Thus

$$x_{i\gamma}(t) - x_{i\gamma}(0) = -(1/2)\partial V/\partial x_{i\gamma}\big|_{o} t^2 \quad . \qquad A2$$

But the distance traveled along the reaction path is, for small steps,

$$\Delta s = \sqrt{\Sigma_{i\gamma}[x_{i\gamma}(t) - x_{i\gamma}(0)]^2}$$
$$= (1/2) \ t^2 \sqrt{\Sigma_{i\gamma}(\partial V/\partial x_{i\gamma})^2} \qquad . \qquad A3$$

Now divide eq. A2 by eq. A3 and take the limit of infinitesimal Δs :

$$\partial x_{i\gamma}/\partial s = -c\partial V/\partial x_{i\gamma} \qquad , \qquad A4$$

where $c = 1/\sqrt{\Sigma_{i\gamma}(\partial V/\partial x_{i\gamma})^2}$, which is the set of 3N differential equations (eq. II-5) we introduced to define the reaction path. Because the formulation is in terms of Cartesian coordinates and is related to classical mechanics, no ambiguities or mathematical difficulties arise.

Appendix B.   Initial Conditions for a Diatomic Molecule

To classically determine probabilities, it is necessary to average over initial conditions. For an isolated diatomic molecule, one can change variables to action-angle variables, (N,Q_V), (J,Q_J), and (M,Q_M) such that $\dot{N}_V = \dot{J} = \dot{M} = 0$, with N_V being the vibrational action, J the rotational action or angular momentum, and M being the projection of the angular momentum onto the z axis. These variables allow a connection with quantum mechanical states to be made easily[57]. The probability P of some event may be obtained by averaging over the initial angle variables Q_V, Q_J, Q_M, for fixed N_V, J, and M,

$$P = (2\pi)^{-3} \int_0^{2\pi} dQ_V \int_0^{2\pi} dQ_J \int_0^{2\pi} dQ_M \ \chi_{N_V J M}(Q_V, Q_J, Q_M) \qquad B1$$

where $\chi = 1$ if the event occurs and 0 if it does not occur for the given initial conditions. Usually, the angular momentum is randomly oriented in space, so an average may be taken over M :

$$\bar{P} = \int_{-J}^{J} dM\ P \Big/ \int_{-J}^{J} dM = \frac{1}{2J} \int_{-J}^{J} dM\ P \qquad . \qquad B2$$

To do the Monte-Carlo integration[45a], the variables of integration are changed to $\vec{\xi}$, with $0 \le \vec{\xi} \le 1$, such that

$$2\,\xi_1 - 1 = M/J = \lambda$$

$$2\pi\,\xi_2 \qquad = Q_v$$

$$2\pi\,\xi_3 \qquad = Q_J$$

$$2\pi\,\xi_4 \qquad = Q_M \qquad \qquad \text{B3}$$

Eq. B2 becomes

$$\bar{P} = \lim_{N \to \infty} \frac{1}{N} \sum_{\vec{\xi}}^{N} \chi_{N_v J M}(\vec{\xi}) \qquad \qquad \text{B4}$$

That is, one averages χ over N random evaluations of $\vec{\xi}$ (each component of $\vec{\xi}$ is taken to be a pseudorandom number for a given evaluation).

Approximate relations between the action-angle variables and ordinary molecular coordinates have been given by Porter, Raff, and Miller[57] for a rotating Morse oscillator. The orbits given by them for θ and ϕ are not strictly correct. The corrected orbits are

$$r(t) = r_e \quad - \frac{1}{\alpha}\,\ell n\,\{(-2a)[b + \sqrt{b^2 - 4ac}\ \sin\,(\omega_N\,t + Q_N)] \qquad \text{B5a}$$

$$\theta(t) = \arccos\ [\sqrt{1 - \lambda^2}\,\cos\,(\omega_J\,t + Q_J + \text{sign}\,(p_r)\,J\Delta_J)] \qquad \text{B5b}$$

$$\phi(t) = Q_M + \text{sign}\,(p_\theta)\,\arccos\left(\frac{\lambda\,\cot\,[\theta(t)]}{\sqrt{1 - \lambda^2}}\right) \qquad \text{B5c}$$

where the formulae for $a, b, c, \omega_N, \omega_J$, and Δ_J may be found in Ref. 57. The errors in the angular orbits arose from omission of a $\text{sign}(p_r)$ and a $\text{sign}(p_\theta)$ factor in the generators W_r and W_θ, respectively (eqs. 8a and 8b of Ref. 57). Another slight error is in eqs. 30b and

30c of Ref. 57. Here, the factor r^2 should be replaced by the expansion

for r^2 given by their eq. 5.

Thus, to generate the initial conditions for a diatomic we first

pick λ, Q_v, Q_J, and Q_M randomly according to eqs. B3. Then, since the

calculations are to be made in spherical coordinates, r, θ, and ϕ are

calculated from eqs. B5. p_r and p_θ may be obtained by either

conservation of energy and angular momentum, or by differentiation of

eqs. 30 of Ref. 57. This procedure is completely equivalent to

randomly orienting the molecule and its angular momentum vector and

picking only r and p_r from the action-angle variable formulae, which

is the more standard approach[45a]. Thus, the present approach offers

no technical advantage over the ordinary approach for most applications,

including the present one, except when rotational angle variables

play an important role, as in some semiclassical applications.

The vibrational action N_v is calculated at a time t from the

approximate formula of Ref. 57,

$$N_v = -\frac{\hbar}{2} + \frac{\sqrt{2\mu}}{\alpha}\left(\frac{b}{2\sqrt{-c}} - \sqrt{-a}\right)$$
B6

and only depends on the molecular energy and angular momentum state,

$J(J + \hbar) = (p_\theta^2 + p_\phi^2/\sin^2\theta)$. N_v was also calculated numerically (from

$N_v = -\hbar/2 + (2\pi)^{-1} \oint p_r \, dr$) as a check on eq. B6 and, for all N_v and J

with $J \lesssim 10$, N_v from eq. B6 is accurate to three significant figures.

Thus, essentially no error is introduced by the use of eq. B6.

Appendix C. Fixed Points of the Period Advance Map

An approximate, but surprisingly accurate estimate of the period 1 fixed points is as follows. Starting from eq. IV-29 of the text,

$$K = H_o(\hat{p} + n_1) - \varepsilon V_1(\hat{p} + n_1) \cos\hat{q} - \hat{p}\Omega \quad , \qquad \qquad C1$$

where $\hat{q} = q - \Omega t$ and $\hat{p} = n - n_1$, one then uses the harmonic oscillator[8] $x(n,q)$ to estimate V_1, rather than the exact form eq. IV-26b. This is valid for small n and simplifies the calculations. Thus

$$V_1(n) = (2\pi)^{-1} \int_{-\pi}^{\pi} x(n,q) \cos q \, dq$$

$$= (2\pi)^{-1} \int_{-\pi}^{\pi} \sqrt{(2n + 1)/\mu\omega_o} \, \cos^2 q \, dq$$

$$= \sqrt{(2n + 1)/\mu\omega_o} \, /2 \quad . \qquad \qquad C2$$

Eq. C1 becomes

$$K = H_o(\hat{p} + n_1) - (\varepsilon/2) \sqrt{[\, 2(\hat{p} + n_1) + 1 \,]/\mu\omega_o} \, \cos\hat{q} - \hat{p}\Omega \, . \qquad C3$$

The equations of motion consistent with the Hamiltonian above are

$$\dot{\hat{p}} = - (\varepsilon/2) \sqrt{[2(\hat{p} + n_1) + 1]/\mu\omega_o} \, \sin\hat{q}$$

$$\dot{\hat{q}} = \omega(\hat{p} + n_1) - \frac{(\varepsilon/2) \cos\hat{q}}{\sqrt{\mu\omega_o \, [2(\hat{p} + n_1) + 1]}} - \Omega \qquad \qquad C4$$

For a fixed point, we require $\dot{\hat{p}} = \dot{\hat{q}} = 0$. Replacing $\hat{p} + n_1$ by n, and setting $t = 0$ so that $\hat{q} = q$, we obtain the two equations

$$- (\varepsilon/2) \sqrt{(2n+1)/\mu\omega_o} \, \sin q = 0 \qquad\qquad \text{C5a}$$

$$\omega(n) - \frac{(\varepsilon/2) \cos q}{\sqrt{\mu\omega_o (2n+1)}} - \Omega = 0 \; . \qquad\qquad \text{C5b}$$

Eq. C5a is satisfied for $q = 0$ and π. Inserting either of these into eq. C5b yields a simple one-dimensional root equation for n, which can be solved by iteration. With the parameters of sec. IVC, one finds the fixed points $(n,q) = (0.6218, \pi)$, $(0.3610, 0)$, and $(-0.4828, 0)$, which are in remarkably good agreement with the more exact fixed points, which were found to be $(0.6173, \pi)$, $(0.3603, 0)$, and $(-0.4821, 0)$.

References

1. See, for example, (a) M.A.D. Fluendy and K.P. Lawley, " Chemical Applications of Molecular Beam Scattering", (Chapman and Hall Ltd., London, 1973), and (b) R.D. Levine and R.B. Bernstein, "Molecular Reaction Dynamics", (Clarendon Press, Oxford, 1974).

2. An excellent but somewhat outdated review of classical trajectory applications is (a) R.N. Porter, Ann. Rev. Phys. Chem. 25,317(1974). A more recent discussion is (b) R.B. Walker and J.C. Light, Ann. Rev. Phys. Chem. 31,401(1980).

3. M. Karplus, R.N. Porter, and R.D. Sharma, J. Chem. Phys. 43, 3259(1965).

4. (a) G.C. Schatz and A. Kuppermann, J. Chem. Phys. 62,2502(1975).

    (b) A.B. Elkowitz and R.E. Wyatt, J. Chem. Phys. 62,2504(1975).

    (c) A.B. Elkowitz and R.E. Wyatt, J. Chem. Phys. 63,702(1975).

    (d) G.C. Schatz and A. Kuppermann, J. Chem. Phys. 65,4668(1976).

5. (a) J.T. Muckerman, J. Chem. Phys. 54,1155(1971).

    (b) J.T. Muckerman, J. Chem. Phys. 56,2997(1972).

    (c) J.T. Muckerman, J. Chem. Phys. 57,3388(1972).

6. W.L. Hase, R.J. Wolf, C.S. Sloane, J. Chem. Phys. 71,2911(1979).

7. R.E. Wyatt, in "Atom - Molecule Collision Theory, A Guide for the Experimentalist", edited by R.B. Bernstein, (Plenum, New York, 1979),pp. 567-94.

8. W.H. Miller, Adv. Chem. Phys. 25,69(1974).

9. For a good treatment of the WKB approximation, see (a) E. Merzbacher, "Quantum Mechanics", (Wiley, New York, 1970), and (b) D. Rapp, "Quantum Mechanics", (Holt, Rinehart, and Winston, New York, 1971).

10. W.H. Miller, N.C. Handy, and J.E. Adams, J. Chem. Phys. 72, 99(1980).

11. W.H. Miller, J. Am. Chem. Soc. 101,6810(1979).

12. (a) W.H. Miller and C.W. McCurdy, J. Chem. Phys. 69,5163(1978).

   (b) H-D. Meyer and W.H. Miller, J. Chem. Phys. 70,3214(1979).

   (c) H-D. Meyer and W.H. Miller, J. Chem. Phys. 71,2156(1979).

   (d) H-D. Meyer and W.H. Miller, J. Chem. Phys. 72,2272(1980).

13. V.I. Arnold, "Mathematical Methods of Classical Mechanics", (Springer-Verlag, New York, 1978), p. 114.

14. B.V. Chirikov, Phys. Rep. 52,263(1979)

15. P.J. Robinson and K.A. Holbrook, "Unimolecular Reactions", (Wiley, New York, 1972).

16. W.L. Hase, in "Dynamics of Molecular Collisions, Part B", edited by W.H. Miller, (Plenum, New York, 1976), pp.121-69.

17. W. Forst, "Theory of Unimolecular Reactions", (Academic, New York, 1973), p.61.

18. H.S. Johnston, "Gas Phase Reaction Rate Theory", (Ronald Press, New York, 1966), pp.37-47.

19. (a) P. Pulay, in "Applications of Electronic Structure Theory", edited by H.F. Schaefer, (Plenum, New York,1977),pp.153-85. For details on analytic configuration interaction derivatives, see (b) B.R. Brooks, W.D. Laidig, P. Saxe, J.D. Goddard, Y. Yamaguchi, and H.F. Schaefer, J. Chem. Phys. 72,4652(1980), and (c) R. Krishnan, H.B. Schlegal, and J.A. Pople, J. Chem. Phys. 72,4654(1980).

20. See, for example, T. Takada, M. Dupuis, and H.F. King, J. Chem. Phys. 75,332(1981), and references therein.

21. C.J. Cerjan and W.H. Miller, J. Chem. Phys. 75,2800(1981).

22. Y. Osamura, H.F. Schaefer, S.K. Gray, and W.H. Miller, J. Am. Chem. Soc. 103,1904(1981). See also Y. Osamura and H.F. Schaefer, Chem. Phys. Lett. 79,412(1981).

23. (a) P.S. Skell and J.H. Plonka, J. Am. Chem. Soc. 92,5620(1970); P.S. Skell, F.A. Fagone, and K.J. Klabunde, J. Am. Chem. Soc. 94,7862(1972); P.S. Skell, J.J. Havel, and M.J. McGlinchey, Acc. Chem. Res. 6,97(1973).

    (b) C. Reiser, F.M. Lussier, C.C.Jensen, and J.I. Steinfeld, J. Am. Chem. Soc. 101,350(1979); C. Reiser and J.I. Steindeld. J. Phys. Chem. 84,680(1980).

24. R. Krishnan, M.J. Frisch, J.A. Pople, and P.V.R. Schleyer, Chem. Phys. Lett. 79,408(1981).

25. M. Born, "The Mechanics of the Atom", (Ungar, New York, 1960),pp.249-56.

26. See, for example, S. Chapman, B.C. Garrett, and W.H. Miller, J. Chem. Phys. 64,502(1976).

27. S.K. Gray, W.H. Miller, Y. Yamaguchi, and H.F. Schaefer, J. Chem. Phys. 73,2733(1980).

28. See, for example, F.B. Hildebrand, "Introduction to Numerical Analysis",(McGraw-Hill, New York,1956),Chap. 6.

29. K. Ishida, K. Morokuma, and A. Komornicki, J. Chem. Phys. 66, 2153(1977).

30. A good introduction to formaldehyde dissociation is the review article, W.M. Gelbart, M.L. Elert, and D.F. Heller, Chem. Rev. 80,403(1980).

31. J.C. Weisshaar and C.B. Moore, J. Chem. Phys. 70,5135(1979)

32. J.D. Goddard and H.F. Schaefer, J. Chem. Phys. 70,5117(1979).

33. J.D. Goddard, Y. Yamaguchi, and H.F. Schaefer, J. Chem. Phys. 75,3459(1981).

34. S.K. Gray, W.H. Miller, Y. Yamaguchi, and H.F. Schaefer, J. Am. Chem. Soc. 103,1900(1981).

35. J.L. Duncan and P.D. Mallison, Chem. Phys. Lett. 23,597(1973).

36. B.A. Waite, W.H. Miller, and S.K. Gray, to be published; see also B.A. Waite and W.H. Miller, J. Chem. Phys. $\underline{76}$, 2412(1982).

37. M.J. Frisch, R. Krishnan, and J.A. Pople, J. Phys. Chem. $\underline{85}$, 1467(1981).

38. H.F. King, M. Dupuis, and J. Rys, National Resource for Computation in Chemistry Software Catalog, Vol.1 , Program No. QHO2 (HONDO), 1980.

39. K. Yamashita, T. Yambe, and K. Fukui, Chem. Phys. Lett. $\underline{84}$,123(1981).

40. See, e.g., K. Lacman, Adv. Chem. Phys. $\underline{42}$,513(1980).

41. M.B. Faist and R.D. Levine, J. Chem. Phys. $\underline{64}$,2953(1976).

42. (a) J.C. Tully and R.K. Preston, J. Chem. Phys. $\underline{55}$,562(1971).
    (b) J.R. Krenos, R.K. Preston, R. Wolfgang, and J.C. Tully, J. Chem. Phys. $\underline{60}$,1634(1974).

43. W.H. Miller, J. Chem. Phys. $\underline{68}$,4431(1978).

44. F.T. Smith, Phys. Rev. $\underline{179}$,111(1969); see also M. Baer, Chem. Phys. Lett. $\underline{35}$,113(1975).

45. (a) R.N. Porter and L.M. Raff, in "Dynamics of Molecular Collisions", edited by W.H. Miller, (Plenum, N.Y.,1976),p.1.
    (b) D.L. Bunker, Meth. Comp. Phys. $\underline{10}$,287(1971).

46. A.E. Orel, D.P. Ali, and W.H. Miller, Chem. Phys. Lett. $\underline{79}$,137 (1981).

47. W.H. Miller and F.T. Smith, Phys. Rev. $\underline{17A}$,939(1978).

48. See the initial value representation, discussed in W.H. Miller, J. Chem. Phys. $\underline{53}$,3578(1970).

49. See, e.g., M.S. Child, "Molecular Collision Theory",(Academic, N.Y.,1974),pp. 161-79.

50. See, for example, papers in "Advances in Laser Chemistry", edited by A.H. Zewail, (Springer, N.Y.,1978) and "Laser-Induced Processes in Molecules", edited by K.L. Kompa and S.D. Smith, (Plenum, N.Y.,1978).

51. (a) D. Poppe, Chem. Phys. $\underline{45}$,371(1980).

    (b) D.W. Noid, C. Bottcher, and M.L. Koszykowski, Chem. Phys. Lett. $\underline{72}$,397(1980).

    (c) D.W. Noid, M.L. Koszykowski, R.A. Marcus, and J.D. MacDonald, Chem. Phys. Lett. $\underline{51}$,540(1977).

52. R.B. Walker and R.K. Preston, J. Chem. Phys. $\underline{67}$,2017(1977).

53. (a) D.W. Noid and J.R. Stine, Chem. Phys. Lett. $\underline{65}$,153(1979).

    (b) J.R. Stine and D.W. Noid, Chem. Phys. lerr. $\underline{77}$,287(1981).

    (c) K.M. Christoffel and J.M. Bowman, J. Phys. Chem. $\underline{85}$,2159(1981).

54. (a) S.C. Leasure and R.E. Wyatt, Opt. Eng. $\underline{19}$,46(1980).

    (b) S.C. Leasure and R.E. Wyatt, Chem. Phys. Lett. $\underline{61}$,625(1979).

    (c) S.C. Leasure, K.F. Milfeld, and R.E. Wyatt, J. Chem. Phys. $\underline{74}$,6197(1981).

55. W.H. Flygare, "Molecular Structure and Dynamics",(Prentice-Hall, Englewood Cliffs, N.J., 1978),p.11.

56. W.H. Miller, J. Chem. Phys. $\underline{69}$,2188(1978).

57. R.N. Porter, L.M. Raff, and W.H. Miller, J. Chem. Phys. $\underline{63}$, 2214(1975).

58. (a) M.L. Sage, Chem. Phys. $\underline{35}$,375(1978).

    (b) R. Wallace, Chem. Phys. Lett. $\underline{37}$,115(1976).

59. L.F. Shampine and M.K. Gordan, "Computer Solution of Ordinary Differential Equations : The Initial Value Problem", (Freeman, S.F., 1975). The actual program used was ODE from the SANDIA Laboratory.

60. C.W. Gear, SIAM Rev. $\underline{23}$,10(1981).

61. (a) M. Sargent, M.O. Scully, and W.E. Lamb, "Laser Physics", (Addison-Wesley, Reading, MA,1974).

    (b) S. Flugge, "Practical Quantum Mechanics",(Springer,N.Y.,1971), Vol. II,p.138.

    (c) M. Quack, J. Chem. Phys. $\underline{69}$,1282(1978).

62. J.V. Moloney and W.J. Meath, Mol. Phys. $\underline{31}$,1537(1976).

63. P.S. Dardi and S.K. Gray, J. Chem. Phys.,to be published.

64. M.V. Berry, N.L. Balazs,M. Tabor, and A. Voros, Ann. Phys. $\underline{122}$, 26(1979).

65. H.T. Davis, "Introduction to Nonlinear Differential and Integral Equations", (Dover, N.Y., 1962).

66. (a) L.F. Shampine and R.C. Allen, "Numerical Computing : An Introduction", (Saunders, Philadelphia, 1973).

66. (b) D.R. McLaughlin and D.L. Thompson, J. Chem. Phys. <u>59</u>,

4393(1973); see also N. Sathyamurthy and L.M. Raff, J. Chem.

Phys. <u>63</u>,464(1975).

67. C.C. Rankin and W.H. Miller, J. Chem. Phys. <u>55</u>,3150(1971). Note

that their phase convention for q differs by π from ours and their

energy is with respect to the separated atoms as zero.

68. See, e.g., M.V. Berry in "Topics in Nonlinear Dynamics", edited

by S. Jorna, (AIP, N.Y., 1978), Chapter 2.

69. H. Goldstein, "Classical Mechanics",(Addison-Wesley, Reading,

MA, 1950).

70. I.S. Gradshetyn and I.M. Ryzhik, "Table of Integrals, Series, and

Products",(Academic, N.Y., 1965).

71. M.J. Davis and R.E. Wyatt, Chem. Phys. Lett. <u>86</u>,235(1982).

72. D.W. Oxtoby and S.A. Rice, J. Chem. Phys. <u>65</u>,1676(1976).

73. Robert E. Wyatt, personal communication.

74. E.A. McCullough and D.M. Silver, J. Chem. Phys. <u>62</u>,4050(1975).

75. (a) K. Fukui, J. Phys. Chem. <u>74</u>,4161(1970).

      (b) H.F. Schaefer, Chem. Brit. <u>11</u>,227(1975).

112

Table I. Predicted DZ+P CI harmonic vibrational frequencies
for vinylidene, acetylene, and the transition state
connecting them.

Species	Frequency	Normal Mode Description
vinylidene	3344	CH asym. stretch
	3239	CH sym. stretch
	1710	CC stretch
	1288	CCH bend
	787	out of plane
	444	CH_2 rock
transition state	3454	CH_a stretch
	2699	CH_b stretch
	1874	CC stretch
	937	HCC bend
	573	out of plane
	1029i	reaction coordinate
acetylene	3583	CH asym. stretch
	3488	CH sym. stretch
	2073	CC stretch
	764	CCH bend
	610	CCH bend

Table II. Harmonic Vibrational Frequencies[a] of H_2CO.

	DZ-SCF[b]	DZP-SCF	DZ-CI	DZP-CI	EXP[c]
$\omega_1(a_1)$	3223	3149	3028	3074	2944
$\omega_2(a_1)$	1878	2006	1703	1869	1764
$\omega_3(a_1)$	1651	1656	1544	1596	1563
$\omega_4(b_1)$	1324	1335	1194	1243	1191
$\omega_5(b_2)$	3315	3226	3112	3155	3009
$\omega_6(b_2)$	1349	1367	1263	1306	1287

[a]Units for frequencies are cm^{-1}.

[b]Various column headings refer to the various ab initio basis sets and extent of configuration interaction included in the calculations.

[c]The experimental harmonic frequencies given in reference 35 .

Table III. Transition State Parameters[a,b] for $H_2CO \rightarrow H_2 + CO$.

	DZ-SCF	DZP-SCF	DZ-CI	DZP-CI	SCALED[c]
$\omega_1(a')$	3156	3243	3159	3263	3125
$\omega_2(a')$	1948	2092	1764	1939	1830
$\omega_3(a')$	1371	1526	1310	1555	1523
$\omega_4(a')$	800	829	803	876	839
$\omega_5(a')$	2320i	2305i	1997i	2124i	2026i
$\omega_6(a'')$	1015	1024	889	$\sim$ 950	936
$V_0(\frac{kcal}{mole})^d$	113.7	105.9	100.3	98.1	92[e]

[a,b] See Table II .

[c] Scaled frequencies , see text.

[d] Barrier height relative to vibrationless H_2CO.

[e] The best estimates of Goddard et al. (reference 33) of the classical barrier, with a probable error of ± 1 kcal/mole.

Table IV. Rate Constants via Simple RRKM + Tunneling Model.

$E-V_0$(kcal/mole)	log k (sec^{-1})				
	DZ-SCF	DZP-SCF	DZ-CI	DZP-CI	SCALED
-2	3.57	3.41	2.91	2.99	2.95
0	4.41	4.26	3.90	3.92	3.92
2	5.24	5.10	4.87	4.83	4.88
4	6.06	5.93	5.83	5.74	5.81
6	6.88	6.76	6.77	6.63	6.75
8	7.68	7.57	7.71	7.51	7.67
10	8.43	8.34	8.57	8.36	8.55
12	9.02	9.00	9.17	9.05	9.21

Table V. Frequency Variation along the Reaction Path.

	s ($\sqrt{amu}$ Å)		
	-0.21	0	$+0.21$
ω_1	3517	3263	2642
ω_2	1932	1939	1981
ω_3	1594	1555	1648
ω_4	953	876	738
$\omega_6{}^a$	($\sim$ 950)	$\sim$ 950	($\sim$ 950)

---

[a]The out-of-plane bending frequency.

Table VI. Effect on Rate of More Rigorous Dynamical Model.

E-V$_0$(kcal/mole)	log k (sec^{-1})[a]				
	A	B	C	D	E
-2	2.99	3.14	3.17	3.14	2.98
0	3.92	4.00	4.03	4.00	3.86
2	4.83	4.86	4.89	4.86	4.74
4	5.74	5.72	5.75	5.72	5.62
6	6.63	6.58	6.61	6.58	6.50
8	7.51	7.50	7.52	7.49	7.41
10	8.36	8.34	8.35	8.33	8.25
12	9.05	9.04	9.04	9.02	8.97

[a]See text for a description of the theoretical models corresponding to columns A-E.

Table VII. Comparison of semiclassical perturbation theory (SCL)
and exact quantum (QM) probabilities for the Landau-Zener model.

z	$P_{1 \leftarrow 0}(SCL)$	$P_{1 \leftarrow 0}(QM)$
0.	0.	0.
0.2	0.0099	0.0099
0.4	0.0384	0.0392
0.6	0.0822	0.0861
0.8	0.1360	0.1479
1.0	0.1937	0.2212
1.2	0.2483	0.3023
1.4	0.2936	0.3874
1.6	0.3248	0.4727
1.8	0.3381	0.5551
2.0	0.3326	0.6321
∞	0.	1.

Table VIII. Some relevant energy levels for HF, according to the
rotating Morse oscillator approximation.

| v | j | $\varepsilon_{v\,j}^{\,o}$ | |
		a.u.	cm^{-1}
0	0	0.0093309	2048
0	1	0.0095187	2089
0	2	0.0098941	2171
1	0	0.0274001	6014
1	1	0.0275819	6054
1	2	0.0279454	6133
2	0	0.0446793	9806
2	1	0.0448551	9845
2	2	0.0452065	9922

Table IX. Approximate time averaged probabilities for vibrational transitions of HF in a 1.0 TW/cm^2 laser.

$\bar{\nu}(cm^{-1})$	non-rotating			rotating		
	P_0	P_1	P_2	P_0	P_1	P_2
3850	0.88(QM)	0.08	0.04	0.99	0.01	0.00
	1.00(CL)	0.00	0.00			
3879	0.47	0.08	0.45	0.53	0.03	0.44
	0.88	0.12	0.00	0.99	0.01	0.00
3900	0.83	0.11	0.06	0.96	0.03	0.01
	0.73	0.19	0.08	0.94	0.04	0.02
3937	0.69	0.28	0.03	0.47	0.07	0.46
	0.69	0.24	0.06	0.67	0.27	0.06
3966	0.51	0.47	0.02	0.87	0.12	0.01
	0.63	0.36	0.01	0.58	0.40	0.02
4006	0.69	0.30	0.01	0.50	0.49	0.01
	0.68	0.32	0.00	0.66	0.34	0.00
4085	0.93	0.07	0.00	0.95	0.05	0.00
	0.90	0.10	0.00	0.88	0.12	0.00

Table X.   Approximate time averaged vibrational transition probabilities
for rotating HF in a 2.5 TW/cm^2 laser.[a]

$\overline{\nu}(cm^{-1})$	P_0	P_1	P_2
3879	0.51(QM)	0.07	0.42
	0.88(CL)	0.07	0.05
3900	0.90	0.05	0.05
	0.67	0.17	0.16
3937	0.48	0.10	0.42
	0.50	0.31	0.19
3966	0.77	0.18	0.05
	0.52	0.39	0.09
4006	0.52	0.45	0.03
	0.61	0.37	0.02
4085	0.89	0.11	0.00
	0.78	0.20	0.00

[a]
The classical results shown for $\overline{\nu}$ = 3879 and 3937 cm^{-1} were actually
run at 3870 and 3927 cm^{-1}, respectively. The probabilities will not vary
much since the classical peak is broad. It was displayed in the table
this way to avoid confusion since the overall trends are still clear.

Table XI. Quantum mechanical transition probabilities and energy absorbed as a function of pulse time for laser phases of 0 and $\pi/2$ at $\omega = 4006$ cm^{-1} and $I = 1.0$ TW/cm^2.

t(ps)	P_{00}		P_{11}		$\langle E(t) \rangle_{QM}$ (a.u.)	
	$\delta = 0$	$\delta = \pi/2$	$\delta = 0$	$\delta = \pi/2$	$\delta = 0$	$\delta = \pi/2$
0.0	1.00	1.00	0.00	0.00	0.0000	0.0000
0.4	0.30	0.32	0.63	0.66	0.0125	0.0126
0.8	0.13	0.14	0.81	0.83	0.0156	0.0158
1.2	0.94	0.95	0.05	0.05	0.0010	0.0009
1.6	0.51	0.53	0.44	0.45	0.0084	0.0086
2.0	0.03	0.03	0.92	0.92	0.0177	0.0179
2.4	0.81	0.81	0.17	0.17	0.0034	0.0033
2.8	0.73	0.73	0.24	0.24	0.0047	0.0048
3.2	0.01	0.01	0.95	0.94	0.0180	0.0182
3.6	0.62	0.62	0.36	0.36	0.0068	0.0069
4.0	0.88	0.90	0.09	0.09	0.0018	0.0017
4.4	0.08	0.09	0.87	0.88	0.0167	0.0169

Table XII. Quantum mechanical transition probabilities and energy absorbed
as a function of pulse times for laser phases of 0 and $\pi/2$ at
$\omega = 3937$ cm^{-1} and I = 1.0 TW/cm^2.

t(ps)	P_{00}		P_{22}		$\langle E(t)\rangle_{QM}$ (a.u.)	
	$\delta = 0$	$\delta = \pi/2$	$\delta = 0$	$\delta = \pi/2$	$\delta = 0$	$\delta = \pi/2$
0.0	1.00	1.00	0.00	0.00	0.0000	0.0000
0.4	0.93	0.93	0.05	0.05	0.0021	0.0019
0.8	0.78	0.80	0.19	0.19	0.0072	0.0071
1.2	0.57	0.58	0.37	0.38	0.0142	0.0144
1.6	0.36	0.37	0.57	0.57	0.0218	0.0219
2.0	0.18	0.18	0.71	0.74	0.0282	0.0284
2.4	0.05	0.05	0.83	0.81	0.0320	0.0324
2.8	0.00	0.00	0.83	0.86	0.0333	0.0338
3.2	0.03	0.03	0.80	0.80	0.0322	0.0324
3.6	0.14	0.13	0.69	0.71	0.0283	0.0287
4.0	0.27	0.29	0.56	0.57	0.0231	0.0233
4.4	0.47	0.47	0.40	0.40	0.0169	0.0170

Table XIII Root mean square deviations between the map predictions and direct numerical integration of trajectories. The results are for 50 trajectories with $n_o = 0$ initially. Typical values of p and x are ± 3 and 2 a.u. respectively.

	R.M.S. deviation	
r	p	x
100	0.005	0.0001
200	0.008	0.0003
300	0.016	0.0010
400	0.024	0.0020
500	0.078	0.0029

Figure Captions

Figure 1. Stationary point geometries at the DZP-CI level of theory
for vinylidene, acetylene, and the transition state
connecting them.

Figure 2. Rate of vinylidene rearrangement to acetylene as a function
of excess vibrational energy in vinylidene, i.e. vibrational
energy in excess of the zero-point energy. The solid curve
is for a classical barrier of 4 kcal/mol, and the dashed
curve is for a barrier of 6 kcal/mol. Arrows on the energy
axis indicate the respective classical thresholds.

Figure 3. Plot of the x and y coordinates of the H atom along the
reaction path for HNC → HCN. The origin of the coordinate
system is the center of mass of CN. Only the region important
for tunneling is shown, and the spurious oscillations have
been smoothed out.

Figure 4. Potential energy (left hand scale) and vibrational frequencies
(right hand scale) as a function of the reaction coordinate
for HNC → HCN.

Figure 5. Vibrational mode coupling constants as a function of the
reaction coordinate.

Figure 6. Microcanonical rate constant for zero total angular
momentum for the reaction HNC → HCN. The classical threshold
is indicated by an arrow.

Figure 7. Potential energy profile along the formaldehyde reaction path for decomposition. The points are the ab initio (DZP-CI) results and the solid curve is an Eckart potential fit.

Figure 8. Potential energy profile, calculated at the DZ-SCF level of ab initio theory, for formaldehyde decomposition.

Figure 9. Vibrational frequencies as a function of reaction coordinate for formaldehyde decomposition, calculated at the DZ-SCF level of theory.

Figure 10. Selected vibrational mode couplings for the formaldehyde reaction path. (a) B_{12}, (b) B_{31}, (c) B_{32} . See text for more discussion.

Figure 11. Classical (points), quantum (solid curve), and perturbative semiclassical (dashed curve) results for Na + I $\rightarrow$ Na$^+$ + I$^-$ cross section.

Figure 12. Classical and quantum mechanical time averaged energy absorption for HF in a 1.0 TW/cm^2 laser. (a) nonrotating HF, (b) rotating HF.

Figure 13. Classical and quantum mechanical time averaged energy absorption for rotating HF in a 2.5 TW/cm^2 laser.

Figure 14. Time-dependent energy absorption for nonrotating HF with laser frequency $\bar{\nu}$ = 3966 cm^{-1} and I = 1.0 TW/cm^2.

Figure 15. Time-dependent energy absorption for rotating HF with $\bar{\nu} = 4006$ cm^{-1} and I = 1.0 TW/cm^2.

Figure 16. Quantum time-dependent energy absorption for rotating HF with $\bar{\nu} = 3937$ cm^{-1} and I = 1.0 TW/cm^2. Jaggedness is due to poor resolution of high frequency oscillations.

Figure 17. Classical time-dependent energy absorption for rotating HF with $\bar{\nu} = 3937$ cm^{-1} and I = 1.0 TW/cm^2.

Figure 18. Classical and quantum probabilities P_{vj} for HF with $\bar{\nu} = 4006$ cm^{-1} and I = 1.0 TW/cm^2.

Figure 19. Classical probabilities for HF with $\bar{\nu} = 3937$ cm^{-1} and I = 1.0 TW/cm^2.

Figure 20. Quantum probabilities P_{00} and P_{22} for HF with $\bar{\nu} = 3937$ cm^{-1} and I = 1.0 TW/cm^2.

Figure 21. Surface of section plots for the period advance map. a) p-x space. b) n-q space. Open circles indicate stable fixed points and filled circles indicate unstable fixed points.

Figure 22. Evolution of an initial n_o = 1/2 state. a) after r = 20 periods, b) after 40 periods, c) after 60 periods. Note the dashed line in a) represents the initial state.

Figure 23. a) result of mapping an n_o = 0 state 40 periods, b) result of mapping an n_o = 1 state 40 periods.

Figure 24. Evolution of the entire n-q phase plane. After a) 20
            periods, b) 40 periods, and c) 60 periods. See text for
            details.

Figure 25. Pendulum model predictions for the fate of initial
            states a) $n_o = 1/2$, b) $n_o = 0$, and c) $n_o = 1$, after
            40 periods.

Figure 1

Figure 2

131
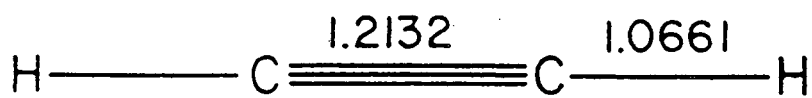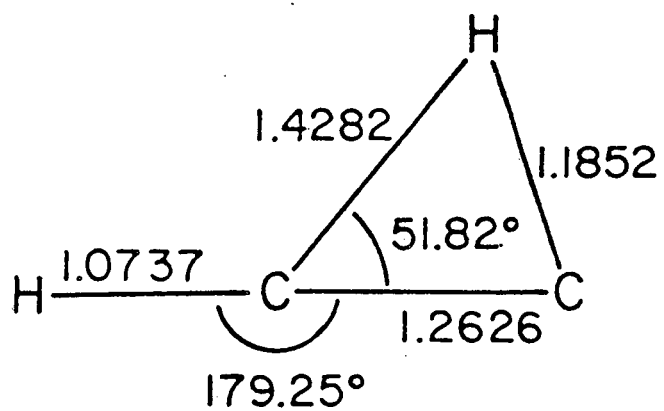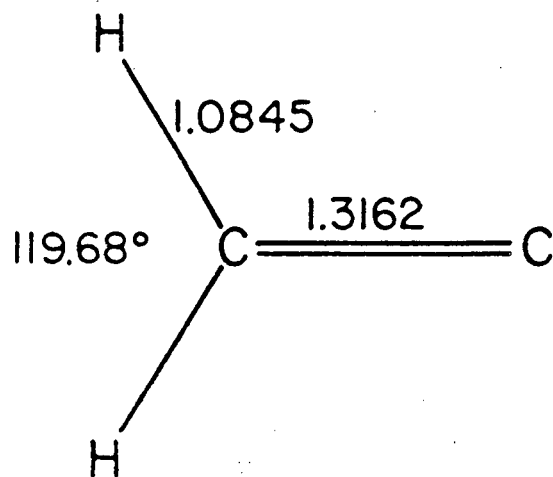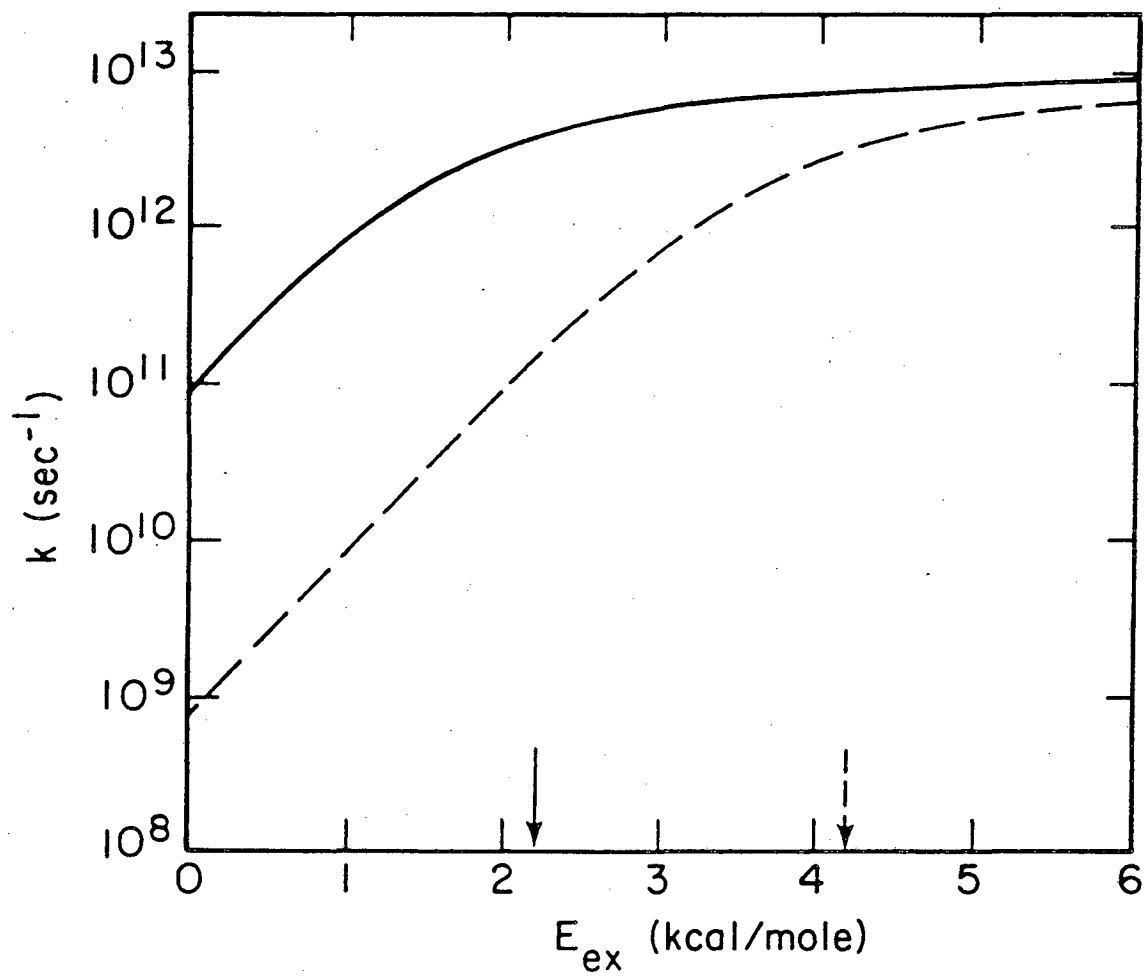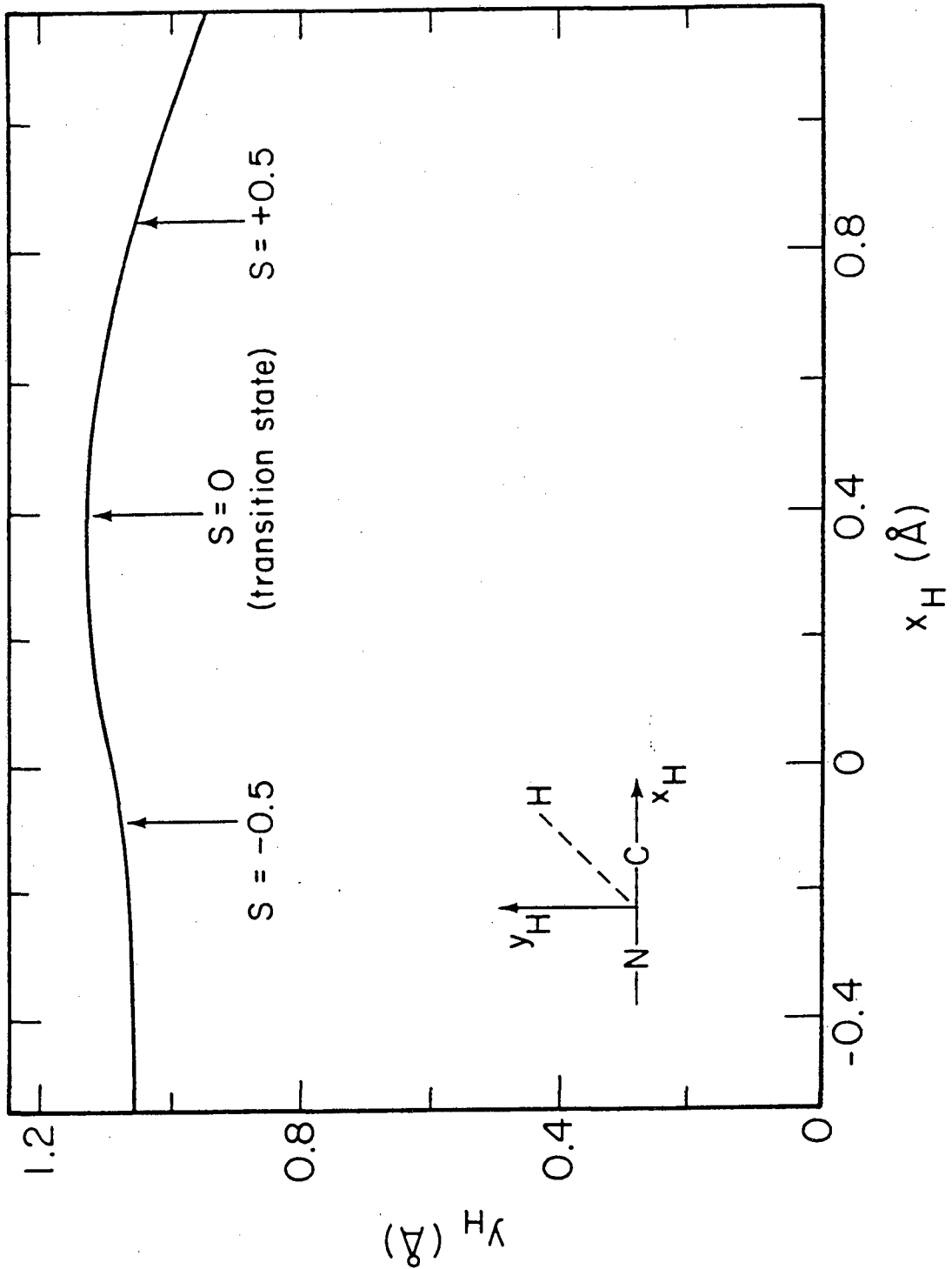
Figure 3.

Figure 4.

XBL 806-9864

Figure 5.

XBL 806-9865

134

Figure 6.

XBL 806-9866

Figure 7.

XBL 808-11071

136
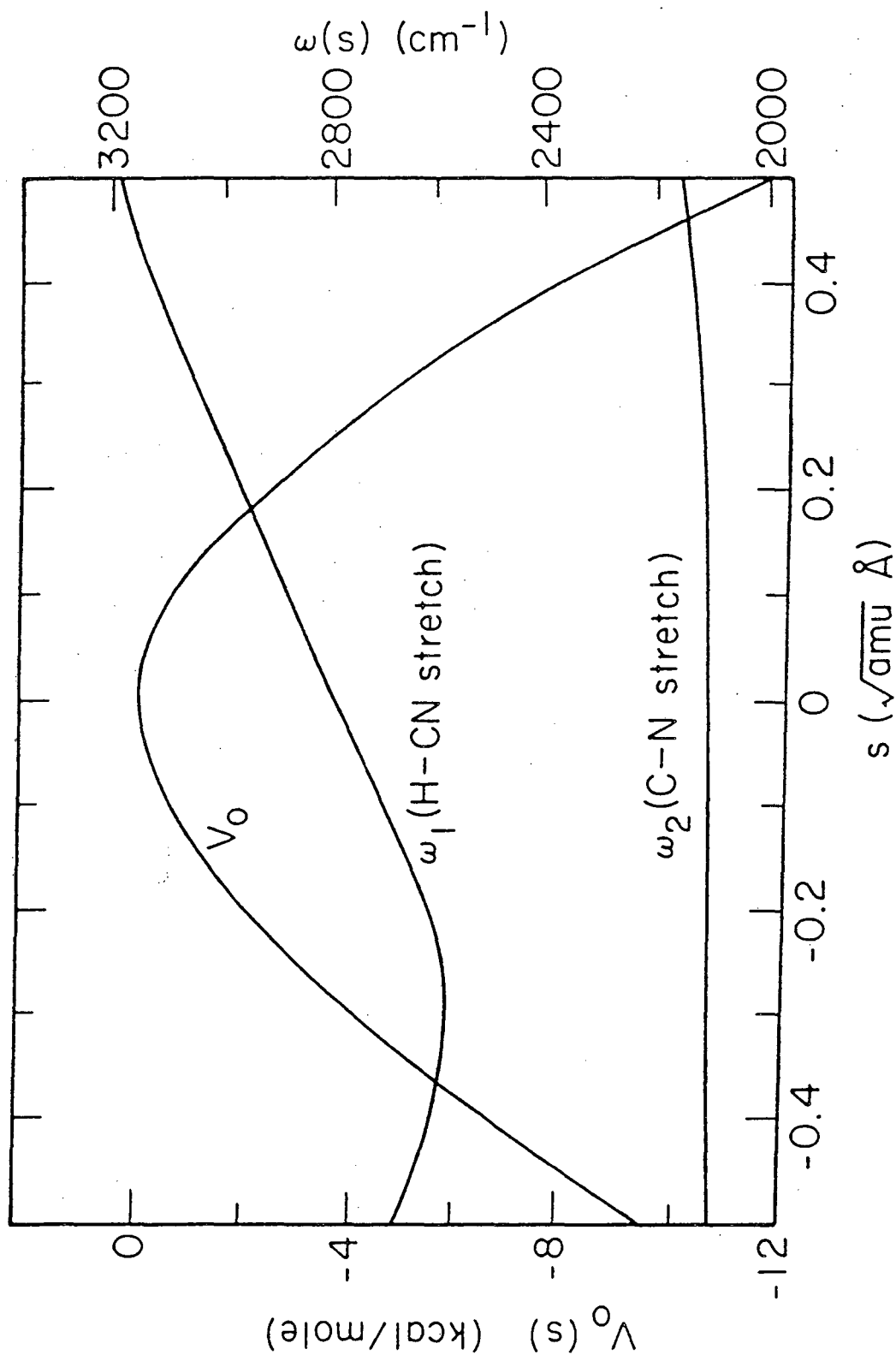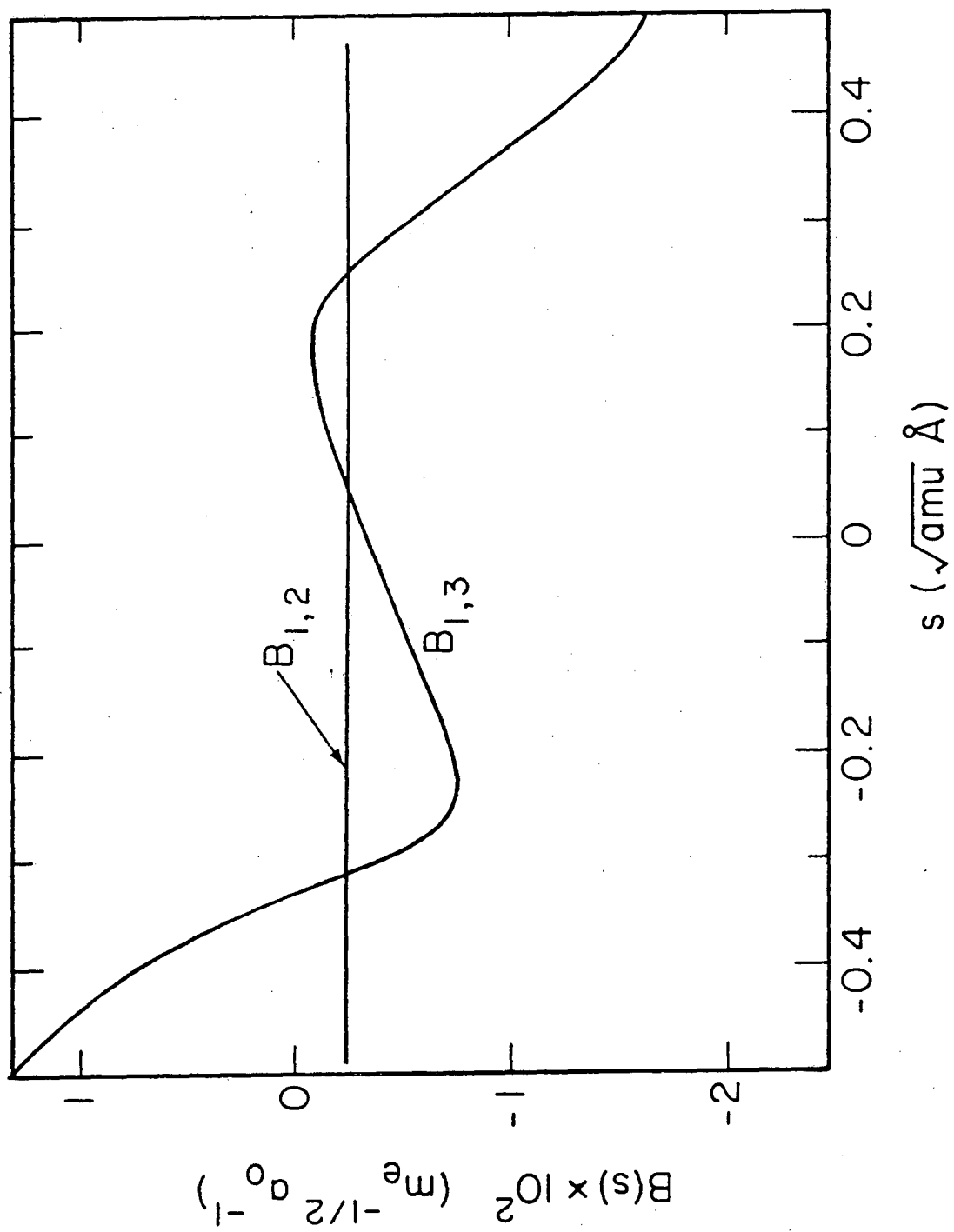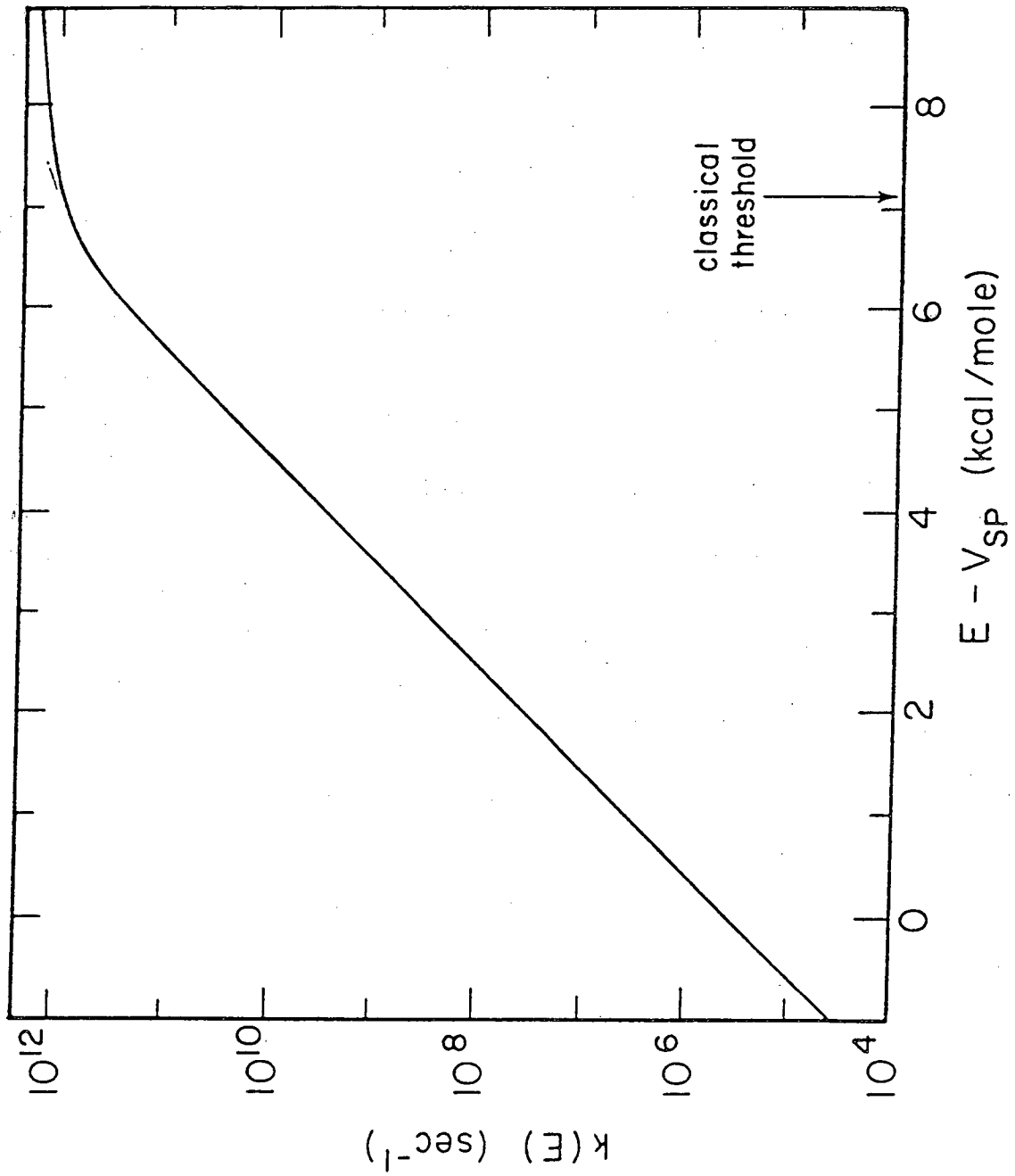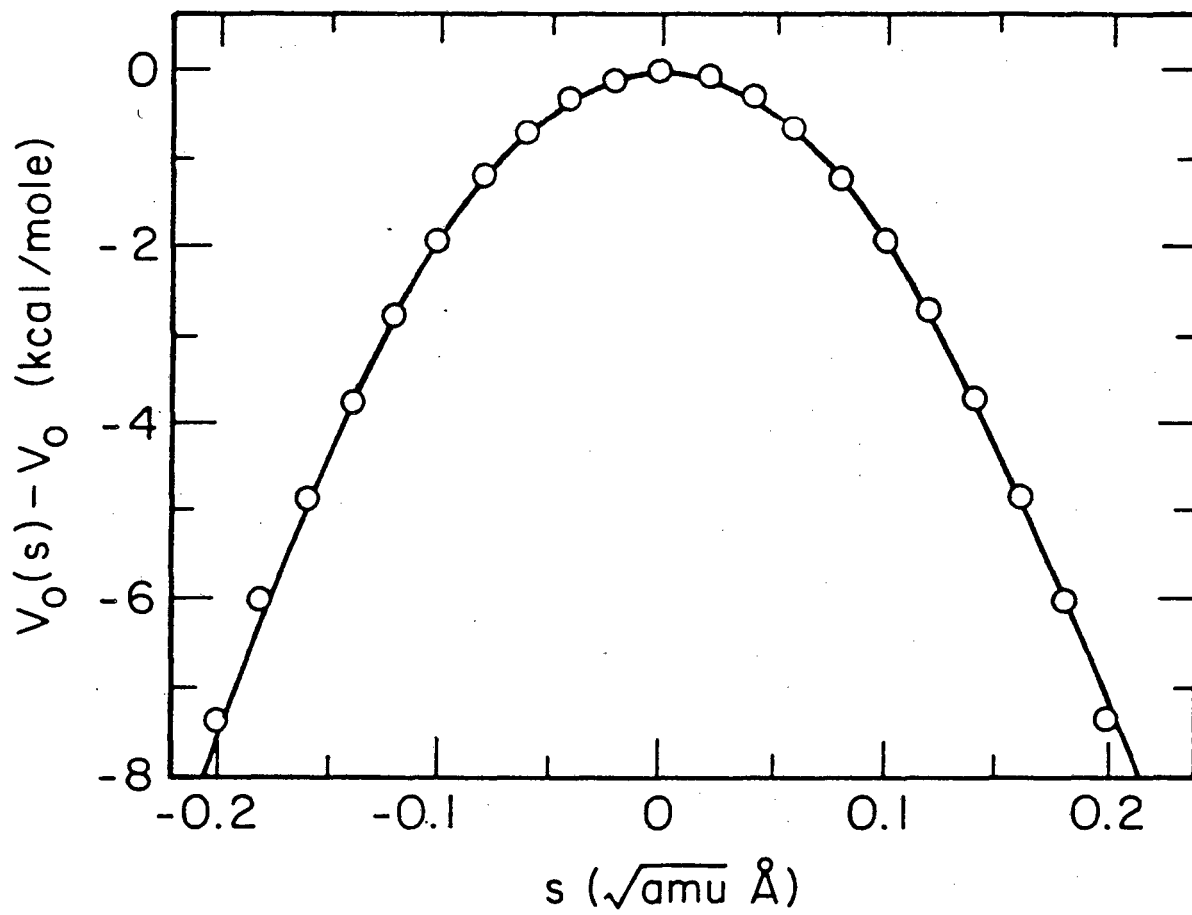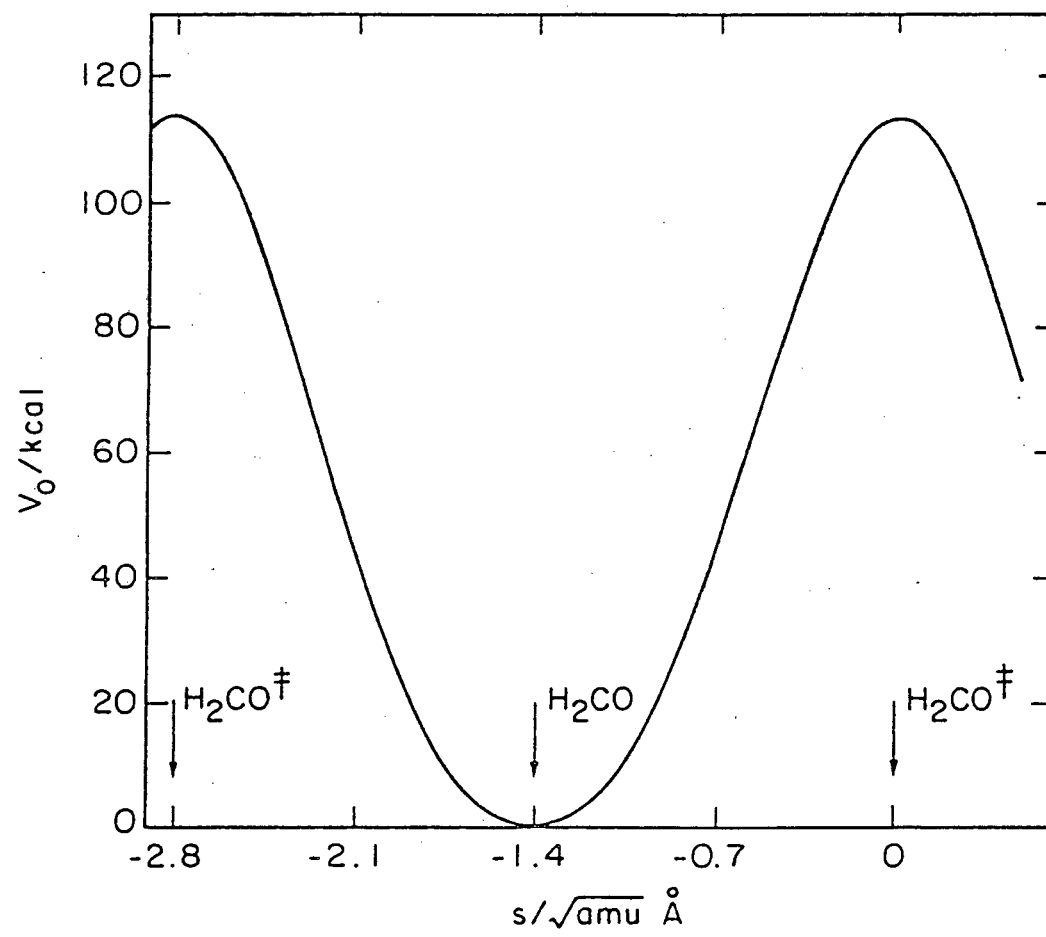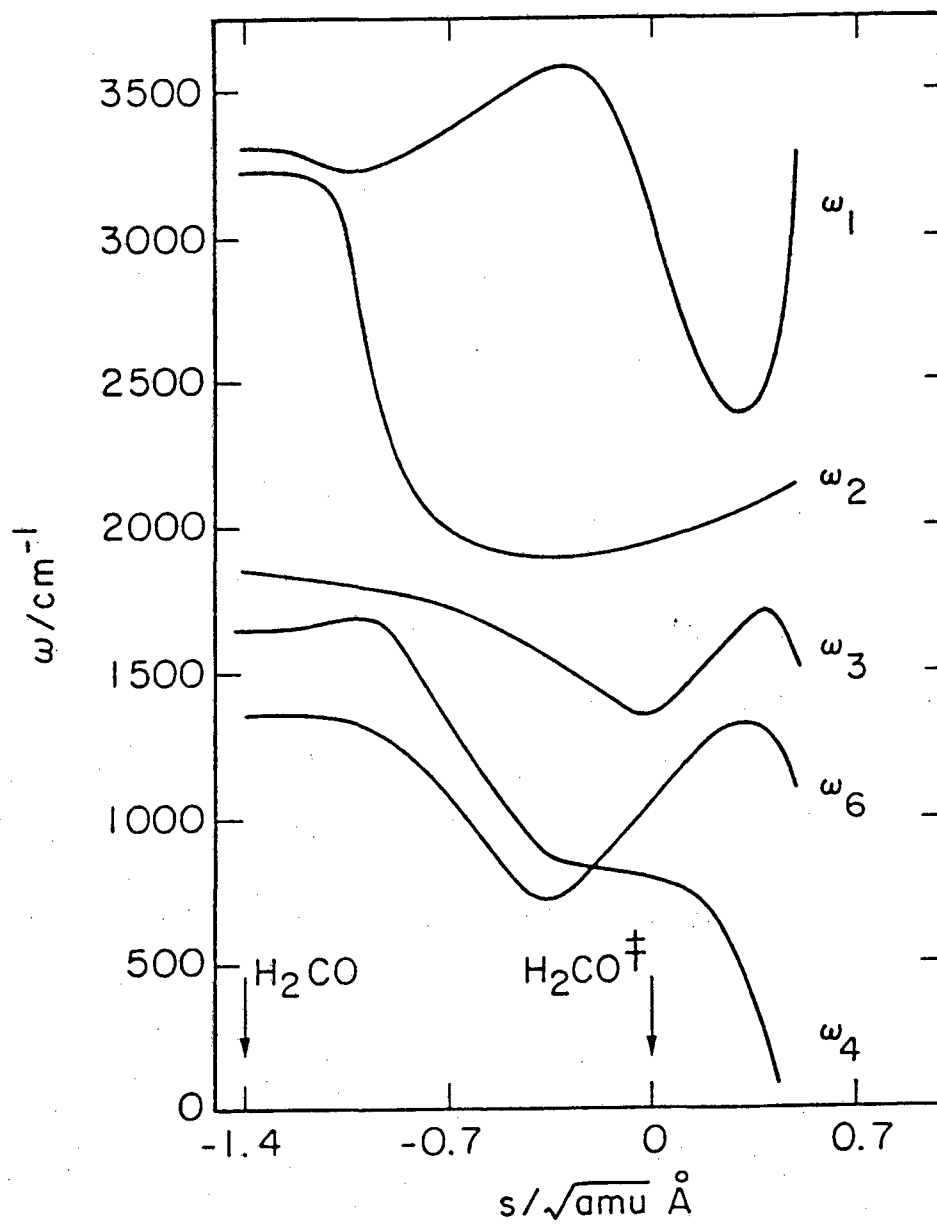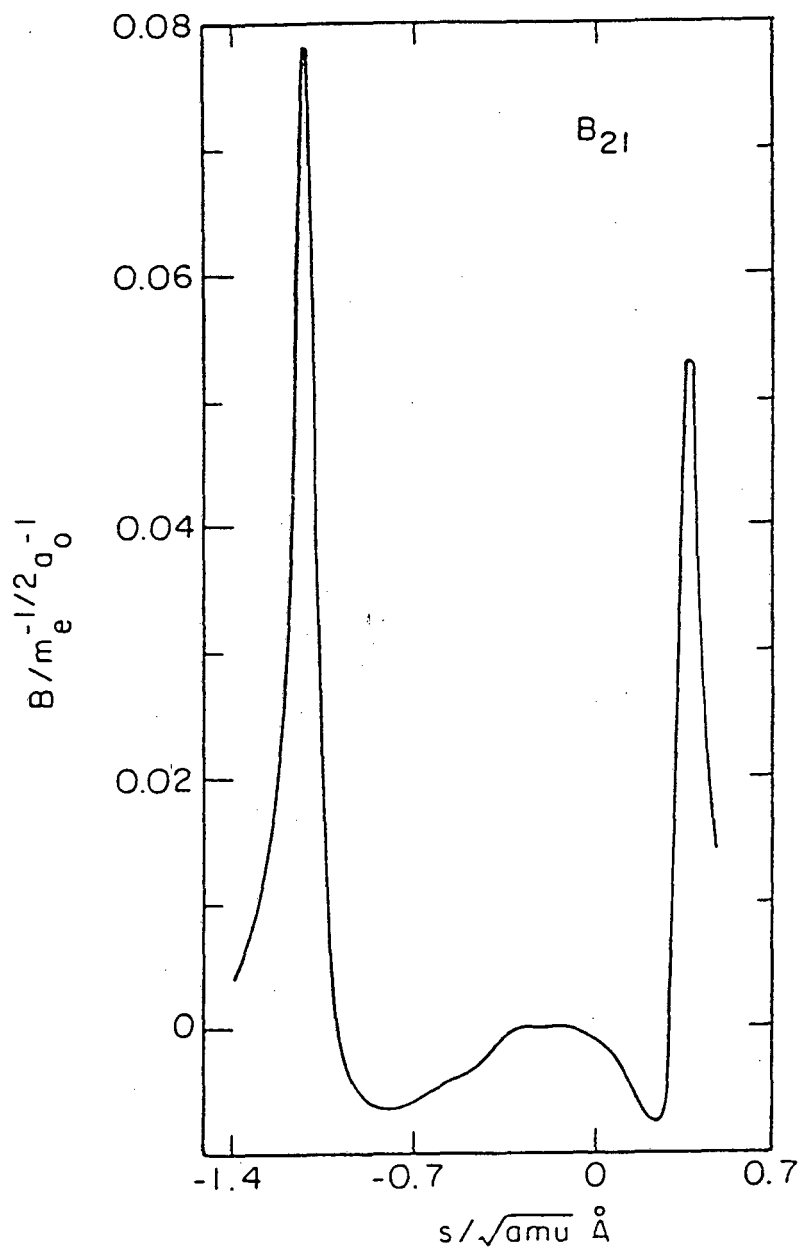
Figure 8

Figure 9

Figure 10a
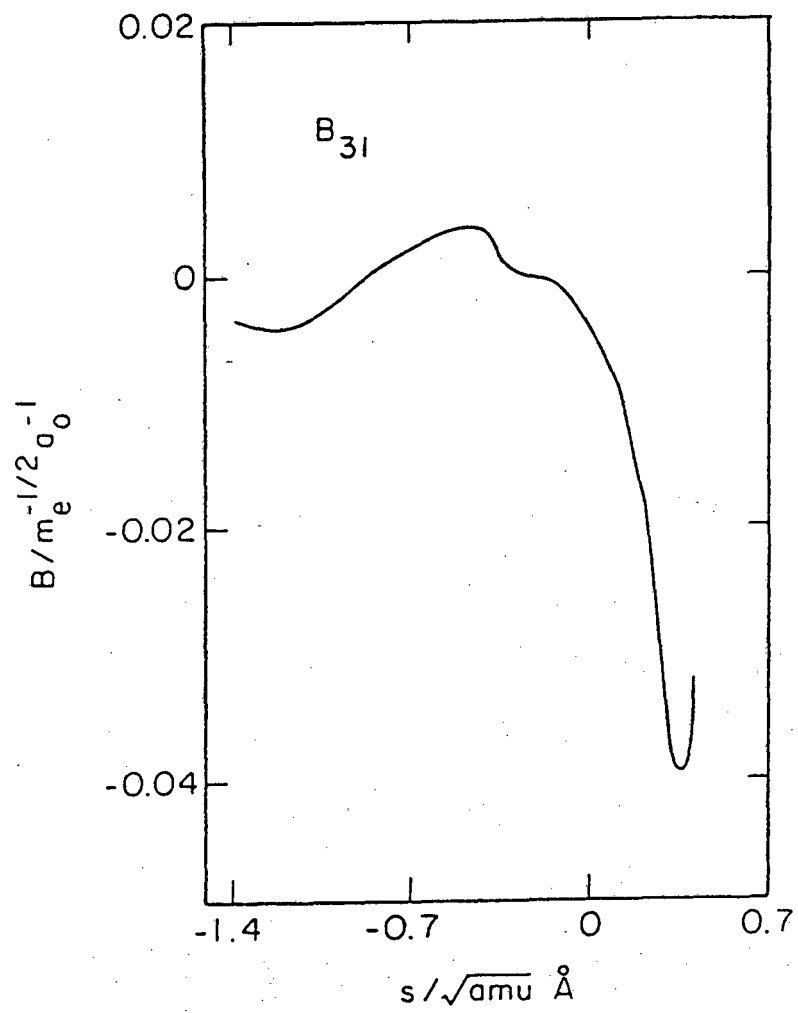
Figure 10b
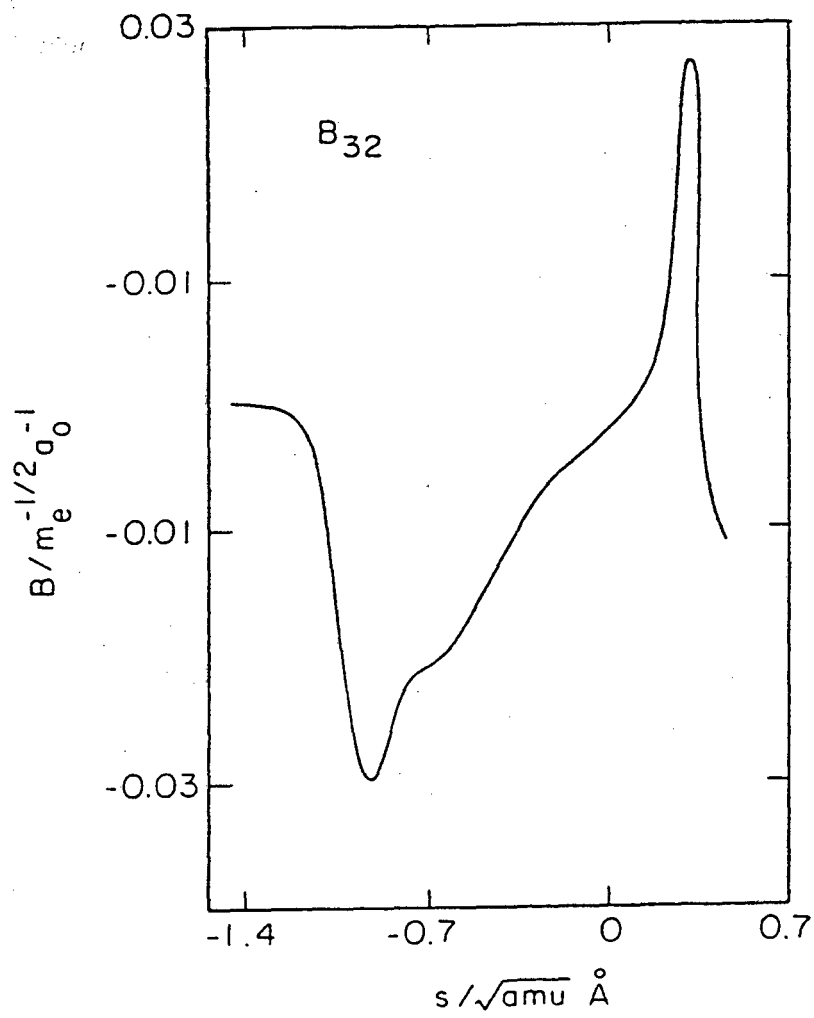
Figure 10c
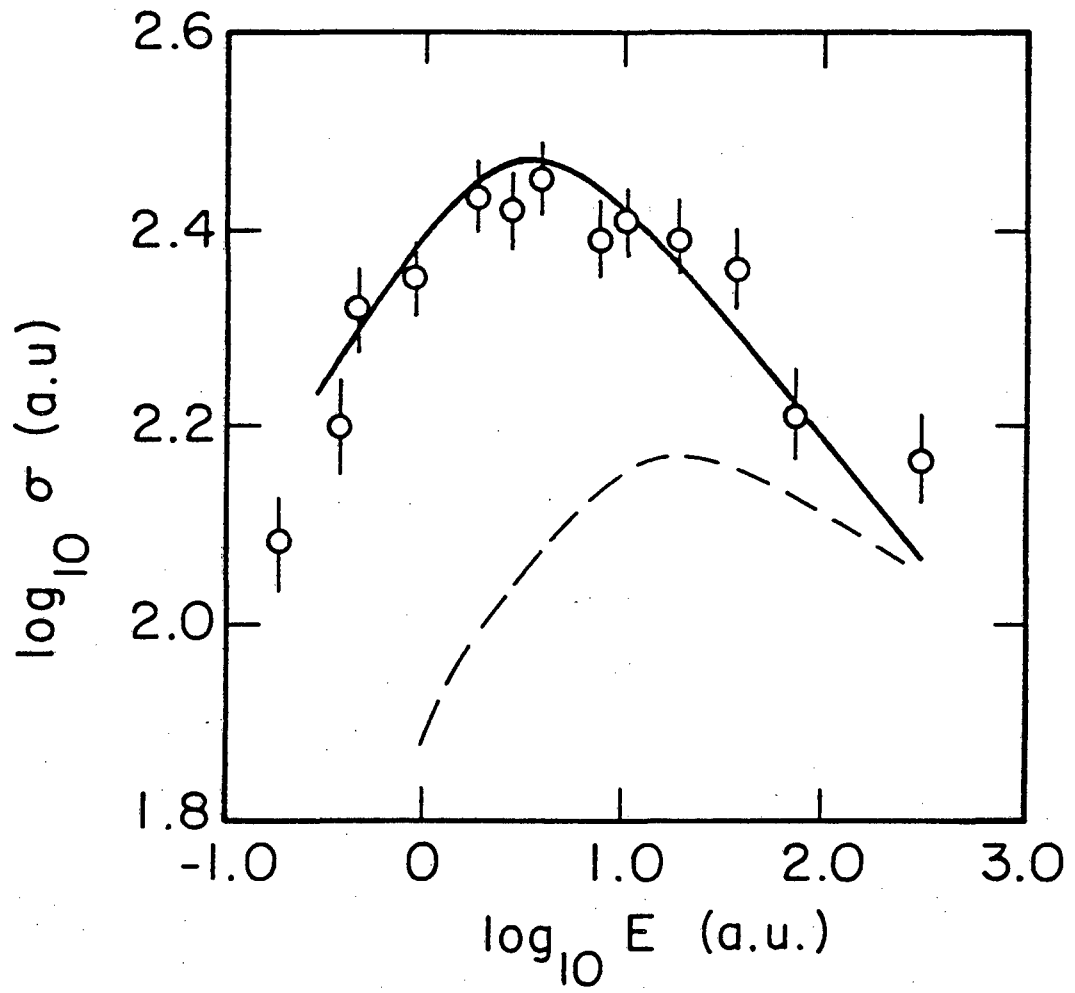
Figure 11
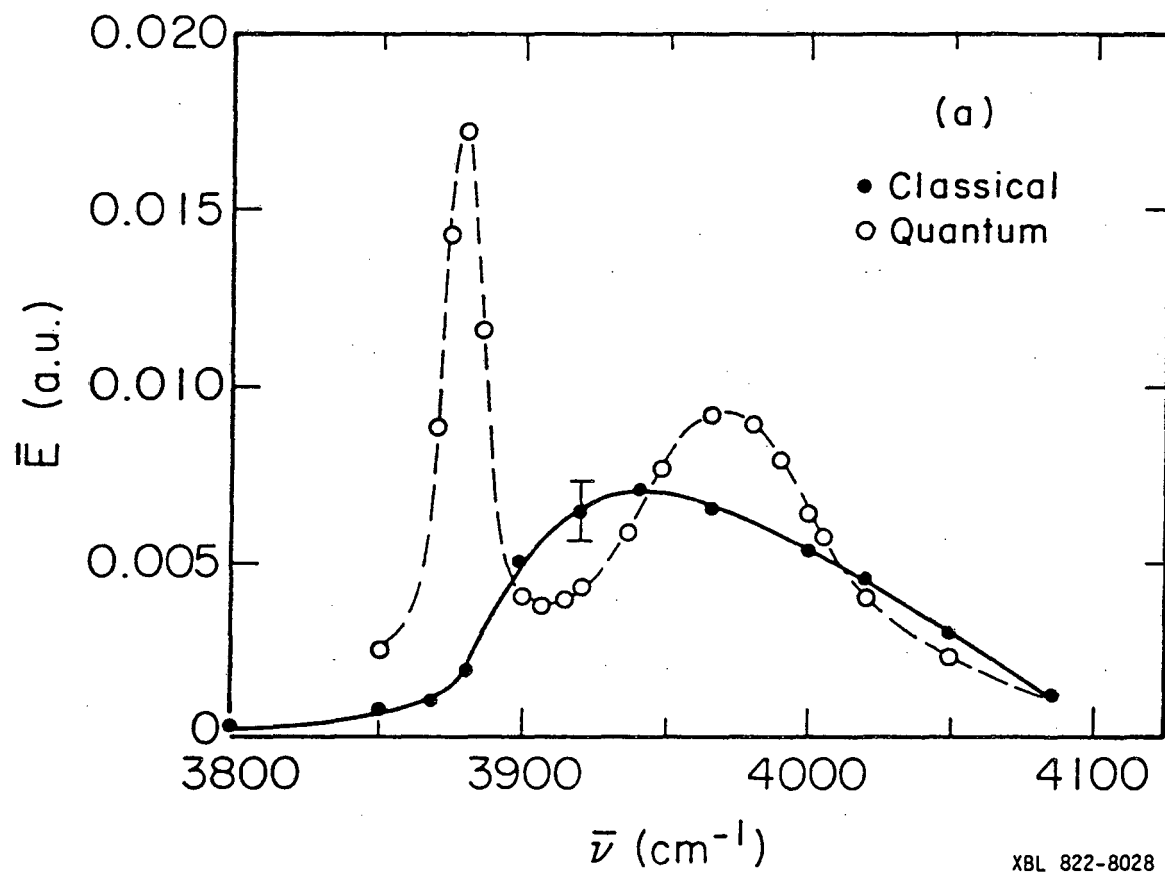
Figure 12a.
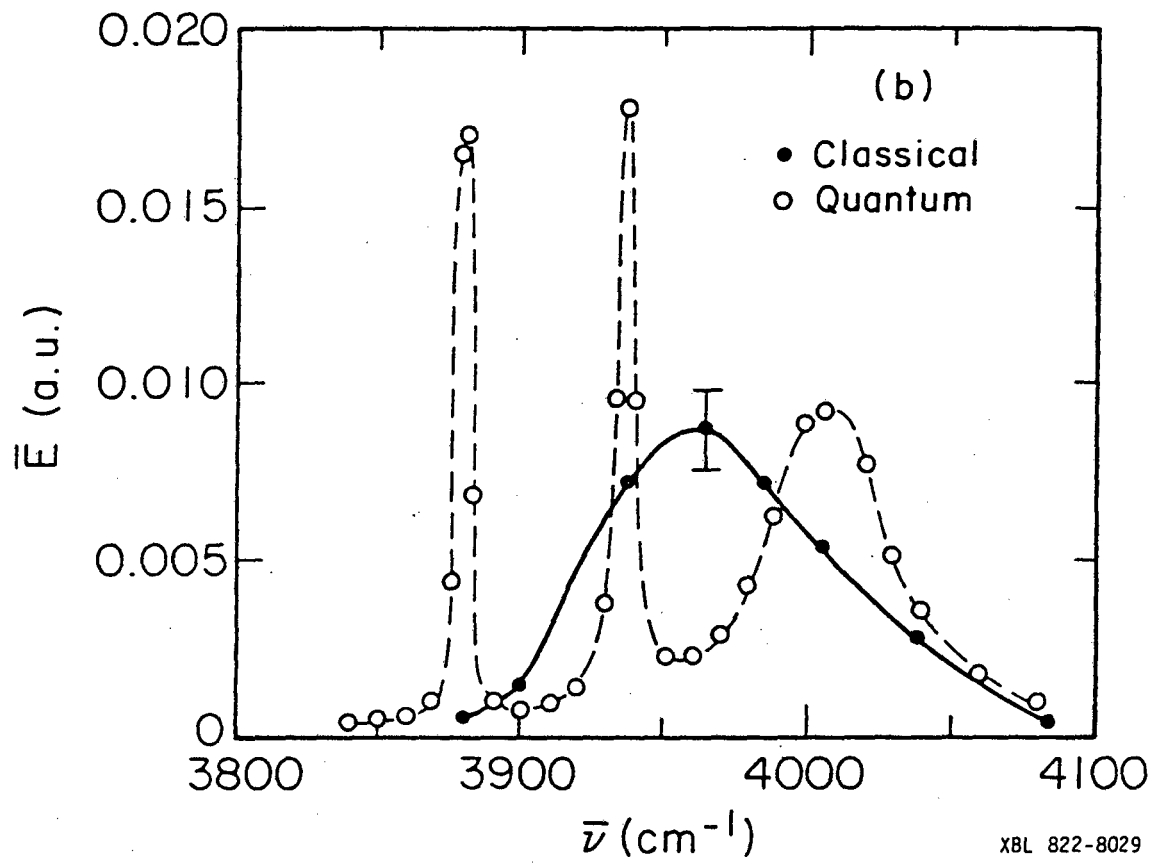
Figure 12b.
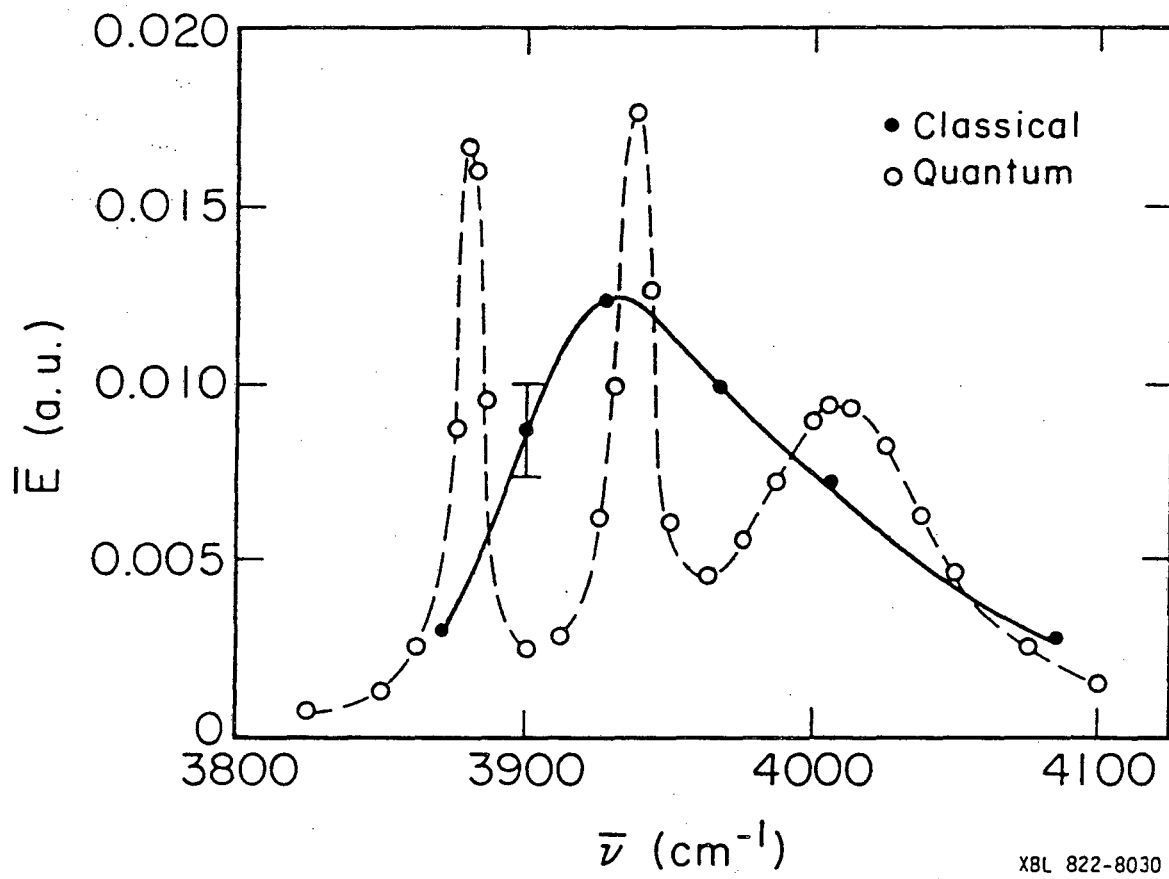
Figure 13.
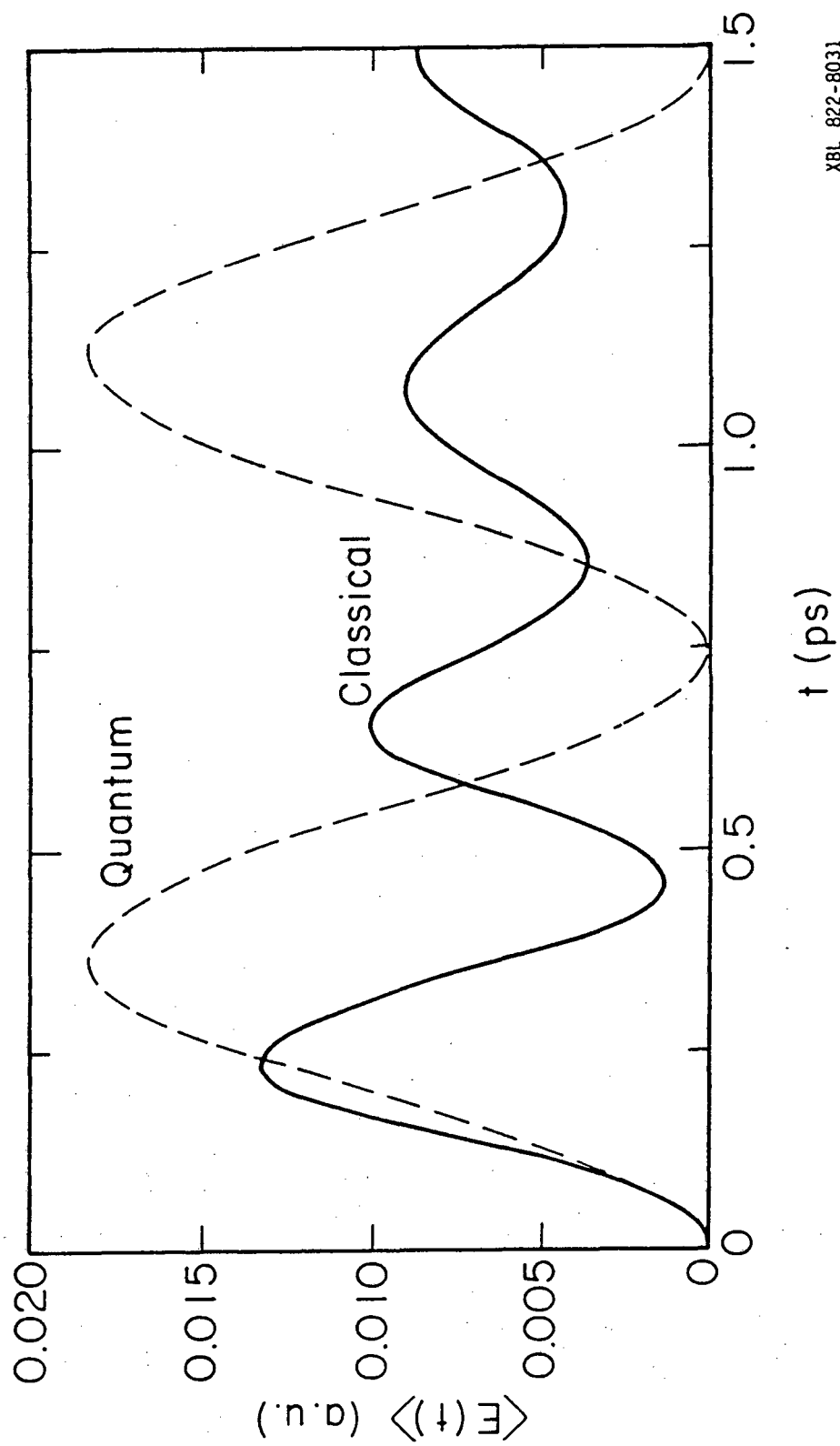
XBL 822-8030

XBL 822-8031

Figure 14.
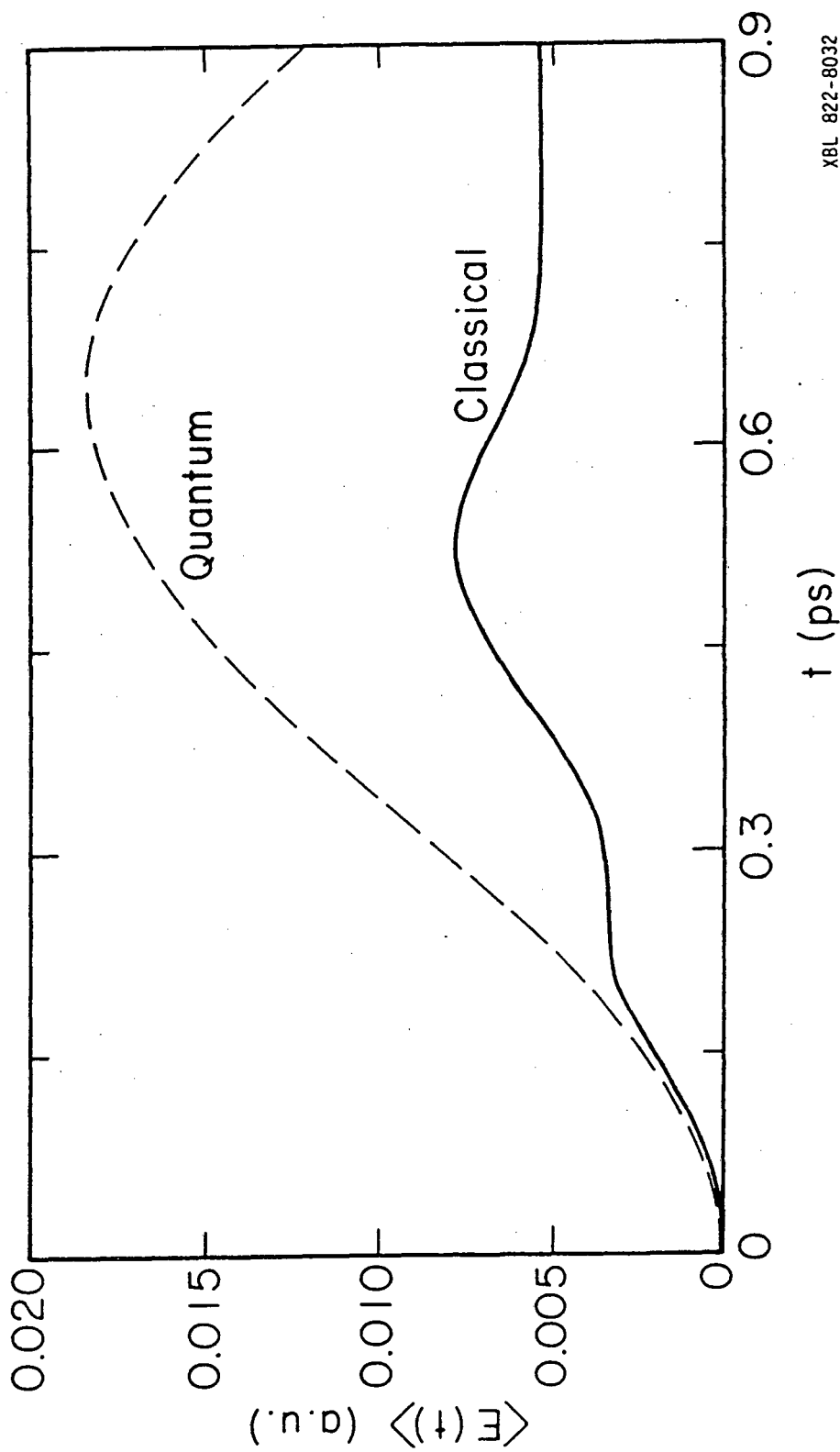
Figure 15.

XBL 822-8032

Figure 16.
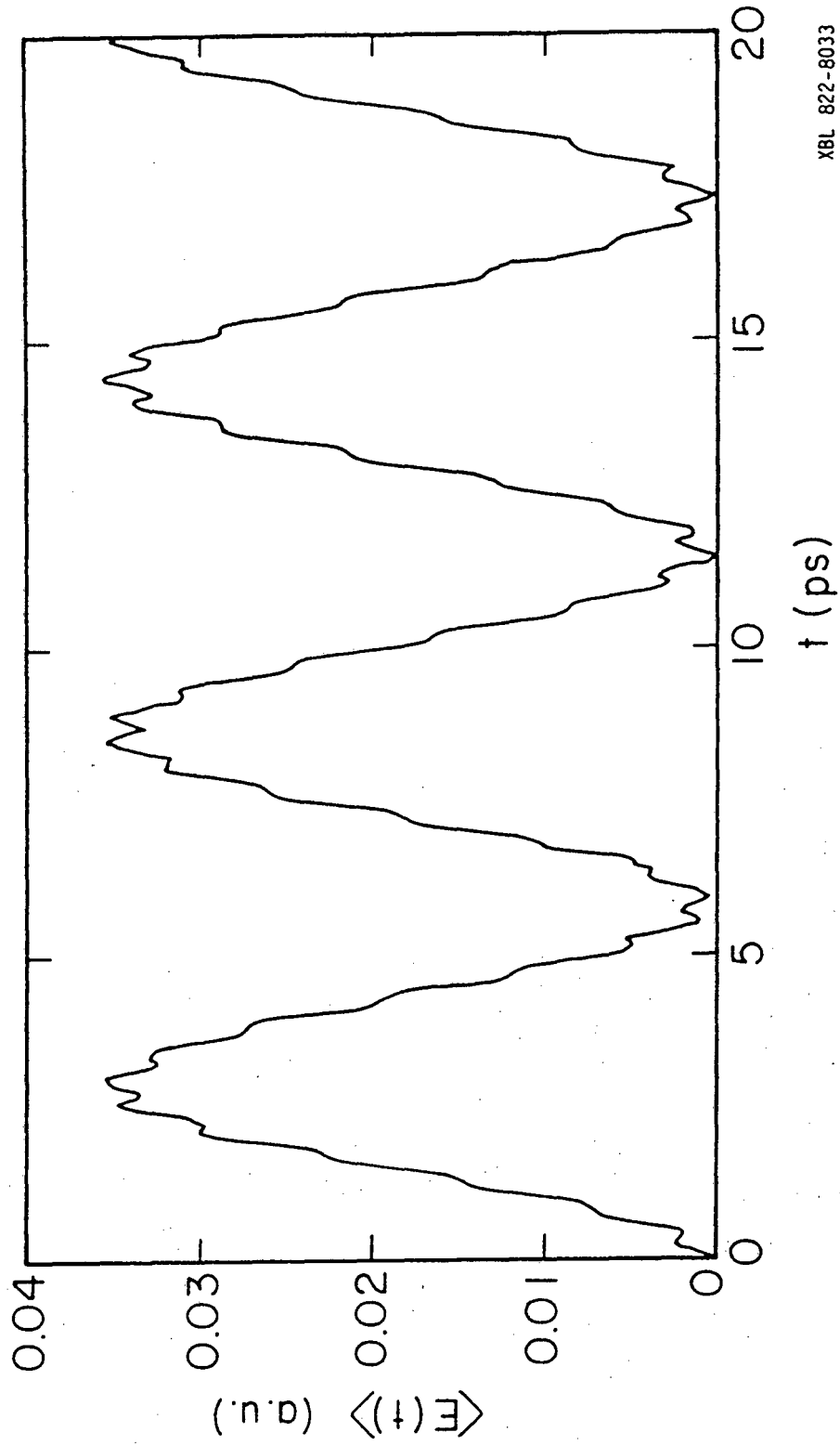
XBL 822-8033
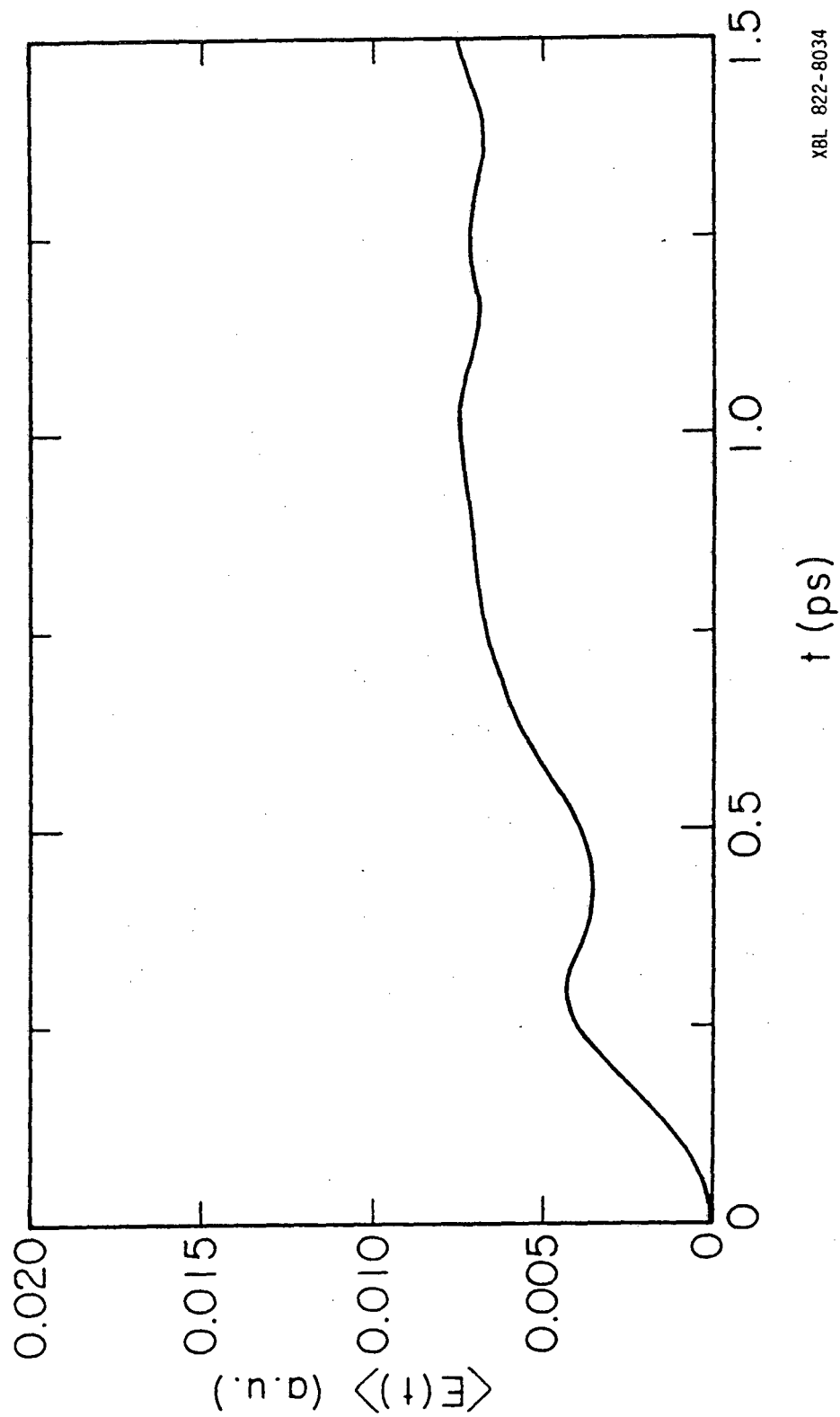
XBL 822-8034
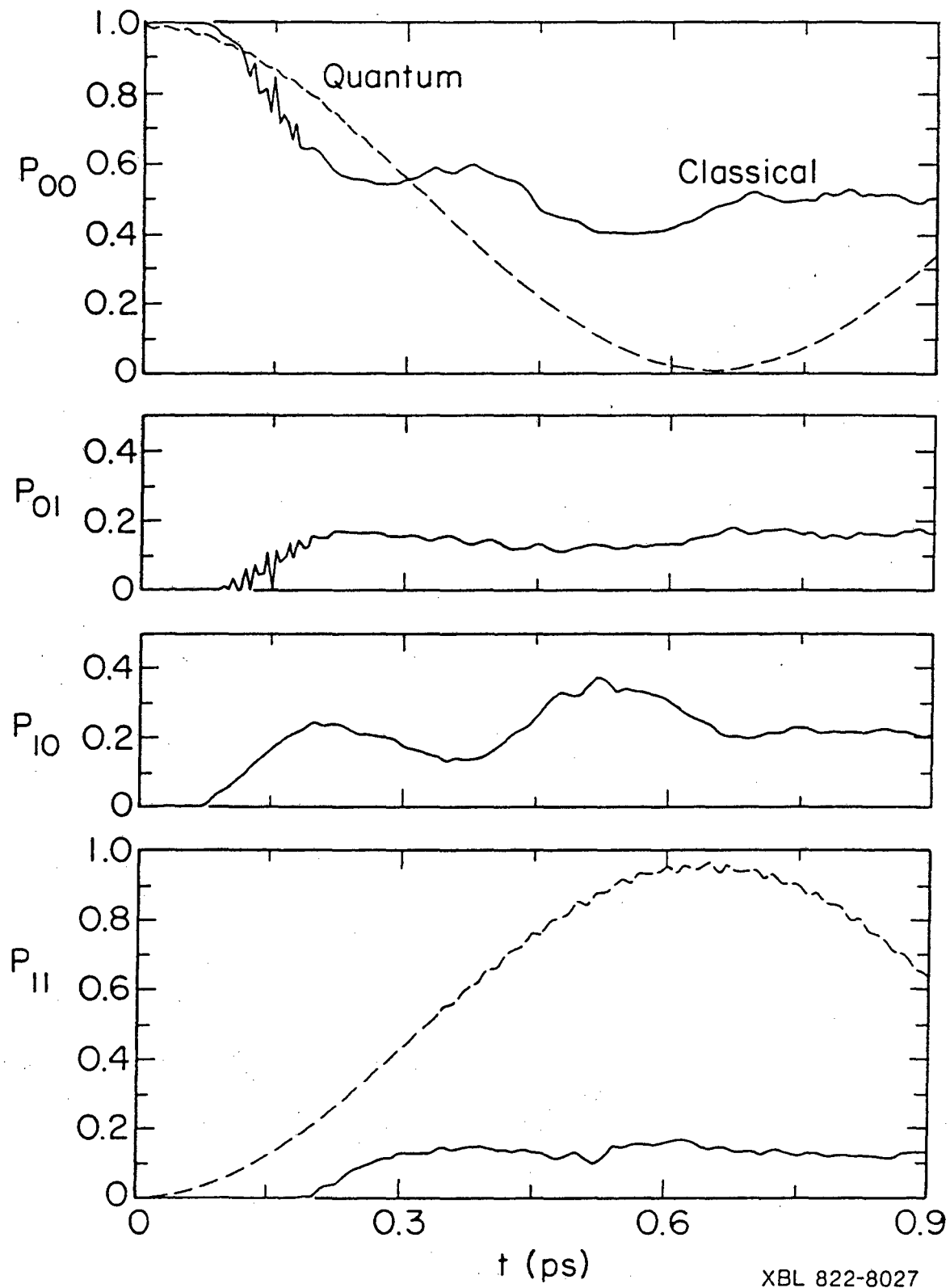
Figure 17.

Figure 18.
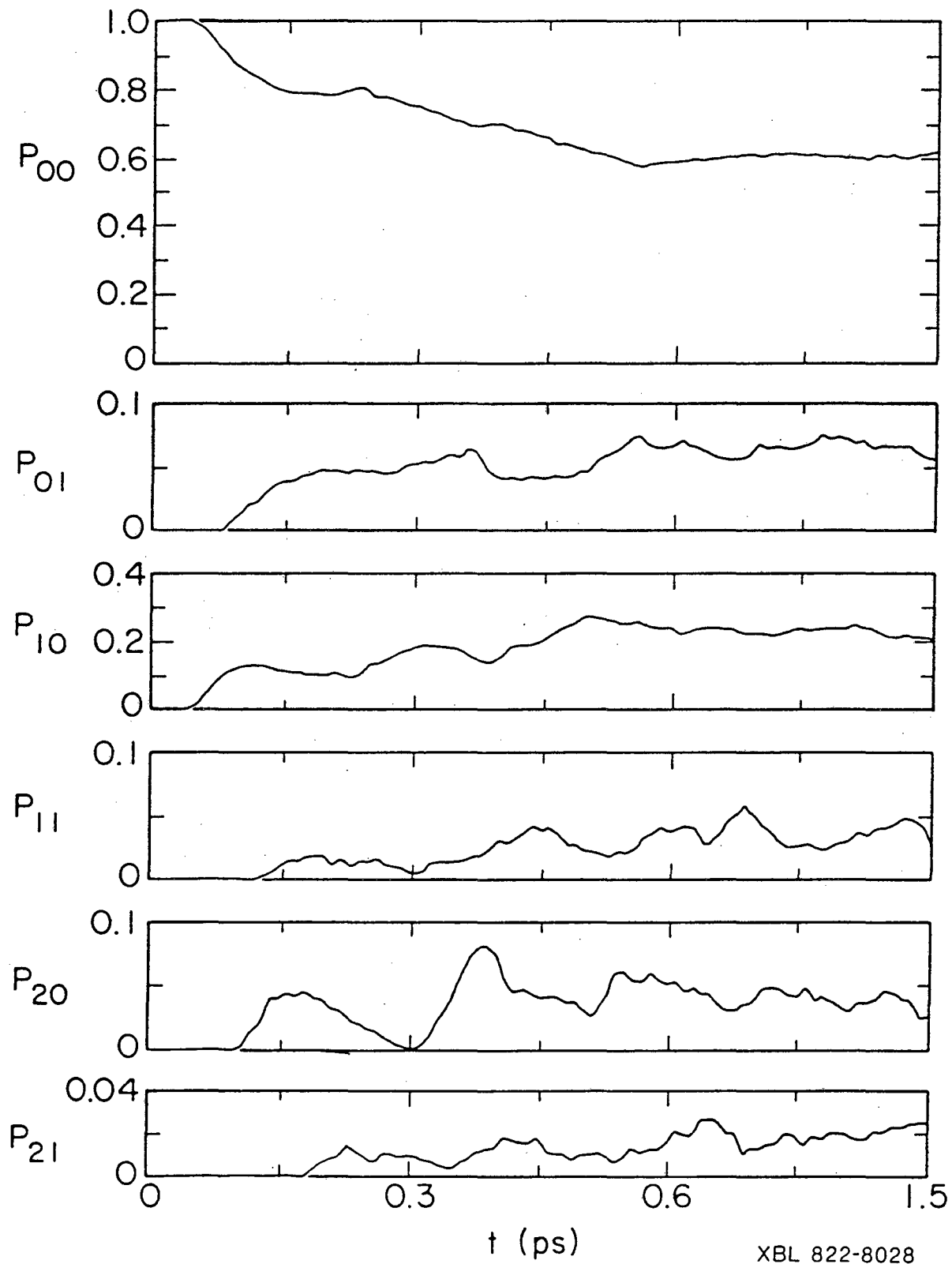
XBL 822-8027

XBL 822-8028

Figure 19.
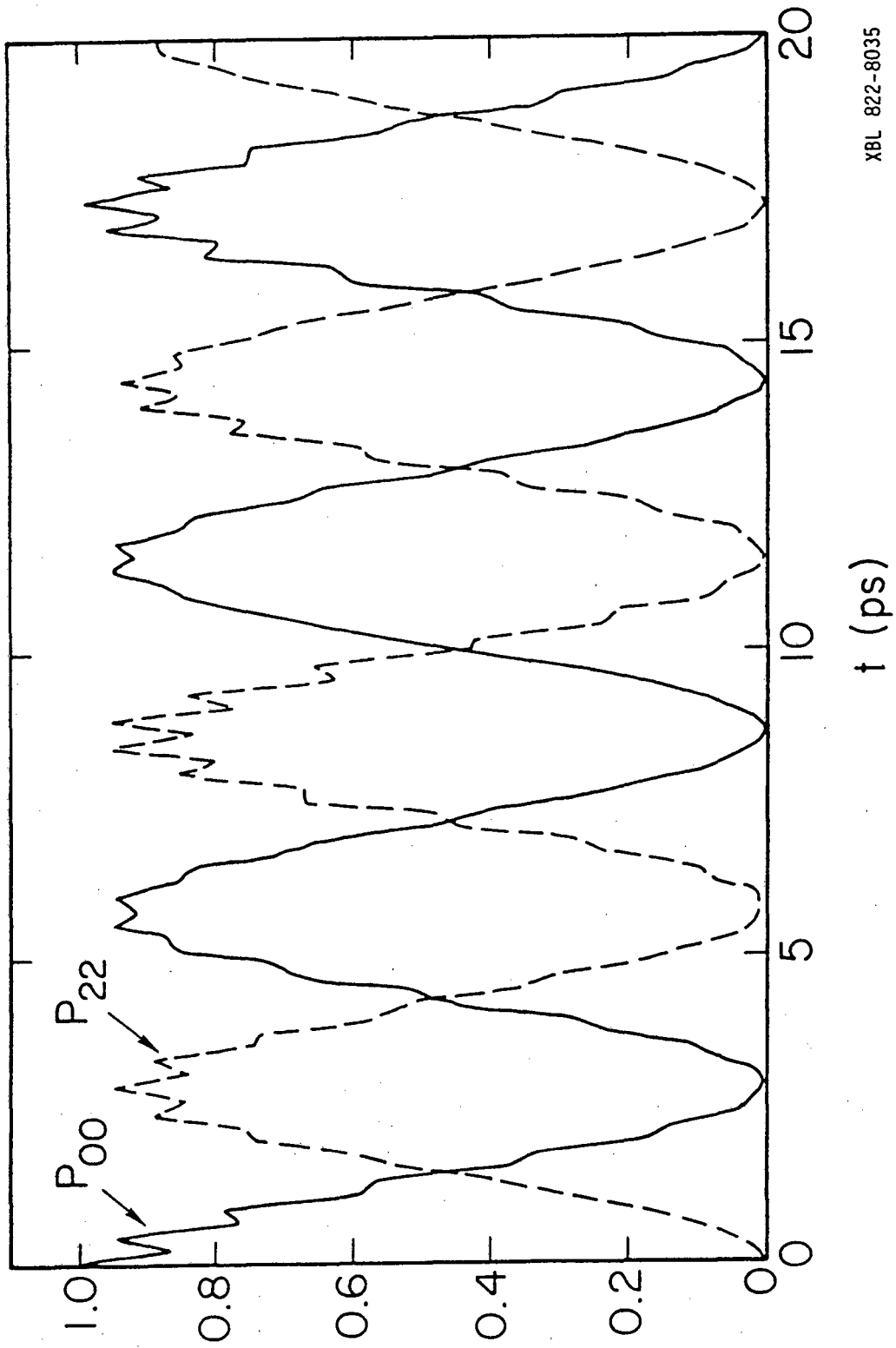
Figure 20.

XBL 822-8035

Figure 21a.

153
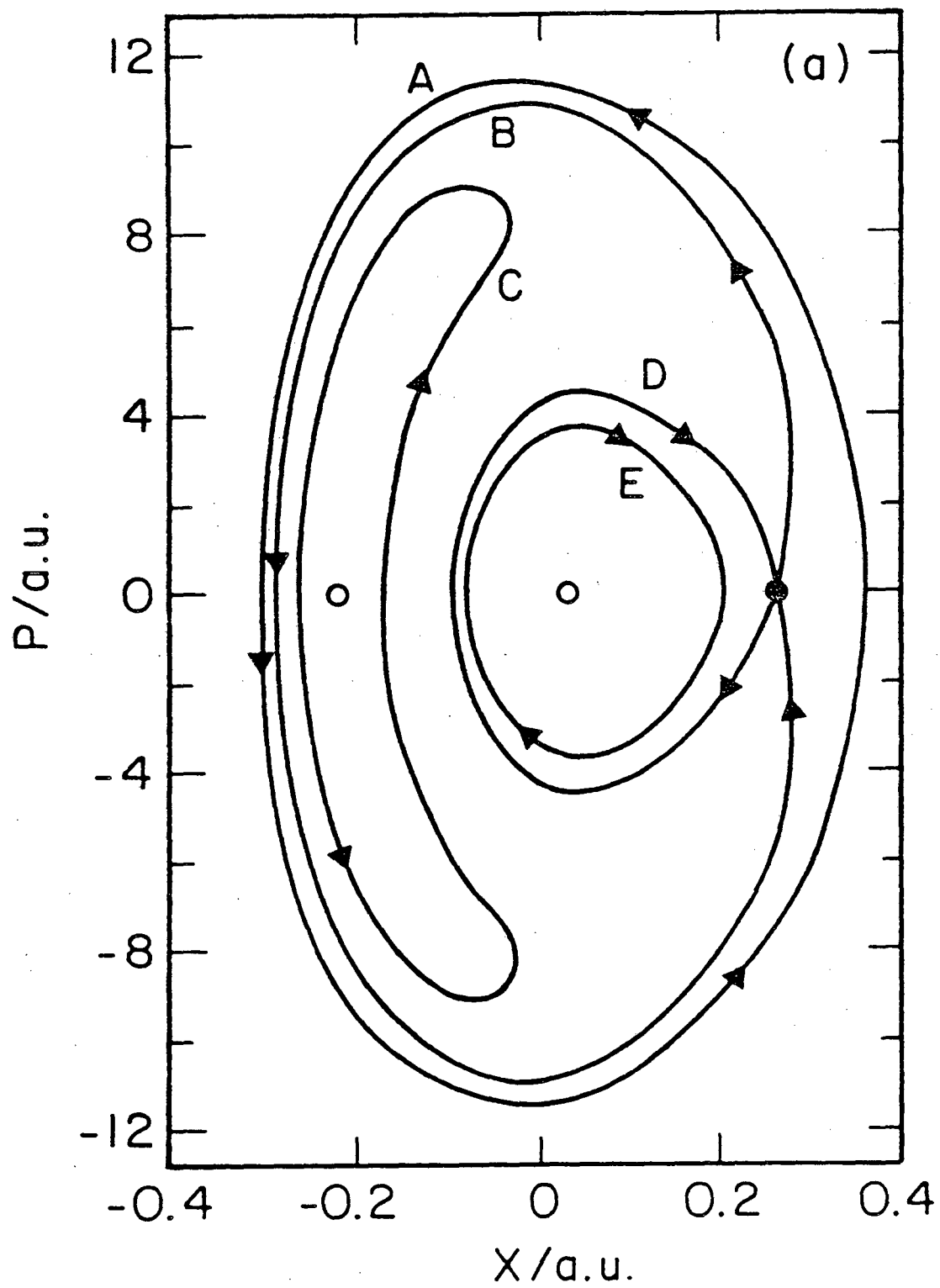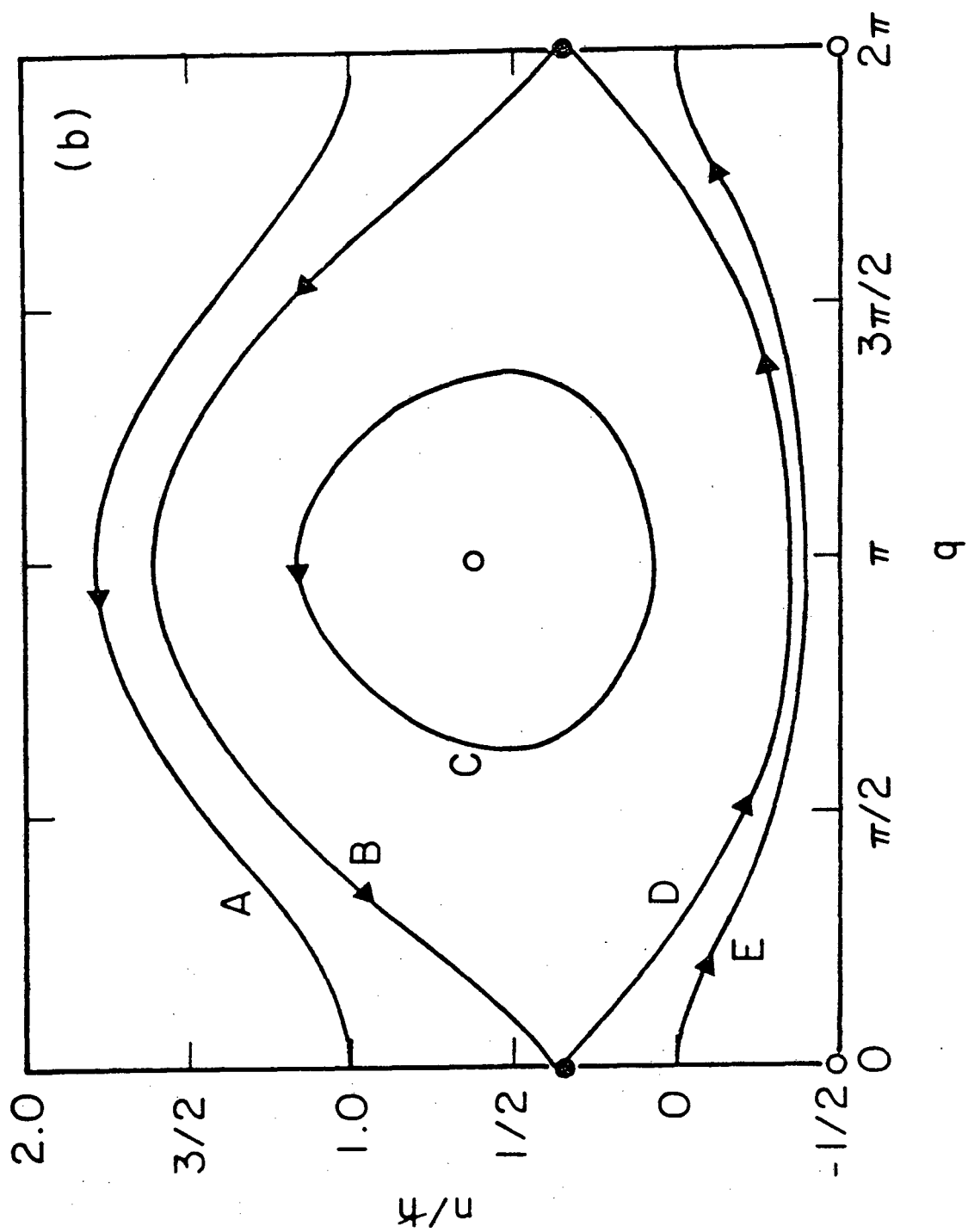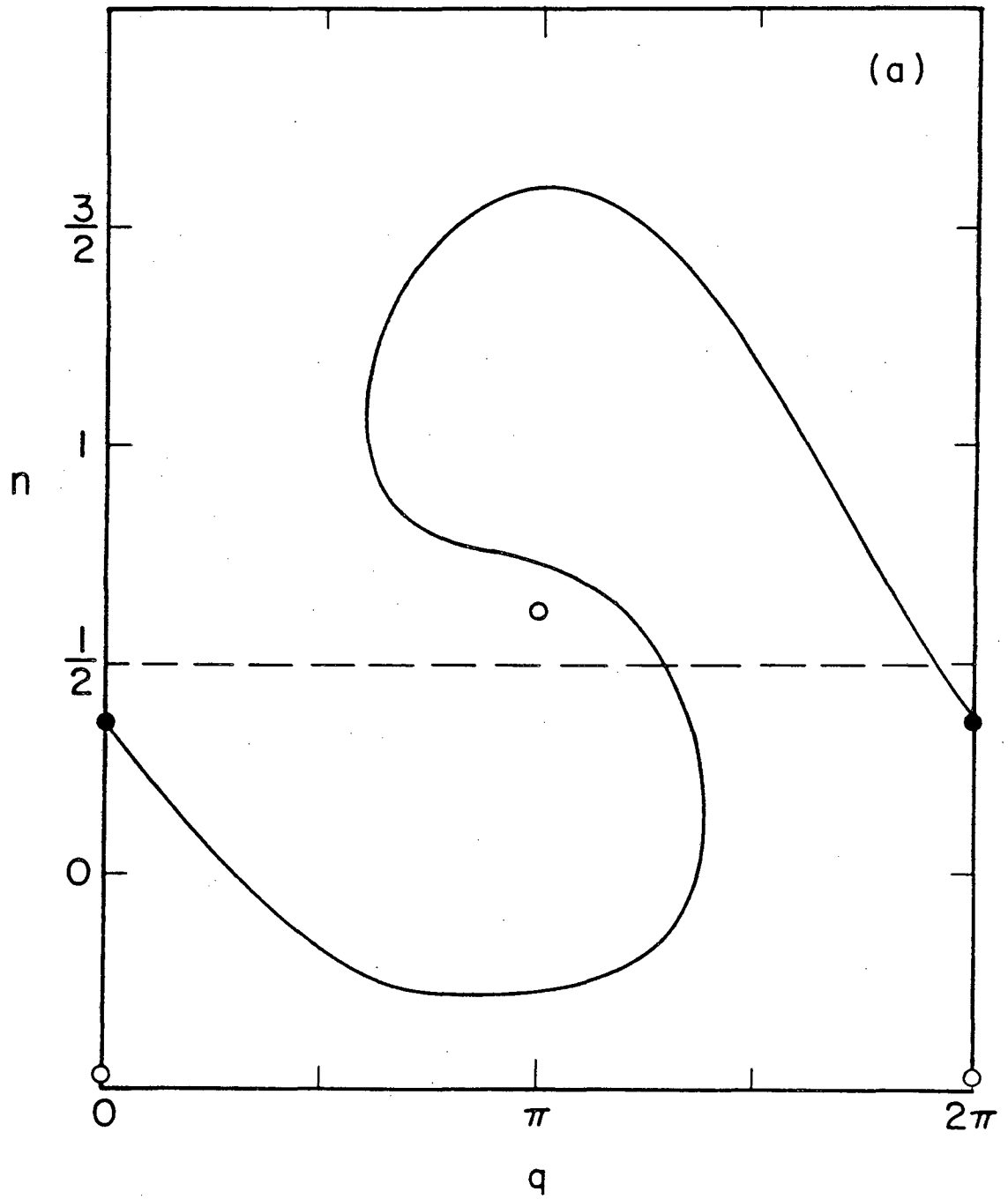
Figure 21b.

Figure 22a.
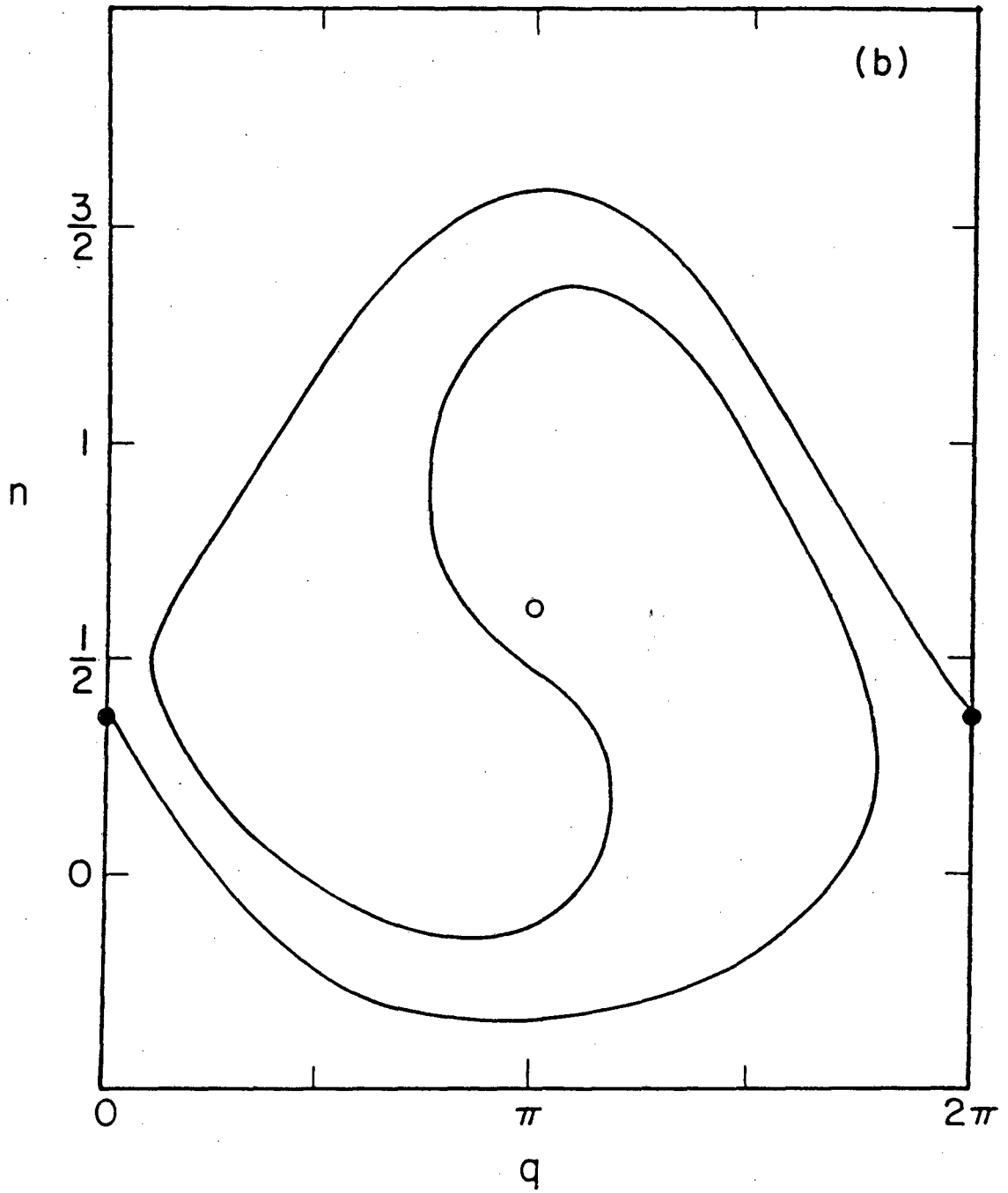
Figure 22b.
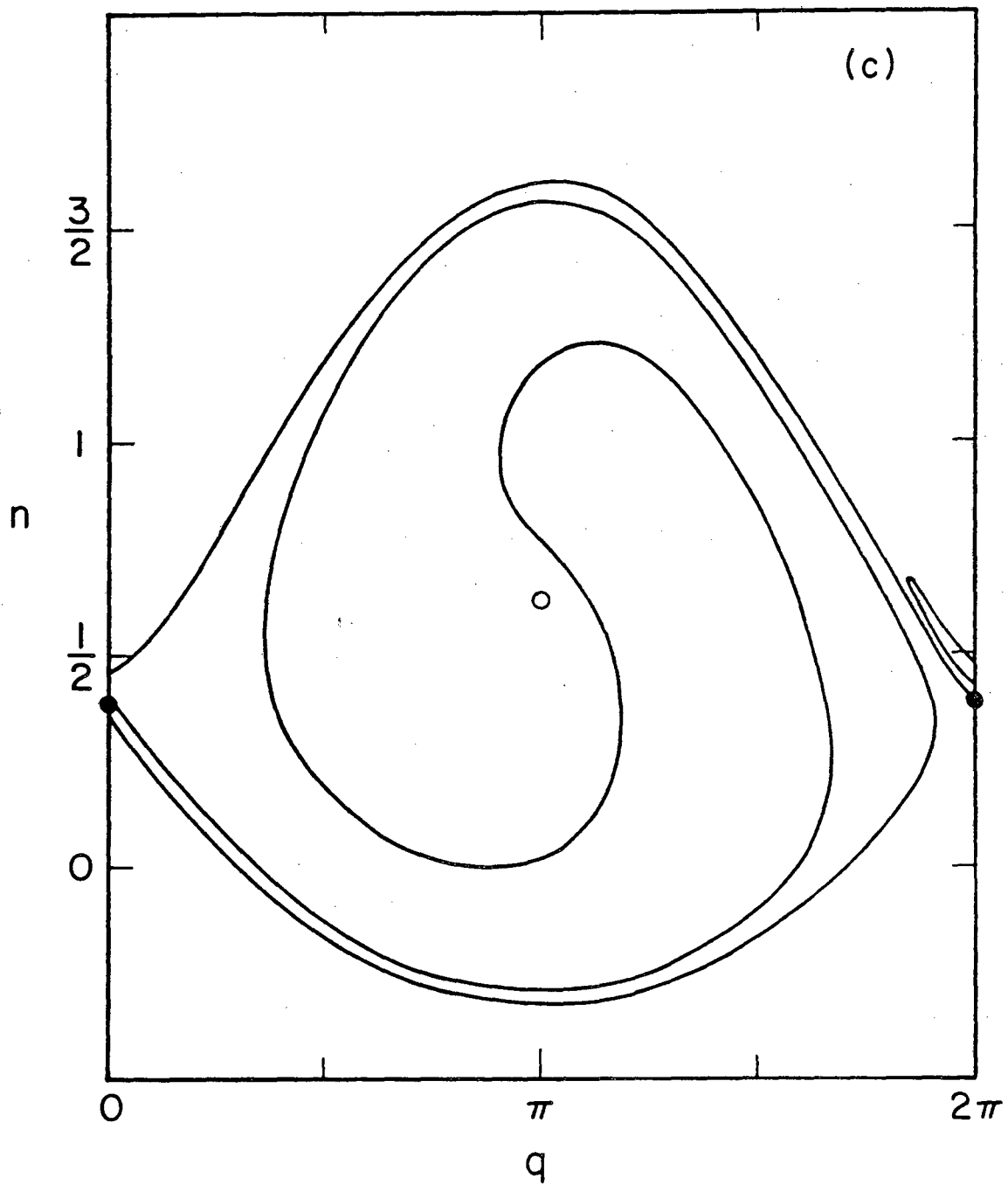
Figure 22c.
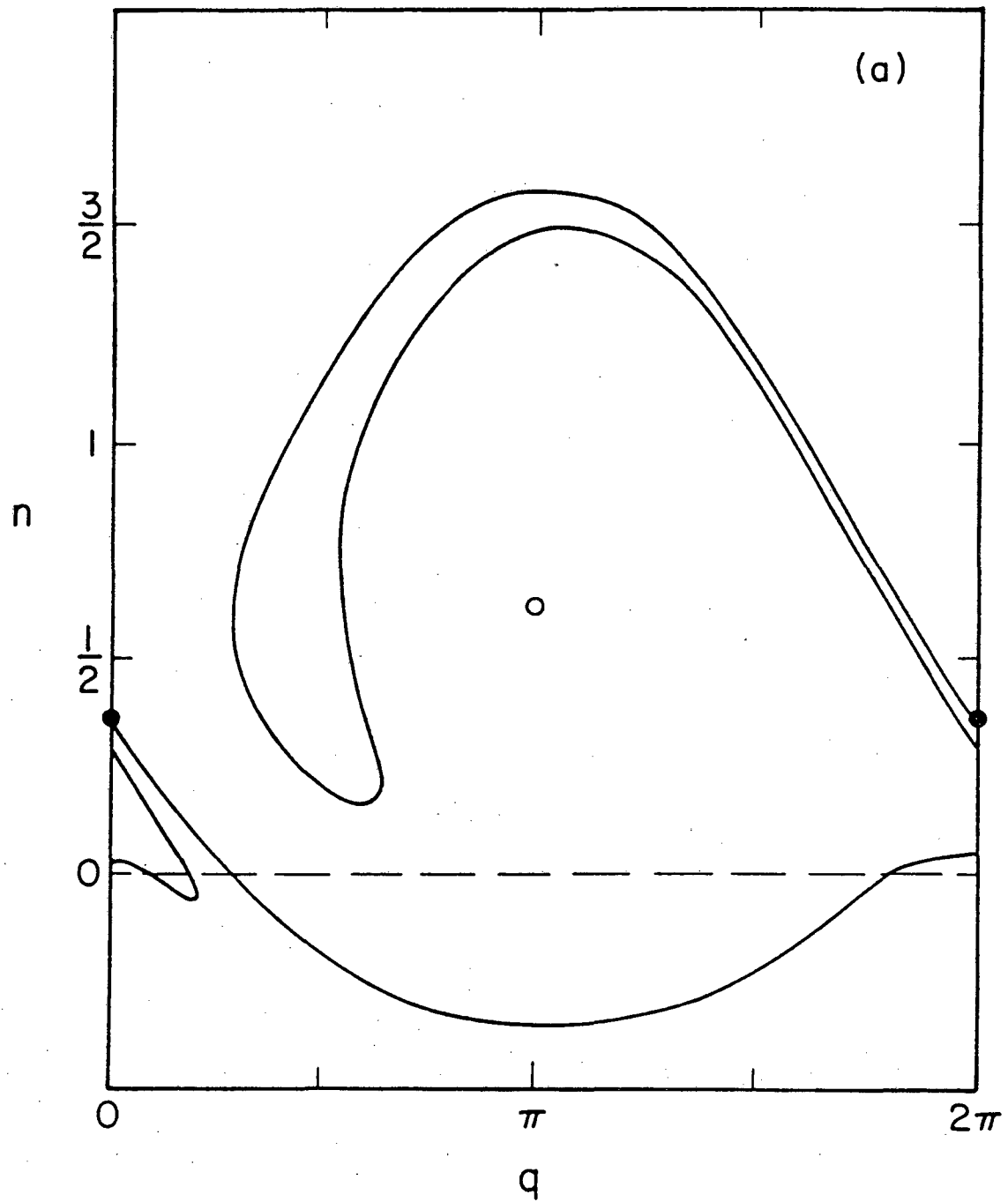
Figure 23a.
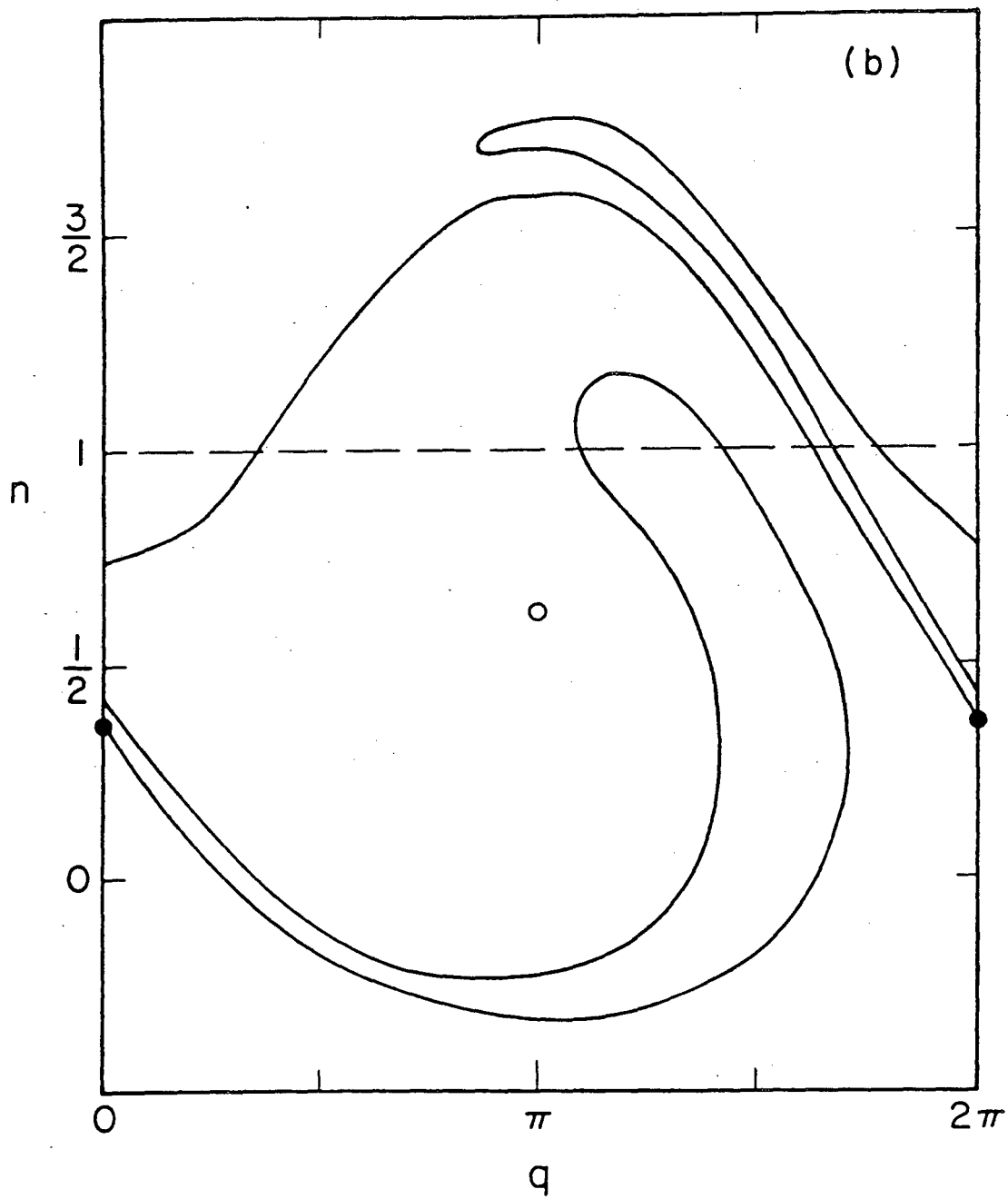
Figure 23b.
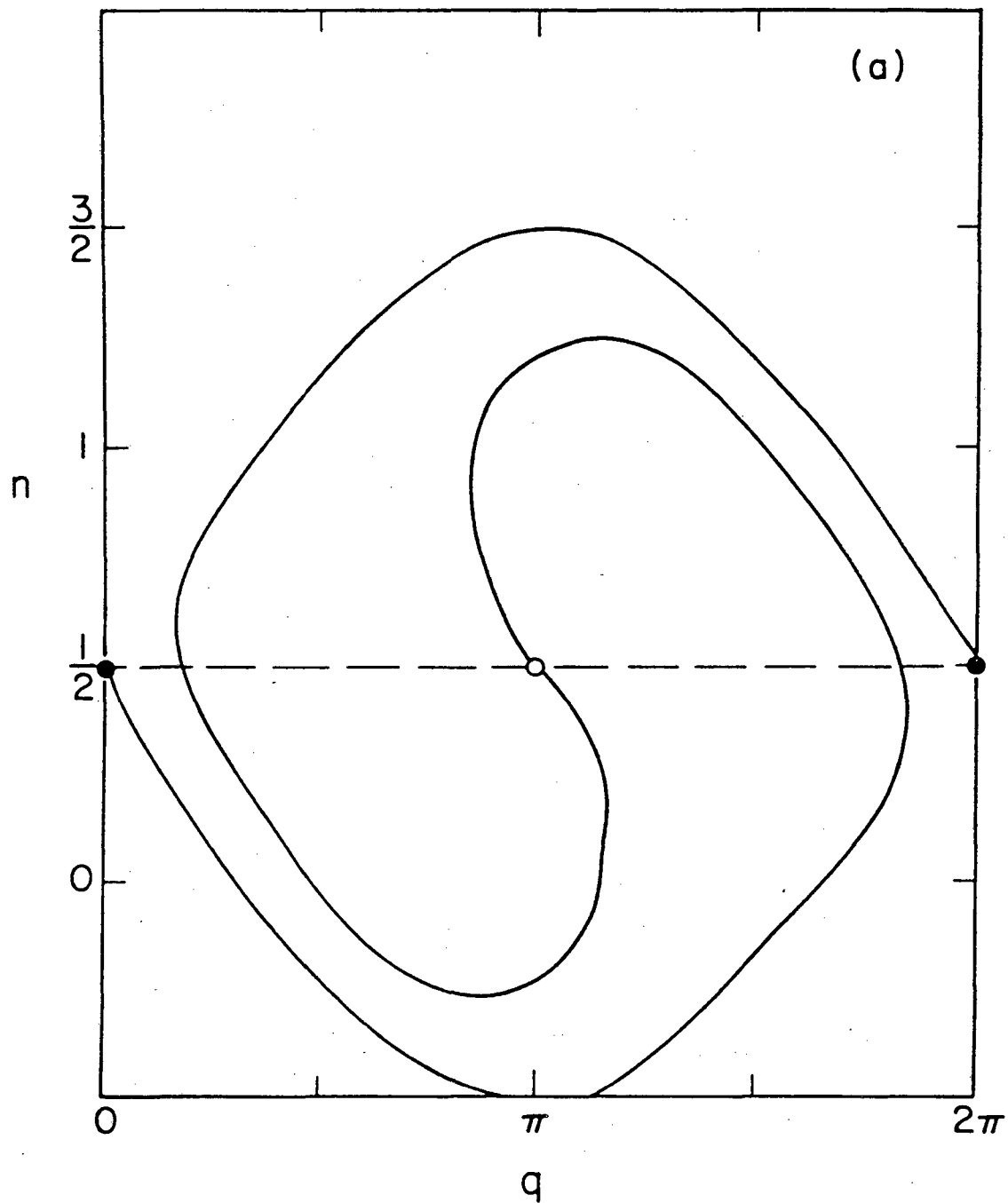
Figure 24a.
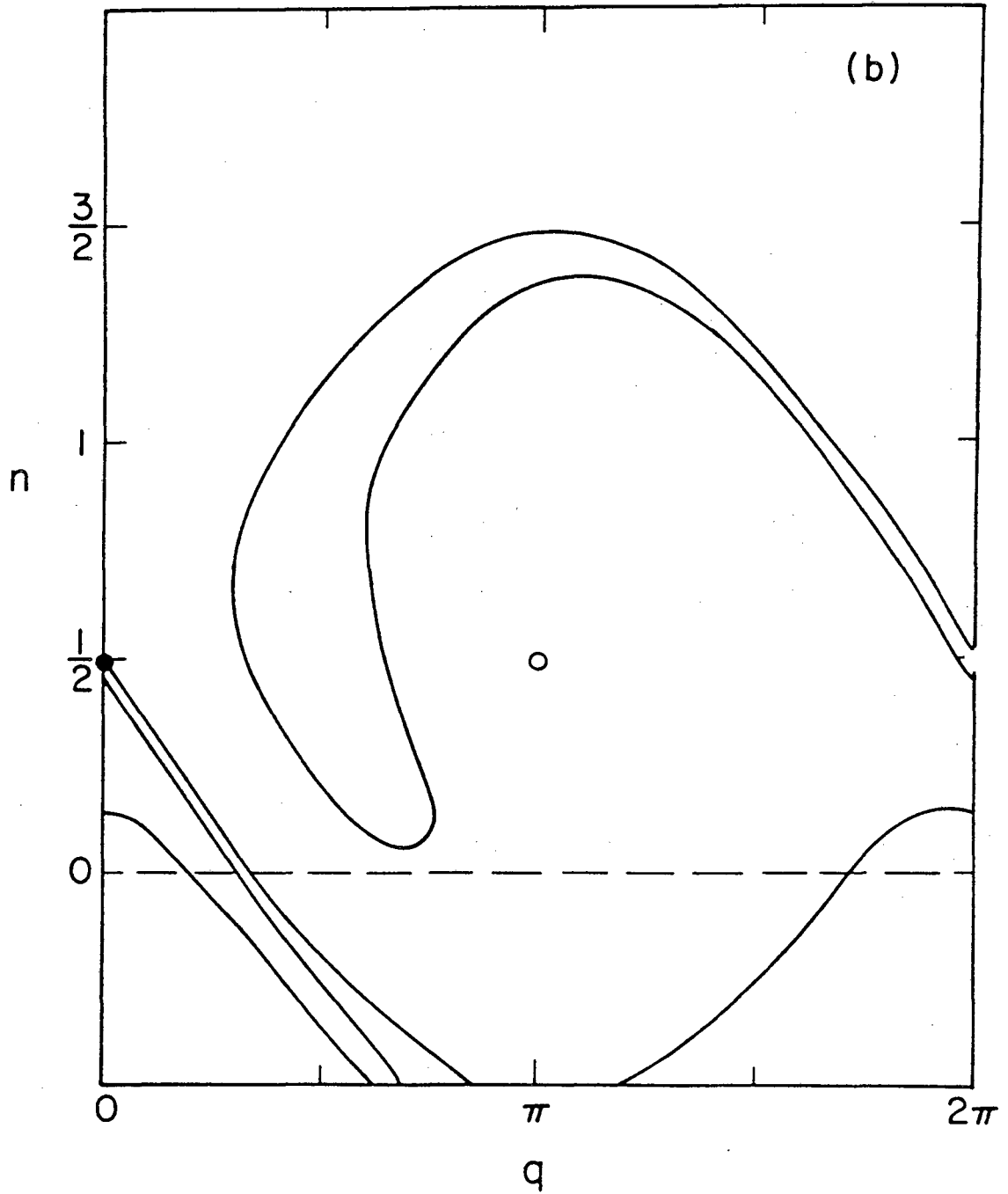
Figure 24b.
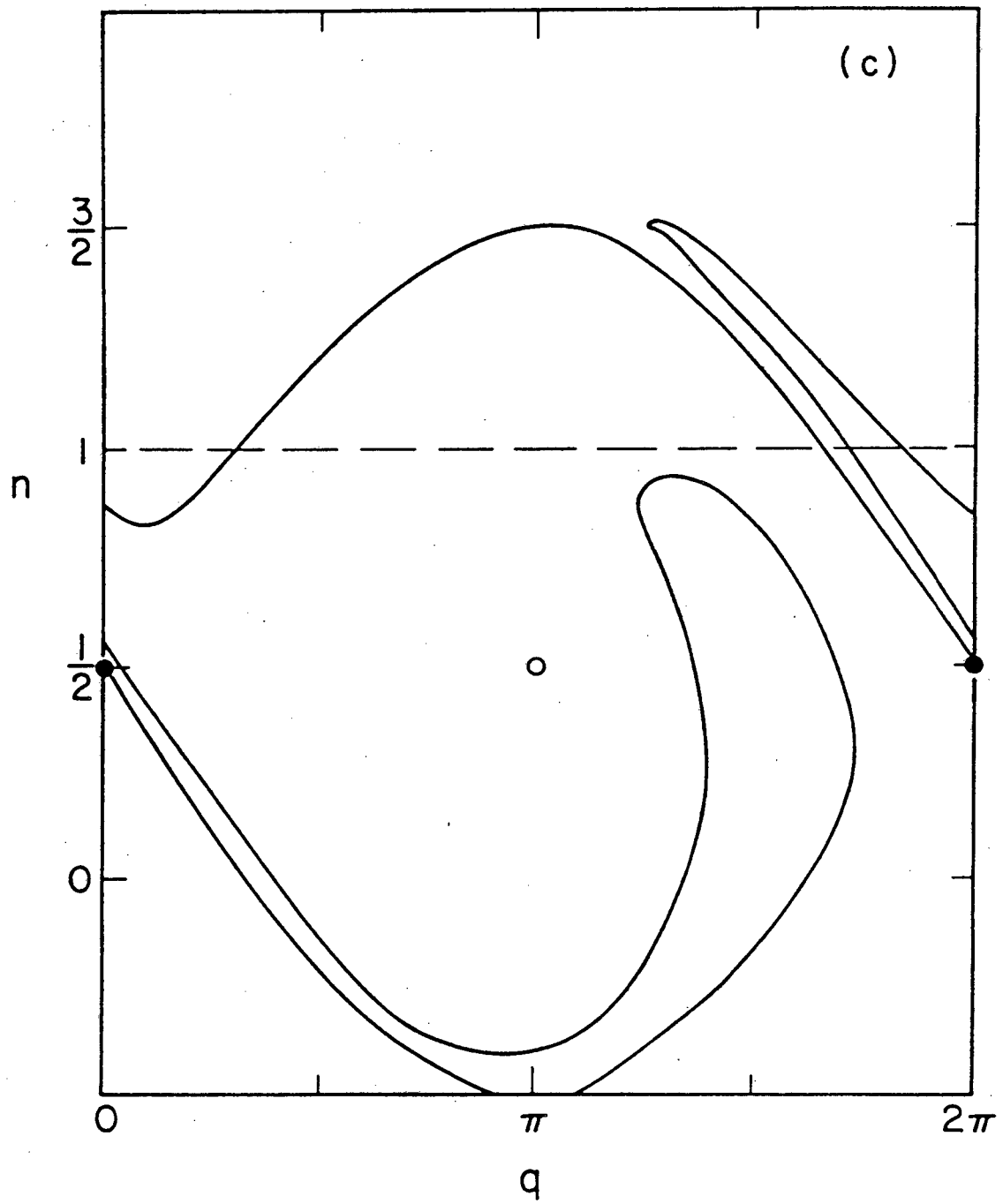
Figure 24c.
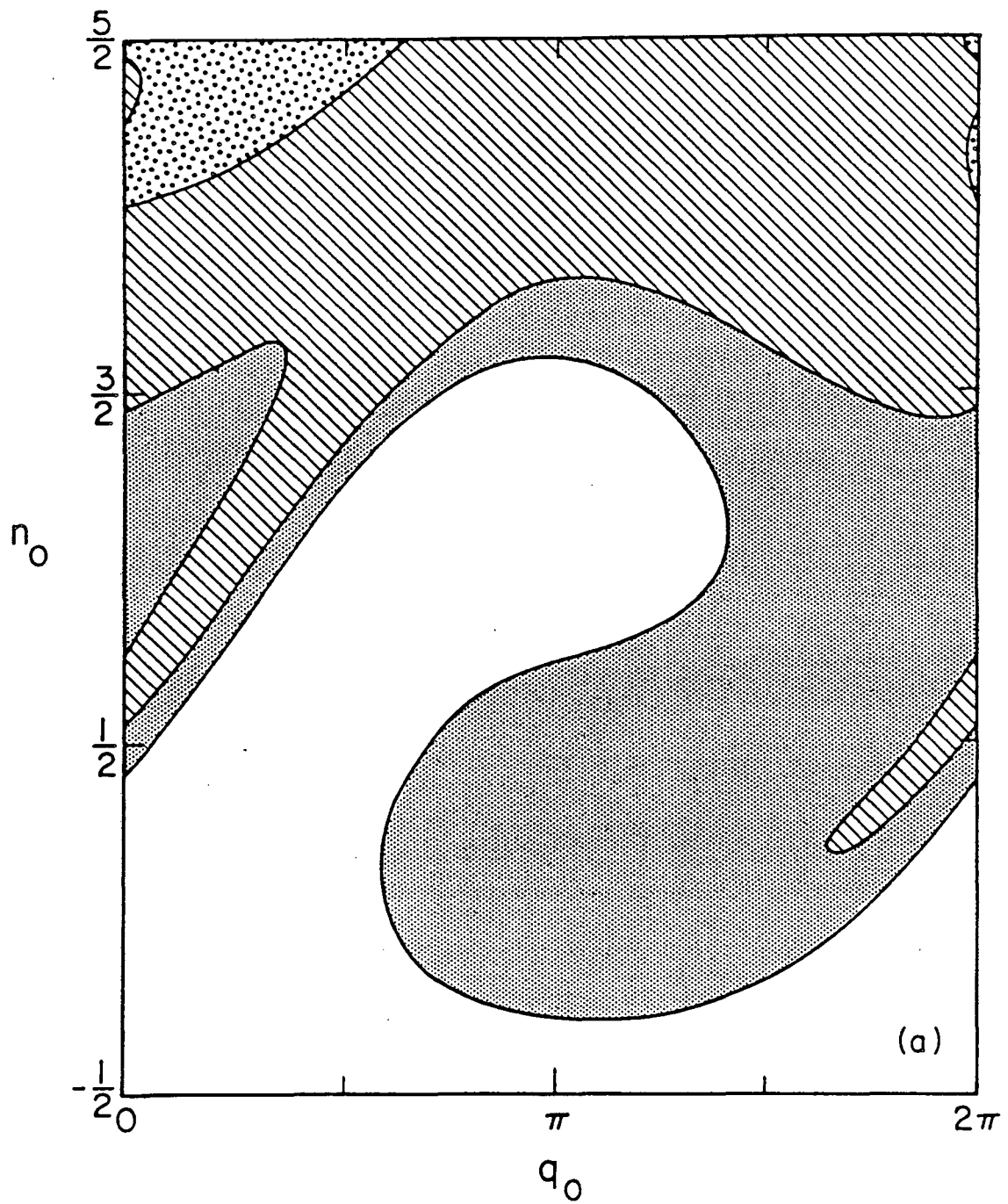
Figure 25a.
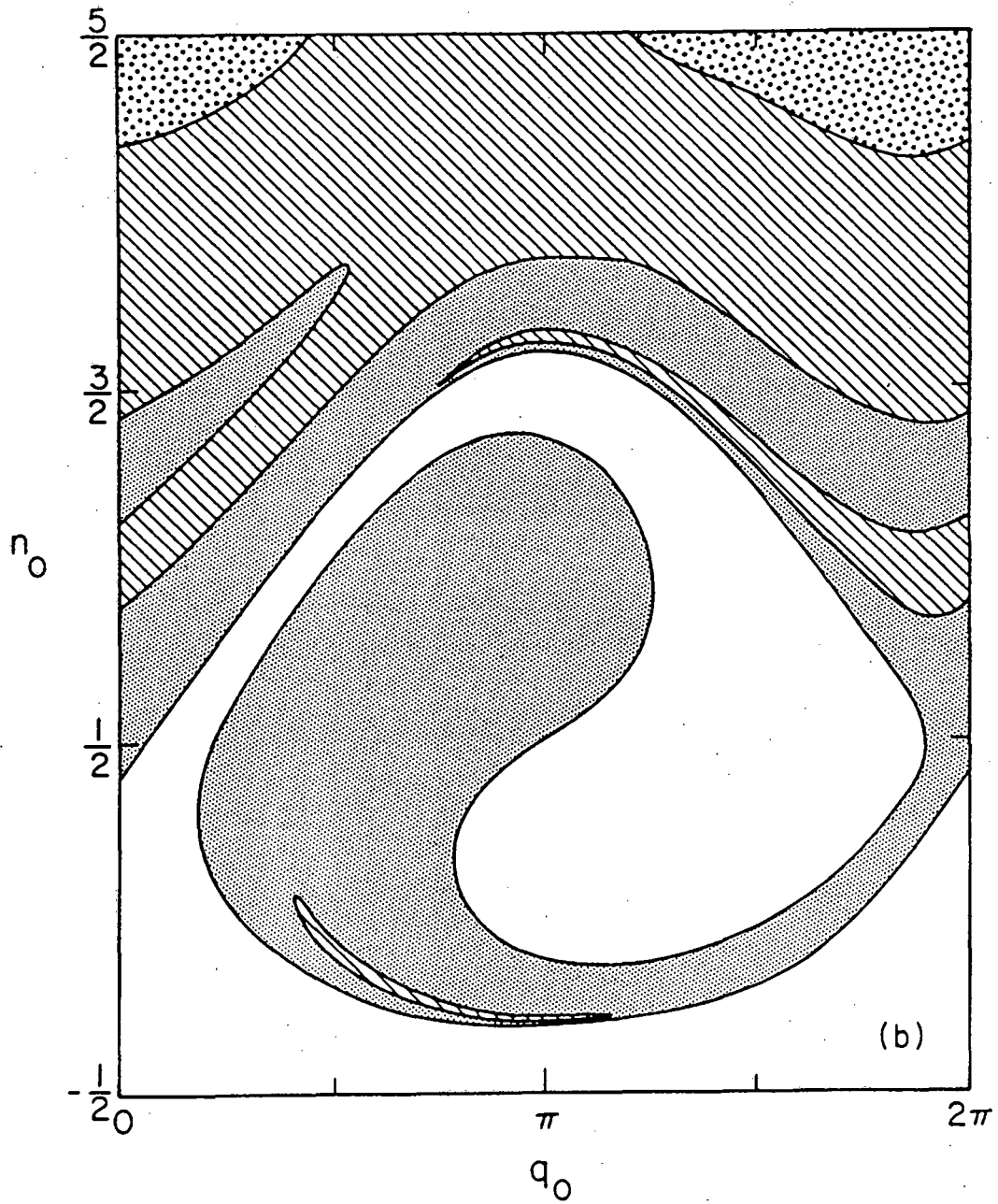
Figure 25b.
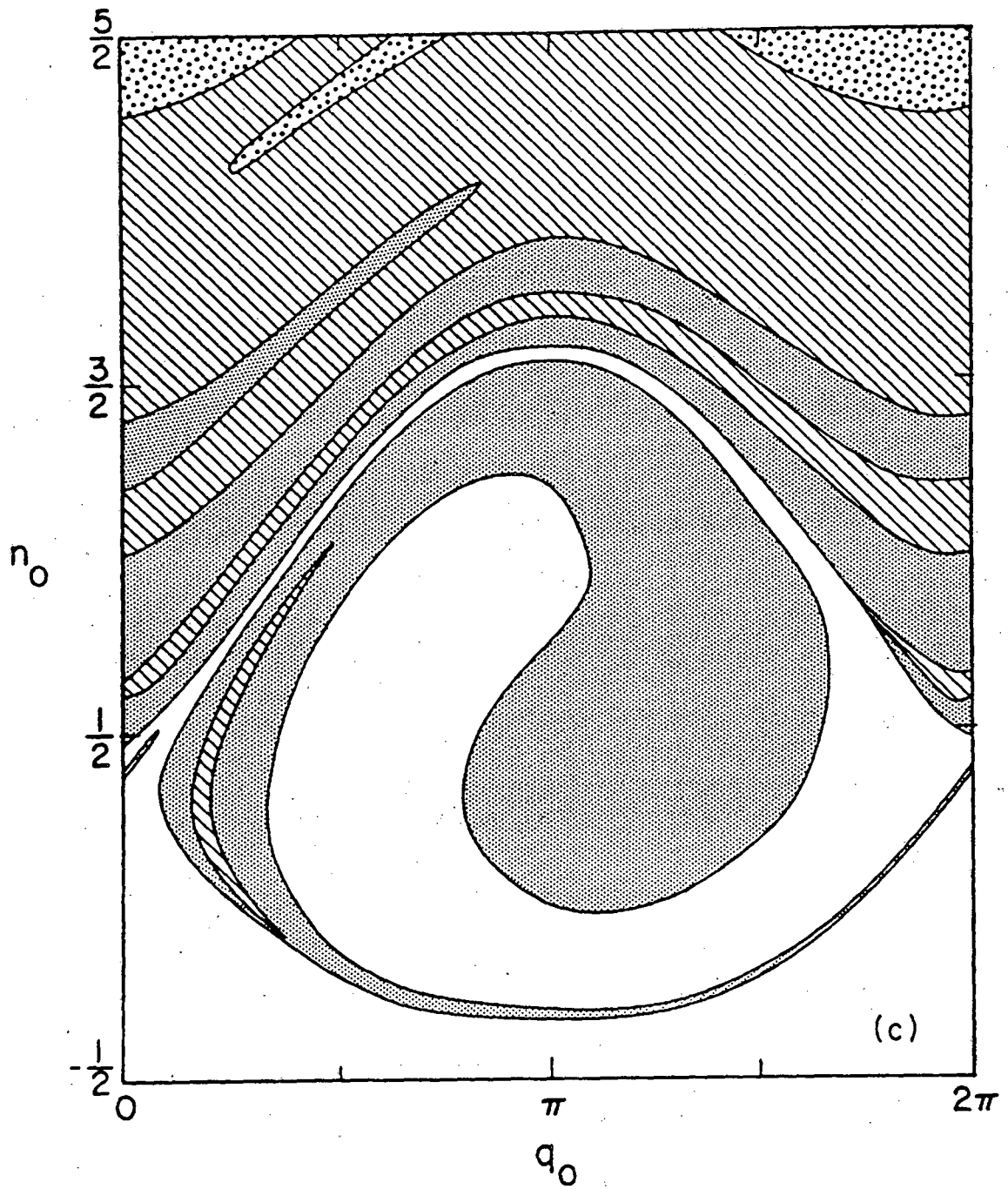
Figure 25c.

TECHNICAL INFORMATION DEPARTMENT
LAWRENCE BERKELEY LABORATORY
UNIVERSITY OF CALIFORNIA
BERKELEY, CALIFORNIA 94720